Thymic self-recognition-mediated TCR signal strength modulates antigen-specific CD8$^+$ T cell pathogenicity in non-obese diabetic mice

Chia-Lo Ho[1], Li-Tzu Yeh[2], Yu-Wen Liu[3], Jia-Ling Dong[4], Huey-Kang Sytwu[1,2,3,4]

[1]Molecular and Cell Biology, Taiwan International Graduate Program, Academia Sinica and Graduate Institute of Life Sciences, National Defense Medical Center, Taipei, Taiwan.

[2]Department and Graduate Institute of Microbiology and Immunology, National Defense Medical Center, Taipei, Taiwan.

[3]National Institute of Infectious Disease and Vaccinology, National Health Research Institutes, Miaoli, Taiwan.

[4]Graduate Institute of Life Sciences, National Defense Medical Center, Taipei, Taiwan.

Address correspondence and reprint request to Dr. Huey-Kang Sytwu, National Institute of Infectious Diseases and Vaccinology, National Health Research Institutes, 35, Keyan Road, Zhunan Town, Miaoli County 350, Taiwan

TEL: +886-37-206166, ext 31011;

FAX: 886-2-87921774

E-mail address of corresponding author: sytwu@nhri.org.tw

Competing interests: All the authors declare no competing interests.

Key words: autoimmune diabetes, CD8, CD5

Public Review #1

Comment 1: Figures 1 through 4 contain data that largely recapitulate published findings (Fulton et al., 2015; Lee et al., 2024; Swee et al., 2016; Dong et al., 2021); it is noted that there is value in confirming phenotypic differences between naive CD5lo and CD5hi CD8 T cells in the NOD background. It is important to contextualize the data while being wary of making parallels with results obtained from CD5lo and CD5hi CD4 T cells. There should also be additional attention paid to the wording in the text describing the data (e.g., the authors assert that, in Figure 4C, the "CD5hi group exhibited higher percentages of CD8+ T cells producing TNF-α, IFN-γ and IL-2" though there is no difference in IL-2 nor consistent differences in TNF-α between the CD5lo and CD5hi populations).

Response: We thank the reviewer for this insightful comment. We agree that the phenotypic differences between $CD5^{hi}CD8^{+}$ and $CD5^{lo}CD8^{+}$ T cells have been previously characterized in other genetic backgrounds. In our study, we aimed to confirm and extend these observations specifically in the autoimmune-prone NOD background, which had not been systematically addressed. Additionally, we carefully reviewed the text describing Figure 4C and revised the wording to accurately reflect the observed data (line 263-264). Specifically, we now state that the $CD5^{hi}$ group exhibited higher levels of IFN-γ and a trend toward increased TNF-α, while IL-2 production did not show a significant difference.

Comment 2: The comparison of CD5 across thymocyte populations is cautioned due to variation in developmental stages, particularly in transgenic models. The reported differences may reflect maturation stages rather than self-reactivity.

Response: We appreciate the reviewer's important point regarding the interpretation of CD5 levels across thymocyte subsets. In our revised manuscript (lines 455–471), we have added clarification that CD5 expression in DN and DP subsets reflects pre-TCR and TCR signaling events during thymic development. We also acknowledge that differences in maturation stages, especially in the NOD8.3 transgenic model, may influence CD5 expression. We now discuss this caveat and interpret our results with caution, particularly emphasizing that our data support but do not sufficiently define their differential self-reactivity.

Comment 3: The conclusion that PTPN22 overexpression does not inhibit the diabetogenic potential of $CD5^{hi}CD8^{+}$ T cells is potentially confounded by differences between polyclonal and TCR transgenic systems.

Response: We thank the reviewer for raising this concern. We acknowledge that this system introduces confounders due to differences in precursor frequencies and clonal expansion compared to polyclonal repertoires. These differences may affect the responsiveness to phosphatase-mediated attenuation of signaling. Therefore, while our results support that high-affinity autoreactive $CD8^{+}$ T cells may be less sensitive to PTPN22 overexpression, we do not claim that this finding generalizes to all autoreactive $CD8^{+}$ T cells. Rather, it highlights a potential inability of peripheral tolerance in T cells with strong intrinsic self-reactivity.

Comment 4: TCR sequencing data shows variability; is this representative of the overall repertoire?

Response: We appreciate the reviewer's comment. We acknowledge that data from bulk TCR sequencing has potential limitations, including variability across experiments and limited resolution at the clonotype level. To improve representativeness and reduce sampling bias, we performed TCR repertoire analysis in two independent experiments. In each experiment, naïve $CD5^{hi}CD8^{+}$ and $CD5^{lo}CD8^{+}$ T cells were sorted from pooled peripheral lymph nodes of at least 20 individual NOD mice per group. This approach allowed us to capture a broader range of clonotypes and ensured that the resulting repertoire profiles reflect the characteristics of the overall $CD5^{hi}$ and $CD5^{lo}$ populations, rather than isolated outliers. Despite some variability, we observed consistent trends in key features, such as shorter CDR3β length, altered TRAV/TRBV usage and reduced diversity in the $CD5^{hi}$ subset across both experiments. To enhance resolution and directly assess clonotype-specific reactivity, we plan to perform single-cell RNA and TCR sequencing in future studies, as noted in the revised Discussion (lines 466–471).

Comment 5: Clarifications are requested regarding naive gating, controls, gMFI reporting, and missing methods.

Response: We thank the reviewer for these specific suggestions. We have revised figure legends to better describe gating strategies and included appropriate controls in Figures or Supplementary Figures. Regarding gMFI reporting, we have now shown in the figure legends whether values are

reported as gMFI. Additionally, we have added the missing methods for cytokine staining, EdU incorporation, overlapped count matrix construction and TCR repertoire diversity metrics.

Public Review #2

Summary Comment: The study is nicely performed, but the definition of naive T cells using only CD44 and CD62L may be oversimplified. CD5hi naive T cells express higher CD44 than CD5lo cells.

Response: We thank the reviewer for the critical evaluation and thoughtful comment. As noted, we defined naïve $CD8^+$ T cells using a well-established gating strategy based on $CD44^{lo}$ and $CD62L^{hi}$ expression, consistent with previous studies (Immunity. 2010; 32(2):214–26; Nat Immunol. 2015; 16(1):107–17). We acknowledge that CD44 is expressed along a continuum, and indeed, within the naïve gate, $CD5^{hi}CD8^+$ T cells exhibited slightly higher CD44 levels compared to their $CD5^{lo}$ counterparts. However, both subsets remained well below the CD44 expression observed in conventional effector/memory $CD8^+$ T cells, supporting their classification as naïve. To further validate this, we assessed additional markers associated with activation and memory differentiation, including CD69, PD-1, KLRG1 and CD25. These analyses confirmed that the sorted $CD5^{hi}$ and $CD5^{lo}$ populations retained a phenotypically naïve profile while exhibiting meaningful differences in baseline activation readiness (Figure 1F).

Public Review #3

Comment 1: CD5 can be regulated by peripheral signals. Therefore, it cannot be concluded that predisposition to effector/memory differentiation is solely programmed in the thymus.

Response: We thank the reviewer for this important point. We agree that CD5 expression can be dynamically regulated in the periphery by tonic TCR signals and antigen encounter, as also reflected in our own data that cells with high CD5 level display elevated activation potential upon encountering antigen (e.g., Figure 3L). To minimize the confounding effects of pre-existing peripheral activation, we performed an adoptive T cell transfer experiment (Figure 4). In this experiment, naïve $CD5^{hi}CD8^+$ and $CD5^{lo}CD8^+$ T cells were sorted from the peripheral lymph nodes of young (6–8-week-old) prediabetic NOD mice and transferred into NOD $Rag1^{-/-}$ recipients. After 4 weeks, we compared the disease phenotypes and functional profiles of $CD8^+$ T cells from these two groups. This approach allowed us to evaluate the stability and

differentiation capacity of $CD5^{hi}$ versus $CD5^{lo}$ cells in a lymphopenic environment, while excluding the possibility that the observed differences were due to already activated $CD8^+$ T cells at the time of isolation. We have revised the Discussion (lines 440–450) to acknowledge these experimental limitations and clarify that, while our findings demonstrate functional differences between $CD5^{hi}CD8^+$ and $CD5^{lo}CD8^+$ T cells, we cannot fully exclude contributions from peripheral influences.

Comment 2: Experiments do not explain why PTPN22 overexpression protects in polyclonal T cells but not in NOD8.3 mice.

Response: We appreciate this critical comment. Our findings support that autoreactive T cells with high-affinity TCRs as in NOD8.3 mice receive strong signaling that even PTPN22 overexpression is insufficient to attenuate their activation and effector function. We acknowledge that further mechanistic studies are needed to fully elucidate the differential effects of PTPN22 in polyclonal versus TCR-transgenic settings.

Comment 3: Evidence that PTPN22 does not regulate TCR signaling in NOD8.3 T cells is weak.

Response: We thank the reviewer for this critical comment. Our data show that NOD8.3 T cells with an intrinsic high CD5-associated self-reactivity are more resistant to transgenic Pep-mediated change in the phosphorylation status of TCR signaling molecules CD3ζ and Erk and CD5 expression (Figure 6, B-D). However, we agree that additional functional assays would strengthen this conclusion.

Comment 4: TCR sequencing does not conclusively link CD5hi cells with autoreactivity; single-cell analysis is needed.

Response: We agree with this critical comment. Bulk TCR sequencing revealed repertoire features associated with autoreactivity, but cannot definitively link specific TCRs to function. We have acknowledged this in the discussion (lines 466–471) and highlighted plans to perform single-cell analysis.

Comment 5: CD5hi cells in the PLNs may reflect antigen exposure rather than basal signaling.

Response: We thank the reviewer for this insightful comment. As also noted in Figure 3L, CD5 expression can be influenced by peripheral tonic TCR signals and recent antigen exposure. To minimize the contribution of peripheral activation, we particularly characterized naïve $CD8^+$ T cells isolated from the peripheral lymph nodes of young (6–8-week-old) prediabetic NOD mice before the onset of overt autoimmunity. Furthermore, we performed an adoptive transfer experiment (Figure 4) using sorted naïve $CD5^{hi}CD8^+$ and $CD5^{lo}CD8^+$ T cells from these mice and characterized their disease phenotype after 4 weeks in lymphopenic NOD $Rag1^{-/-}$ recipients and evaluated the effector function of $CD8^+$ T cells. This approach allowed us to compare the differentiation potential of these subsets in a controlled setting, independent of their activation status at the time of isolation. We have revised the Discussion (lines 440–450) to emphasize that, while our data support functional differences between $CD5^{hi}CD8^+$ and $CD5^{lo}CD8^+$ T cells, we cannot fully exclude the role of peripheral cues in shaping CD5 expression.

Comment 6: Provide proper gating controls and representative flow plots.

Response: We thank the reviewer for this comment. We have revised figure legends to better describe gating strategies and included representative flow cytometry plots and appropriate gating controls in Figures or Supplementary Figures.

Responses to the reviewers' recommendations

Reviewer #1 (Recommendations For The Authors)

(1) The figure presentation is inconsistent and the labels/font are often too small to read easily.

As Reviewer suggested, the figure presentation has been revised for consistency. Labels and fonts have been adjusted for improved readability. Specific figures that were difficult to read have been reformatted with larger fonts and clearer legends.

(2) A careful review of the text to ensure clarity of the content is suggested (e.g., "gratitude" at line 91, "were generally lied" at line 123).

Thanks for Reviewer's comments. The text has been carefully reviewed for clarity and grammatical accuracy. Corrections have been made, including changing "gratitude" to "magnitude" (line 47) and "were generally lied" to "fell between" (line 79).

Reviewer #2 (Recommendations For The Authors)

(1) The definition of naïve T cells based solely on CD44low and CD62Lhigh staining may be oversimplistic. Indeed, even within this definition, naïve CD5high CD8 T cells express much higher levels of CD44 than CD5low CD8 T cells.

Thanks for Reviewer's comments. We used a literature-supported gating strategy (Immunity. 2010; 32(2):214–26; Nat Immunol. 2015; 16(1):107–17) to define naïve T cells based on $CD44^{low}$ and $CD62L^{high}$ expression. It is important to note that CD44 expression exists along a continuum. While we were initially surprised to observe that $CD5^{hi}CD8^{+}$ T cells expressed relatively higher levels of CD44 than $CD5^{lo}CD8^{+}$ T cells within the naïve gate, both populations still exhibited significantly lower CD44 expression compared to conventional effector/memory $CD8^{+}$ T cells. To further validate the distinction between $CD5^{hi}$ and $CD5^{lo}$ subsets, we also examined additional markers such as CD69, PD1, KLRG1 and CD25, which supported their phenotypic differences within the naïve compartment (Figure 1F).

(2) Figure 1G should show the proportion of IGRP-tetramer+ in the three groups of CD8 T cells. Additionally, it would be useful to assess reactivity against a pool of other islet autoantigens using a similar strategy.

As suggested by the reviewer, the revised manuscript now includes additional data showing the proportion of IGRP-tetramer+ cells (Supplementary Figure 1D), as well as reactivity against another islet autoantigen, insulin-1/insulin-2 (Insulin B15–23) (Supplementary Figure 1E). The description of these results, including the proportions of IGRP-tetramer^{+} and Insulin B15–23^{+}CD8^{+} T cells, has been added to lines 126–129 of the revised manuscript.

(3) The resolution of Figure 2 is suboptimal and at places poorly visible. Figure 2D is stated to show "two significant pathways stand out." In fact, the data are barely significant, and the authors may want to correct their statement.

The resolution of Figure 2 has been improved. As Reviewer suggested, the text has been revised to state "two potential pathways stand out" (line 187) instead of "two significant pathways stand out".

(4) Figure 3C-F and 3H, showing fold change over baseline values would be much easier for the reader to grasp the data.

As Reviewer suggested, data in Figures 3C-F and 3H now are shown in fold change over baseline values for clarity. Baseline gMFI is the mean of each group (total CD8^{+}, CD5^{hi}CD8^{+} and CD5^{lo}CD8^{+}) at 0 μg/ml anti-CD3, with fold changes calculated for stimulation conditions (0.625-10 μg/ml anti-CD3). The figure legend has been updated accordingly.

(5) Figure 4A, it would be much more valuable to show the diabetes frequency upon transfer of CD25- CD4 T cells alone and upon transfer of CD5high CD8 T cells alone. The word "spontaneous" in the Figure 4A legend seems inappropriate.

Thanks for the Reviewer's comment. We apologize for not including the data for the CD25^{-} CD4^{+} T cell transfer group in the original manuscript. While this group was part of our initial

experimental design, we had considered it a control group and unintentionally omitted it from the figure. The revised manuscript now includes this group in Figure 4A. In addition, the term "spontaneous" has been replaced with "diabetes incidence" in the Figure 4A legend and manuscript (line 248). Regarding the suggestion to assess $CD5^{hi}CD8^{+}$ T cells transfer alone, we appreciate the Reviewer's point. However, previous studies have shown that $CD8^{+}$ T cells alone are not effective and sufficient to induce diabetes in adoptive transfer models, and that effective β-cell destruction typically requires both $CD4^{+}$ and $CD8^{+}$ T cell subsets. For instance, Christianson et al. (1993) demonstrated that enriched $CD8^{+}$ T cells from NOD mice fail to transfer diabetes on their own, while $CD4^{+}$ T cells—particularly from diabetic donors—can induce disease only under specific conditions and are significantly potentiated by co-transfer of $CD8^{+}$ cells. These findings have contributed to the widely available standard of co-transferring both subsets when studying diabetogenic potential in NOD models (Diabetes. 1993;42(1):44–55).

(6) Line 257-258, please remove "indicating superior in vivo proliferation by the CD5hi subset." Indeed, several other possibilities may explain the phenotype, including survival, migration, etc.

As Reviewer suggested, the phrase "indicating superior *in vivo* proliferation by the $CD5^{hi}$ subset" has been replaced with "implying increased expansion and activation/effector potential" (line 261).

(7) Figure 5A, it is unclear to this referee what is the significance of CD5 and pCD3zeta expression on DN thymocytes. Do these cells express rearranged alpha/beta TCR? Is it signaling through pre-TCRalpha/TCRbeta pairs?

Thanks a lot for this important question. In the revised manuscript, we have expanded the discussion (line 455–471) to address the developmental significance of CD5 and pCD3ζ expression on DN thymocytes. CD5 expression at this stage reflects pre-TCR signaling

strength during early selection, which occurs following successful TCRβ rearrangement. The associated phosphorylation of CD3ζ indicates activation of downstream signaling through the pre-TCRα/TCRβ complex. As discussed in the revised text, these early signals play a critical role in determining lineage progression and self-reactivity tuning. We now acknowledge that signaling at the DN stage occurs through the pre-TCRα/TCRβ heterodimer, not a fully rearranged αβ TCR, and that CD5 expression serves as a marker of the strength of these initial pre-selection signals (*Sci Signal.* 2022;15(736):eabj9842.). These developmental checkpoints are essential for calibrating TCR sensitivity and ensuring proper thymocyte maturation. This has been clarified in the revised discussion (line 455–471).

(8) Figure 5F, could the DP TCRbeta- CD69- thymocytes from 8.3-TCR NOD mice already express low levels of the self-reactive TCR at this stage to explain their high expression of CD5? Addressing the question experimentally would be useful.

Thanks a lot for this useful comment. According to a review by Huseby et al. (2022), expression of a functional TCRβ chain begins at the DN3 stage, initiating progression through the β-selection checkpoint. This is followed by TRAV locus recombination, resulting in the generation of αβ TCR-expressing double-positive 1 (DP-1) thymocytes. At the DP-1 stage, the quality of TCR signaling driven by self-pMHC interactions governs both positive and negative selection, as well as the development of nonconventional T cell lineages. We hypothesize that in transgenic NOD8.3 mice, which express pre-rearranged *Tcra* and *Tcrb* transgenes derived from the islet-reactive $CD8^+$ T cell clone NY8.3, thymocytes undergo allelic exclusion and lack the clonal diversity seen in non-transgenic mice. As a result, NOD8.3 thymocytes may receive strong TCR signals from early developmental stages (DN3 and DP-1) even without undergoing normal selection checkpoints. While the elevated TCR signal observed in NOD8.3 is indeed artificial, this model provides a unique system to test our hypothesis—namely, whether a strongly self-reactive TCR can generate high basal signaling during thymic

development that overrides the negative regulatory effects of phosphatases like Pep. This possibility has been acknowledged in the revised Discussion section, along with a plan to validate the hypothesis experimentally (line 455–471).

(9) Figure 7, single-cell TCR-seq would be much more appropriate to tackle the question of self-reactivity of CD5hi vs. CD5low CD8 T cells.

Thanks a lot for this useful comment. The limitations of bulk TCR-seq are acknowledged, and single-cell TCR-seq is proposed as a future direction (line 455–471).

Note, for Reviewer #2 (Recommendations For The Authors) (7) (8) (9), the discussion paragraphs are included to address the reviewers' questions (line 455–471).

Reviewer #3 (Recommendations For The Authors)

(1) Positive controls (activated T cells from PLN or spleen), gating controls (whole naïve T cells), and representative flow-cytometry plots are needed for T-bet, EOMES, GzmB, and cytokine staining in Figure 1.

As Reviewer suggested, we added representative gating controls for T-bet, EOMES, GzmB and cytokine staining in Supplementary Figure 1 of revised manuscript.

(2) For Figure 1F, MFI for activation markers for the CD44hiCD62Llo cells should be provided for the comparison of PLN data.

As Reviewer suggested, MFI data for these markers have been included in Figure 1F of revised manuscript.

(3) In many places and figure legends, it is not mentioned from which organ cells were collected, i.e., spleen or PLN.

As Reviewer suggested, the origin of cells for each experiment has been explicitly indicated in the figure legends or figure content to ensure clarity.

(4) In the pancreatic lymph node, autoreactive T cells might be upregulating CD5 because they are encountering antigens. This should be addressed in the discussion.

As Reviewer suggested, this issue has been included in the discussion of revised manuscript (line 440-450).

(5) It is not clear if T cells from the spleen and PLN were stimulated to detect the production of pro-inflammatory cytokines.

Thanks for the critical comment. The stimulation protocol and cytokine staining method have been added to the Supplementary material's Supplementary methods section *Cytokine staining* in revised manuscript.

(6) Figure 4C-D: It is not clear if analysis was done on naïve T cells or if they were stimulated.

Thanks for the comment. Additionally, the stimulation and cytokine staining methods used in Figure 4C-D have been described in detail in the Supplementary Materials section *Cytokine staining* of revised manuscript.

(7) IGRP gating in Figure 4F should be revisited with negative controls.

Thanks for the critical comment. Negative controls have been added and used to adjust IGRP gating, and this is now mentioned in the figure legend of revised manuscript.

(8) Interpretation that only CD5hi cells form a central memory T cell population (Figure 4F) could be misleading.

Thanks for this valuable comment. We agree with that in conventional $CD8^+$ T cell immune responses, both $CD5^{hi}$ and $CD5^{lo}$ subsets have the potential to differentiate into central memory T cells. In our experimental approach, we adoptively transferred sorted $CD5^{hi}CD8^+$ or $CD5^{lo}CD8^+$ cells into $Rag1^{-/-}$ recipients and specifically analyzed PLNs four weeks after transfer. Using CD44 and CD62L expression as conventional markers for central memory T cells, we barely observed a $CD44^{hi}CD62L^{hi}$ population in $CD5^{lo}CD8^+$ transferred group. Based on these results, we stated: *"This analysis underscores that the central memory T cell*

population and the frequency of islet autoantigen-specific CD8^{+} T cells are higher in the CD5^{hi} transferred subset within the PLNs, implying more robust immune responses initiated by the CD5^{hi} cells" (line 272–274). Importantly, we did not intend to imply that only CD5^{hi} cells can form central memory T cells, but rather that they were more enriched for this phenotype under the specific conditions and time point analyzed.

(9) IL-2 gating representative plot should be provided for Figure 5A.

As Reviewer suggested, a representative IL-2 gating plot has been included in the revised Supplementary Figure 3B.

Abstract

Our understanding of autoimmune diabetes underscores the critical involvement of $CD8^+$ T cells recognizing islet-specific antigens. However, the influence of thymic positive selection on diabetogenic $CD8^+$ T cell development remains unclear. Using CD5 marker representing T-cell receptor (TCR) signal strength, we illustrated that naïve $CD5^{hi}CD8^+$ T cells of non-obese diabetic (NOD) mice with enhanced TCR signals displayed predisposed differentiated/memory T cell traits with increased activation and proliferation upon TCR stimulation, compared to $CD5^{lo}$ counterparts. Additionally, $CD5^{hi}CD8^+$ T cells exhibited gene expression landscape similar to effector T cells and exacerbated disease in transfer model. Interestingly, the protective effects of transgenic phosphatase Pep expression, which lowers TCR signaling and diabetes incidence, were abolished in NOD strain 8.3 with high CD5 expression linked to increased thymic positive selection. Strikingly, TCR repertoire analysis identified higher frequencies of autoimmune disease-related clonotypes in naïve $CD5^{hi}CD8^+$ cells, supporting that distinct effector functions arise from intrinsic TCR repertoire differences. Overall, $CD5^{hi}CD8^+$ clones may be potential targets for autoimmune diabetes treatment.

Introduction

T cells play a crucial role in inducing immunity by recognizing peptides presented on MHC molecules through their TCR during pathogen infection. The strength of the TCR's reactivity to the foreign antigen is contributed by both the affinity of the TCR for that antigen and the basal TCR signaling level of the T cell, which is determined by weak interactions between the TCR and self-peptides presented during T cell development (1, 2). Previous studies have shown that T cell self-reactivity with weak interaction between TCR and self-peptide-MHC (self-pMHC) not only instructs T cell development and activation thresholds, but also influences their functional response (2-4). It is noteworthy that the strength of the weak interaction can be evaluated through CD5, whose expression level is considered proportional to T cell self-reactivity in the developmental stage, and may reflect the responses of T cells to foreign-pMHC complexes in the future (2, 5, 6).

CD5 is a scavenger receptor cysteine-rich protein expressed on T and B cells that regulates TCR and B-cell receptor signaling (7, 8). It functions as a scaffold protein for the recruitment of phosphatase SHP-1 and E3-ubiquitin ligases CBL and CBLB, to reduce the phosphorylation of proximal TCR signaling molecule Zap70, thereby inhibiting TCR-mediated signaling (9). CD5, as a negative regulator for TCR signaling, also plays a crucial role in fine-tuning the process of positive and negative selection during thymocyte development (8, 10). Specifically, thymocytes with higher self-reactivity TCRs induce CD5 expression, which helps them adapt to strong TCR signaling and reduces the likelihood of negative selection. This, in turn, promotes thymocyte positive selection and broadens the affinity spectrum of the TCR repertoire during the TCR self-recognition process. Therefore, the expression of CD5 is not only a surrogate marker for the strength of TCR-self-peptide-MHC interactions during development but also reflects the intrinsic response set point of T cells to a signal (5, 10). This selection process enriches the mature $CD4^+$ T

24 cell repertoire with clones that exhibit increased responses to self-peptide-MHC, thereby
25 displaying enhanced peripheral immune responses to pathogens and autoantigens *in vivo* (5, 11,
26 12). Not only in $CD4^+$ T cells, previous study has also shown that $CD5^{hi}$ population in $CD8^+$ T
27 cells, characterized by higher reactivity to self-peptide-MHC, are prone to positive selection (5,
28 13). In diabetes-prone NOD mice, though negative selection in central tolerance limits the early
29 contribution of high-avidity T cells to disease development, prolonged inflammation in pancreatic
30 islets still drives the avidity maturation of islet-specific glucose-6-phosphatase catalytic subunit-
31 related protein (IGRP)-specific $CD8^+$ T cells, leading to increased cytotoxicity towards β cells (14-
32 16). This suggests that mechanisms other than incomplete thymic negative selection are involved
33 in generating autoreactive T cells. Here, we investigate whether the CD5-correlated self-pMHC
34 reactivity, which attributes to TCR signal strength in autoreactive $CD8^+$ T cells during thymic
35 positive selection, contributes to the development of autoimmune disease.

36 The NOD mouse model is commonly used for studying autoimmune diabetes. NOD mice
37 spontaneously develop autoimmune diabetes similar to human type 1 diabetes (T1D) with
38 immune-mediated destruction of β cells in the pancreas (17-20). Additionally, genetic variation
39 influences cell lineage decisions during T cell development, affecting positive and negative
40 selection processes and contributing to the emergence of pathogenic $CD4^+$ T cells in diabetes-
41 prone NOD mice (16). Both $CD4^+$ and $CD8^+$ T cells play critical roles in pathogenic diabetogenesis,
42 in which $CD4^+$ T cells drive disease onset and $CD8^+$ T cells mediate β cell destruction (21).
43 However, little is known about the factors affecting $CD8^+$ T cell activity, and the extent to which
44 $CD8^+$ T cell reactivity to self-pMHC during thymic positive selection affects its responses to
45 autoantigens during autoimmune processes remains unclear.

46 We hypothesize that the spectrum of $CD8^+$ T cell diabetogenicity correlates with its

47 expression level of CD5, representing the magnitude of self-pMHC-mediated TCR signaling. In
48 this study, we use *Ptpn22* (22-24) and islet antigen-specific 8.3 TCR transgenic (NOD8.3) (25, 26)
49 mice in addition to conventional NOD mice to investigate this hypothesis. The *Ptpn22* gene
50 encodes PEST domain-enriched tyrosine phosphatase (Pep), which negatively regulates TCR
51 signaling. We have previously demonstrated that different modulation of Pep in effector and
52 regulatory $CD4^+$ T cells leads to attenuation of autoimmune diabetes in distal Lck promoter-driven
53 Pep transgenic NOD mice (dLPC/NOD) (27). Here, we crossed dLPC/NOD to NOD8.3 transgenic
54 mice to generate dLPC/NOD8.3 double transgenic mice and further investigate whether transgenic
55 Pep-mediated protective potential in $CD4^+$ T cells with lower TCR signaling (27) can also be
56 applied to an autoantigen-specific $CD8^+$ T cells with higher CD5 and TCR basal signaling in 8.3
57 TCR transgenic mice. Our data reveal that the activation and proliferation of $CD8^+$ T cells from
58 dLPC/NOD8.3 mice was not attenuated, compared to $CD8^+$ T cells from NOD8.3 mice, suggesting
59 that a dominant role of autoantigen reactivity in $CD8^+$ T cell with high TCR basal signaling and
60 CD5 overrides the transgenic Pep-mediated signaling attenuation during autoimmune
61 diabetogenesis. Exploring a potential modulation of CD5-dependent TCR basal signaling and its
62 impact on T cell reactivity may offer a promising therapeutic strategy for the treatment of T1D in
63 the future.
64
65
66
67
68
69

70 **Results**

71 **Phenotypic difference exists in naïve $CD5^{hi}CD8^{+}$ and $CD5^{lo}CD8^{+}$ T cells of NOD**

72 **mice.**

73 Given that CD5 can serve as a surrogate marker of TCR basal signal strength, which
74 correlates with T cell's self-recognition capability, our initial analysis aimed to determine whether
75 naïve ($CD44^{lo}CD62L^{hi}$) $CD8^{+}$ T cells from NOD mice with different CD5 levels ($CD5^{hi}CD8^{+}$ and
76 $CD5^{lo}CD8^{+}$ T cells) display distinct levels of the TCR basal signal markers p-CD3ζ and p-Erk.
77 The histograms and gMFI analysis revealed significantly increased levels of p-CD3ζ and p-Erk in
78 $CD5^{hi}CD8^{+}$ T cells, in comparison to $CD5^{lo}CD8^{+}$, while the amounts of p-CD3ζ and p-Erk in total
79 naive $CD8^{+}$ T cells fell between the $CD5^{hi}$ and $CD5^{lo}$ subsets (Figure 1, A and B, and
80 Supplementary Figure 1A) in both spleen and pancreatic lymph nodes (PLNs). This result implies
81 an enhanced signaling potential and activation status of $CD5^{hi}CD8^{+}$ T cells, compared to
82 $CD5^{lo}CD8^{+}$ cells, in NOD mice. Since two critical T-box transcription factors, T-bet and Eomes,
83 are regulators of differentiation and effector functions of $CD8^{+}$ T cells (28-30), we further
84 investigated whether intrinsic differences in self-recognition capabilities and subsequent
85 functional heterogeneity between $CD5^{hi}CD8^{+}$ and $CD5^{lo}CD8^{+}$ populations correlate the expression
86 levels of T-bet and Eomes. Our results indicated higher levels of T-bet and Eomes in the naïve
87 $CD5^{hi}CD8^{+}$ population in both spleen and PLNs, compared to $CD5^{lo}$ counterparts (Figure 1C and
88 Supplementary Figure 1B). Elevated expressions of T-bet and Eomes in $CD8^{+}$ T cells have been
89 reported to play critical role in promoting T cell migration to inflamed tissues through induction
90 of chemokine receptors (31, 32) in addition to their association with the differentiation of activated
91 $CD8^{+}$ T cells (28). These upregulated T-bet and Eomes in naïve $CD5^{hi}CD8^{+}$ T cells (Figure 1C)
92 were consistent with elevated levels of Granzyme B, TNF-α, IFN-γ and IL-2 (Figure 1D and

93 Supplementary Figure 1C), indicating the potential of these cells in cytokine production and
94 effector functions. Additionally, $CD5^{hi}CD8^{+}$ subset expressed higher level of chemokine receptor
95 CXCR3 (Figure 1E) than $CD5^{lo}CD8^{+}$ counterparts, a characteristic often associated with effector
96 and memory T cell populations, implying a enhanced ability for migration and localization in
97 response to specific chemotactic signals.

98 Building upon our observations of the phenotypic and functional differences between naïve
99 $CD5^{hi}$ and $CD5^{lo}CD8^{+}$ T cell subsets in NOD mice (Figure 1, A-D), as well as previous research
100 highlighting T-bet- and Eomes-related regulatory mechanisms within $CD8^{+}$ T cell populations (3,
101 28), we next sought to investigate whether CD5-associated self-recognition capabilities influence
102 specific gene regulation in $CD8^{+}$ T cells via distinct levels of T-bet and Eomes. It is well
103 documented that T-bet and Eomes work together to control CD122 expression, a common β chain
104 receptor for IL-2 and IL-15, which is crucial for the survival of IL-15-dependent memory $CD8^{+}$ T
105 cells (30, 33). Additionally, CD122, in cooperation with CD127 (IL-7Rα), represents essential
106 receptors for IL-2, IL-15, and IL-7. They play a pivotal role in regulating $CD8^{+}$ T cell subsets
107 during the memory phase of the immune response (34-37), which is crucial for maintaining
108 memory T cell homeostasis. As shown in Figure 1E, higher expression of CD122 and CD127 was
109 observed in the $CD5^{hi}CD8^{+}$ population, supporting that the overall phenotypic traits of naïve
110 $CD5^{hi}CD8^{+}$ T cells resemble those of memory $CD8^{+}$ T cells (Figure 1E), particularly in their ability
111 to maintain T cell homeostasis.

112 In addition to distinct expression patterns of these memory T cell-related homeostasis
113 markers, like CD122 and CD127 (Figure 1E), we also identified higher expressions of other T cell
114 activation markers, including CD69 (38, 39), PD-1 (40, 41), and KLRG-1 (37, 42), in naïve
115 $CD5^{hi}CD8^{+}$ T cells compared to their $CD5^{lo}$ counterparts (Figure 1F). Similar to PD-1, the

116 activation marker CD44, an adhesion molecule and marker for antigen-experienced T cells, was
117 up-regulated in the $CD5^{hi}CD8^{+}$ population (Figure 1F), as previously reported (3, 34, 43, 44).
118 Additionally, $CD5^{hi}$ cells also exhibit elevated expression of CD25 (IL-2Rα), supporting the
119 presence of intrinsic phenotypic distinction between the $CD5^{hi}$ and $CD5^{lo}$ populations in NOD
120 naïve $CD8^{+}$ T cells (Figure 1F). Since the increased number of islet antigen IGRP-specific $CD8^{+}$
121 T cells positively correlate with insulitis progression both in human T1D and NOD mice, we thus
122 used MHC-tetramer technique to trace $IGRP_{206–214}$-specific $CD8^{+}$ T cells in NOD mice. Our results
123 revealed that $CD5^{hi}CD8^{+}$ T cells compared to $CD5^{lo}CD8^{+}$ counterpart had significant increase in
124 IGPR-tetramer staining level (Figure 1G and Supplementary Figure 1D), suggesting that
125 $CD5^{hi}CD8^{+}$ T cells with higher self-antigen recognizing ability contribute more to islet-destructive
126 pathogenesis in T1D. To further evaluate antigen specificity, we also examined Insulin B15-23
127 (InsB15–23)-specific $CD8^{+}$ T cells using MHC-pentamer staining and observed increased
128 frequencies in the $CD5^{hi}$ subset compared to $CD5^{lo}$ and total naïve $CD8^{+}$ T cells (Supplementary
129 Figure 1E), reinforcing their enriched autoreactive potential. Collectively, in line with previous
130 findings, our results indicate that the phenotypic characteristics of naïve $CD5^{hi}CD8^{+}$ T cells
131 resemble those of effector/memory T cells and confer distinct functional capabilities in
132 autoimmune diabetogenesis compared to $CD5^{lo}CD8^{+}$ cells.
133

134 **Differential gene expression profiling of naïve $CD8^{+}$ T cells stratified by CD5**
135 **levels identifies autoimmune disease-associated gene signatures.**

136 To unveil the underlying differences in phenotypic characteristics between $CD5^{hi}CD8^{+}$ and
137 $CD5^{lo}CD8^{+}$ T cells, we analyzed the gene expression profiling by sorting the 10% upper and lower
138 CD5-expressing naïve $CD8^{+}$ T cells from prediabetic mice at the age of 6 to 8 weeks old (Figure

139 2A). We performed differentially expressed genes (DEGs) analysis using multiple platforms and
140 bioinformatic tools to compare the transcriptomic profiles of $CD5^{hi}$ versus $CD5^{lo}$ T cells. Our
141 DEGs results showed that a total of 185 genes were found to be differentially expressed between
142 $CD5^{hi}$ and $CD5^{lo}$, with a fold change greater than 2 and a p-value less than 0.05 cutoffs; within
143 these genes, 133 were upregulated and 52 were downregulated (Supplementary Table 1 and 2).
144 The significantly upregulated DEGs revealed by the volcano plot (Figure 2B) in $CD5^{hi}$ subset
145 include memory T cell homeostasis marker *Il2rb* (CD122), T cell effector/memory function-
146 associated markers *Tbx21*, *Eomes*, and chemokine receptor *Cxcr3*, consistent with the results
147 obtained in Figure 1. Interestingly, the *Xcl1* gene, which encodes the ligand XCL1 exclusively
148 binding to XCR1 on dendritic cells and facilitating antigen-specific $CD8^+$ T cell expansion, IFN-
149 γ secretion and cytotoxicity, was also upregulated in the $CD5^{hi}$ population (28, 45, 46), implying
150 that $CD5^{hi}CD8^+$ T cells are poised for efficient priming upon antigen encounter.

151 To further characterize DEGs for their functional implications, we performed gene set
152 analysis based on the gene ontology (GO). A gene-concept network by $CD5^{hi}$ versus $CD5^{lo}$ DEGs
153 was associated with the three GO terms: external side of plasma membrane (GO:0009897), T cell
154 activation (GO:0042110), and cytokine production involved in immune response (GO:0002367)
155 (Supplementary Figure 2A). Among the notable findings, genes such as *Cd5*, *Cd83*, *Eomes*, *Xcl1*,
156 *Tbx21*, *Il18rap*, *Klra1*, *Cxcr3*, and *Pdcd1* were significantly upregulated within $CD5^{hi}CD8^+$ T cells,
157 with fold changes equal to or greater than 2. Specifically, within the GO term cytokine production
158 involved in immune response, genes such as *Crlf2*, *Kit*, *F2rl1*, *Xcl1*, *Tbx21*, *Tnfrsf1b* and *Il18rap*
159 showed upregulated expression patterns. Overall, these results provide insights into the potential
160 mechanisms underlying T cell activation and cytokine production in $CD5^{hi}$ population.

161 To thoroughly analyze the intrinsic kinetics and expression profiles of $CD5^{hi}CD8^{+}$ versus
162 $CD5^{lo}CD8^{+}$ T cells under conditions resembling antigen encounter, we cross-referenced our
163 findings with a dataset that delineates the functional relevance of ten gene clusters established in
164 a prior study (47). This study identified core transcriptional signatures governing $CD8^{+}$ T cell
165 activation and effector/memory cell differentiation during infections, defining ten temporal gene-
166 regulated patterns (clusters I~X) in $CD8^{+}$ T cells. Using a $\chi 2$ test to examine gene expression
167 variations in these ten clusters between $CD5^{hi}$ and $CD5^{lo}$ cells (Table 1), we found that the $CD5^{hi}$
168 subset has a significantly higher expression of genes linked to the initial cytokine or effector
169 response (cluster I) and preparation for cell division (cluster II). Additionally, it exhibits a
170 moderately higher expression of genes associated with cell cycle and division (cluster III), early
171 effector and late memory (cluster V), short-term effector or memory (clusters IX), and late effector
172 or memory (clusters X) in the $CD8^{+}$ T cell response (Table 1 and Supplementary Figure 2B).
173 Collectively, these data support that the $CD5^{hi}$ T cells are better prepared for initial activation and
174 late memory formation compared to the $CD5^{lo}$ population.

175 In addition, we performed gene set enrichment analysis (GSEA) on DEGs using the Broad
176 Institute's GSEA desktop software. GSEA analysis indicate that $CD5^{hi}$ cells were enriched for GO
177 terms such as T cell activation (GO:0042110), external side of the plasma membrane
178 (GO:0009897), positive regulation of immune system process (GO:0002684), regulation of
179 catalytic activity (GO:0050790) and other GO terms with similar biological process (BP) functions
180 (Figure 2C, Supplementary Figure 2C and Supplementary Table 3), similar to the results in
181 Supplementary Figure 2A. Collectively, these results of cluster analysis (Table 1) and GSEA
182 (Figure 2C) indicate that $CD5^{hi}CD8^{+}$ T cells in NOD mice possess a greater inherent potential for

183 T cell activation and memory cell formation, which may contribute to the initiation and persistence
184 of autoimmune diabetes.

185 Moreover, we analyzed DEGs by applying Kyoto Encyclopedia of Genes and Genomes
186 (KEGG) database to further investigate whether $CD5^{hi}CD8^{+}$ subset is enriched in any potential
187 disease-related pathways. Strikingly, two potential pathways stood out: the inflammatory bowel
188 disease (IBD)- and type 1 diabetes mellitus-associated pathways (Figure 2D). The enrichment
189 results for IBD and TID pathways suggest that naïve $CD5^{hi}CD8^{+}$ T cells with heightened self-
190 reactivity have the intrinsic capacity to induce T1D and IBD. In summary, our data from gene-
191 concept interactions, GSEA and KEGG pathways reveal distinct phenotypes in $CD5^{hi}CD8^{+}$ subset,
192 indicating their potential for autoimmune predisposition even in their naïve state.

193

194 $CD5^{hi}CD8^{+}$ and $CD5^{lo}CD8^{+}$ T cell subsets have distinct activation and 195 proliferation levels.

196 To examine whether variations in self-recognition, as indicated by CD5 expression,
197 determine diabetogenic $CD8^{+}$ T cell proliferation after TCR stimulation, we isolated naïve $CD8^{+}$
198 T cells and subjected them to 2 days of dose-dependent TCR stimulation using various
199 concentrations of anti-CD3 in combination with a consistent concentration of anti-CD28 (Figure
200 3A). Subsequently, we characterized phenotypic and functional distinctions within the 5% upper
201 and lower CD5-expressing subsets of $CD8^{+}$ T cells. Unlike the lower 5% $CD8^{+}$ groups showing
202 moderate change, the upper 5% $CD8^{+}$ groups exhibited much more significant increase in CD5
203 levels in TCR stimulation dose-dependent manner (Figure 3B). The $CD5^{hi}CD8^{+}$ subset also
204 showed higher p-CD3ζ abundance compared to $CD5^{lo}CD8^{+}$ subset across all TCR stimulation
205 doses. Specifically, p-CD3ζ in $CD5^{hi}CD8^{+}$ peaked at 1.25 μg/ml anti-CD3 stimulation, then

206 gradually declining with increased TCR stimulation doses, possibly due to its faster kinetic
207 expression compared to other T cell activation signaling molecule p-Erk (Figure 3, C and D).
208 Higher p-CD3ζ and p-Erk expressions in NOD $CD5^{hi}CD8^{+}$ cells compared to $CD5^{lo}CD8^{+}$
209 counterparts, consistent across TCR stimulation doses, align with the previous findings in B6 mice
210 (2, 5). The upper 5% $CD5^{hi}$ cells consistently exhibited elevated levels of T cell activation markers
211 CD69 and CD44 (Figure 3, E and F) and showed dose-dependent enhanced proliferation under
212 TCR stimulation (Figure 3G), along with their increased CD127 level (Figure 3H), suggesting
213 heightened capabilities in memory T cell homeostasis.

214 In Figure 3, C-H, we exclusively evaluated the phenotypic and functional differences
215 between $CD5^{hi}$ and $CD5^{lo}$ subsets from activated bulk $CD8^{+}$ T cells following TCR stimulation.
216 To investigate whether these distinctions post TCR activation stem from intrinsic differences
217 between $CD5^{hi}$ and $CD5^{lo}$ cells, we specifically sorted the upper and lower 10% of CD5-expressing
218 $CD8^{+}$ T cells from prediabetic NOD mice aged 6 to 8 weeks, aiming to ascertain whether sorted
219 naive $CD5^{hi}$ and $CD5^{lo}$ T cells maintain these intrinsic differences in their immune responses after
220 TCR or downstream signaling stimulation (Figure 3, I-K). The results revealed that $CD5^{hi}$ cells,
221 after TCR stimulation, displayed increased levels of the T cell activation marker CD69 (Figure 3I),
222 accompanied by higher Ki-67 expression and IFN-γ production (Figure 3J), reflecting their
223 intrinsic distinctions in heightened effector and proliferation functions. Notably, in our T cell
224 stimulation experiment comparing $CD5^{hi}$ and $CD5^{lo}CD8^{+}$ T cells treated with anti-CD3/CD28
225 dynabeads, we observed superior activation potential in $CD5^{hi}$ cells (Figure 3I). After 4 hours of
226 stimulation, CD69 expression in $CD5^{hi}$ cells was significantly higher than in $CD5^{lo}$ cells, with a
227 sharp distinction. As the stimulation time extended to 24 hours, CD69 levels in $CD5^{hi}$ compared
228 to $CD5^{lo}$ remained higher, although the difference reduced, and CD69 expression in both

229 populations became closer. In comparison, with PMA/Ionomycin treatment bypassing TCR
230 signaling initiation, there were almost no distinctions in CD69 levels between $CD5^{hi}$ and $CD5^{lo}$
231 populations, implying cell activation differences between $CD5^{hi}$ and $CD5^{lo}CD8^{+}$ T cells primarily
232 through TCR-proximal signaling. The DNA analog [methyl-3H] thymidine incorporation assay
233 further confirmed the heightened proliferation capacity in $CD5^{hi}$ subset compared to $CD5^{lo}$ subset
234 (Figure 3K). Additionally, we compared CD5 levels between $CD8^{+}CD69^{+}$ and $CD8^{+}CD69^{-}$
235 populations in both the spleen and PLNs. In PLNs, a lymphoid tissue enriched with autoantigens,
236 $CD69^{+}CD8^{+}$ T cells were skewed toward expressing higher CD5 levels compared to the
237 counterparts in spleen (Figure 3L), implying that cells with high CD5 level display elevated
238 activation potential upon encountering antigen. In summary, these results indicate that
239 diabetogenic $CD8^{+}$ T cells exhibiting increased activation and proliferation profiles in NOD mice
240 tend to have elevated CD5-associated auto-immune responses.
241

242 **The CD5 expression level in naïve $CD8^{+}$ T cells is positively correlated with**
243 **diabetes susceptibility in NOD mice.**

244 We further explored potential differences in *in vivo* immune response of $CD5^{hi}$ versus
245 $CD5^{lo}CD8^{+}$ T cells, especially their abilities to induce insulitis and diabetes through an adoptive
246 T cell transfer experiment in NOD model. Following the similar sorting method as in Figure 3, I-
247 K, the naïve $CD5^{hi}CD8^{+}$ and $CD5^{lo}CD8^{+}$ cells from prediabetic NOD mice were then administered
248 separately to immunodeficient NOD $Rag1^{-/-}$ recipients via intraperitoneal injection. The diabetes
249 incidence in $Rag1^{-/-}$ mice was weekly monitored after transfer. Strikingly, the $CD5^{hi}$-transferred
250 group exhibited markedly greater diabetes onset kinetics compared to $CD5^{lo}$ group, with the
251 appearance of diabetes as early as 4 weeks post-transfer. All 10 mice in $CD5^{hi}$ group experienced

252 earlier diabetes onset, in contrast to the $CD5^{lo}$-transferred group, where only 4 out of 11 mice
253 exhibited diabetes after approximately 20 weeks post-transfer (Figure 4A, left panel). Moreover,
254 histological analysis and insulitis scoring of pancreata after the 4-week transfer period revealed
255 heightened severity of insulitis, characterized by profound lymphocytic infiltration in the
256 $CD5^{hi}CD8^{+}$ compared to $CD5^{lo}CD8^{+}$ group (Figure 4A, right panel). This suggests that
257 $CD5^{hi}CD8^{+}$ cells possess more potent diabetogenic properties during the immune responses in
258 autoimmune diabetes.

259 Moreover, flow cytometry analysis revealed a significant increase in both the percentage
260 and the number of CD8 T cells in the spleen and PLNs of the $CD5^{hi}$-transferred group compared
261 to their $CD5^{lo}$ counterparts (Figure 4B), implying increased expansion and activation/effector
262 potential by the $CD5^{hi}$ subset, consistent with the observations in *in vitro* proliferation assay
263 (Figure 3K). Additionally, the $CD5^{hi}$ group exhibited higher levels of IFN-γ and a trend toward
264 increased TNF-α, while IL-2 production did not show a significant difference (Figure 4C) and
265 higher percentages of $CD8^{+}$ T cells expressing the transcription factors T-bet, Eomes and the
266 cytotoxic molecule Granzyme B (Figure 4D). In characterizing other key immune markers
267 between $CD5^{hi}$ and $CD5^{lo}$ groups, as shown in Figure 1, E and F, we observed that $CD5^{hi}$ cells-
268 transferred group in PLNs exhibited high level of CD122 but not in spleen, while also maintaining
269 high CD5 expression (Figure 4E). Furthermore, we assessed the composition of central memory T
270 cells, defined by the $CD44^{hi}CD62L^{hi}$ phenotype, and quantified the percentages of $CD8^{+}$ T cells
271 that recognize islet-specific antigen $IGRP_{206–214}$ by tetramer staining ($IGRP^{+}CD8^{+}$ T cells) in the
272 PLNs (Figure 4F). This analysis underscores that central memory T cell population and the
273 frequency of islet autoantigen-specific CD8 T cells are higher in the $CD5^{hi}$ transferred subset
274 within the PLNs, implying more robust immune responses initiated by the $CD5^{hi}$ cells.

275

276 **The intrinsic high CD5-linked self-reactivity of CD8$^+$ T cells attributed to**
277 **thymic positive selection contributes to the peripheral poised autoimmune**
278 **phenotypes.**

279 Based on our results, phenotypic and functional heterogeneity was observed within naive
280 CD8$^+$ T cells with different CD5 level (Figure 1 and 2), and the further sorted CD5^{hi} and CD5^{lo}
281 cells displayed differential effector/memory functions (Figure 3 and 4). To validate that the
282 differential autoimmune T cell responses in CD5^{hi} and CD5^{lo}CD8$^+$ T cells are linked to
283 heterogeneity in TCR self-reactivity during positive selection, we examined whether the unique
284 TCR basal signal strength and IL-2 production differs in the lower and upper CD5-expressing
285 thymocytes in NOD mice. Indeed, from the immature CD4$^-$CD8$^-$ double-negative (DN),
286 CD4$^+$CD8$^+$ double-positive (DP), to CD4$^-$CD8$^+$ (CD8SP) stages in 6-8-week-old NOD
287 thymocytes, the high self-reactivity CD5^{hi} thymocytes exhibited elevated p-CD3ζ, p-Erk and IL-2
288 expression, supporting their characteristics of survival and proliferation (Figure 5A and
289 Supplementary Figure 3, A and B). These findings are consistent with previous report (2) and may
290 explain a higher CD8$^+$ T cell expansion observed in CD5^{hi}CD8$^+$ cell-transferred recipients
291 compared to CD5^{lo}CD8$^+$ cell-transferred recipients in the adoptive transfer experiment (Figure 4B).
292 We further explored the potential influence of thymic selection on peripheral T cell responses by
293 using the islet antigen-specific 8.3 TCR transgenic NOD8.3 mice, characterized by higher CD5
294 expression, compared to that of NOD mice, and thus an enhanced level of self-recognition.
295 NOD8.3 compared to NOD mice consistently showed elevated CD5 expression from DP to
296 CD8SP stages (Figure 5B), and a significant increase in cell number in the CD8SP subset
297 (Supplementary Figure 3, A and C), suggesting an elevated positive selection in NOD8.3

298 thymocytes. NOD8.3 mice, with elevated CD5 expression linked to basal TCR signal strength (10),
299 showed significantly higher p-CD3ζ level in DP cells compared to NOD mice counterparts (Figure
300 5C and Supplementary Figure 3D). The increase of p-CD3ζ level in DP cells positively correlates
301 with the alterations in thymocyte development reflected in increased cell number and percentage
302 in the CD8SP subset transitioning from the DP stage of NOD8.3 mice (Figure 5D and
303 Supplementary Figure 3C). Additionally, DN thymocytes, marked by CD44 and CD25, undergo
304 crucial β-selection in DN3 ($CD44^{-}CD25^{+}$) and DN4 ($CD44^{-}CD25^{-}$), emphasizing the importance
305 of DN stage in thymocyte development (48-51). NOD8.3 mice showed significantly higher cell
306 numbers in DN4 (Figure 5E and Supplementary Figure 3E), suggesting a selection advantage in
307 these stages due to bypassing the need for TCRβ rearrangement occurred in NOD cells.

308 Positive selection in the DP stage was further characterized by analyzing CD69 and TCRβ
309 levels. In the pre-positive selection population (DP/$TCR\beta^{-}CD69^{-}$), NOD8.3 cells showed
310 significantly higher CD5 expression compared to NOD cells (Figure 5F, upper panel, and
311 Supplementary Figure 3F), implying an enhanced TCR signal perception at the initiation of DP
312 positive selection (52). Consistently, the frequency of $CD69^{+}TCR\beta^{+}$ cells, representing post-
313 positive-selection thymocytes (53), significantly increased in NOD8.3 compared to NOD mice
314 (Figure 5F, lower panel), predisposing to an accelerated accumulation of CD8SP cells (Figure 5D
315 and Supplementary Figure 3C). Additionally, to investigate whether the increased accumulation
316 of CD8SP cell number in NOD8.3 mice is associated with elevated expressions of cytokine
317 receptors crucial for T cell survival in DP stage, we assessed the expression levels of CD122,
318 CD127, CD44 and CD25 in DP thymocytes. Indeed, these receptors showed higher levels in
319 NOD8.3 compared to NOD DP thymocytes (Figure 5G), suggesting their contribution to cell
320 survival into the CD8SP stage. Remarkably, NOD8.3 mice showed an increased percentage of

321 memory-like CD122^{hi}CD44^{hi} cells (V_M; virtually memory) in CD8SP compared to NOD mice
322 (Figure 5H and Supplementary Figure 3G), implying a direct transition to memory T cells upon
323 entering peripheral tissues (54). Furthermore, CD5 expression patterns were compared across
324 thymocyte stages among different NOD strains including NOD, BDC2.5 and NOD8.3 mice.
325 NOD8.3 thymocytes consistently showed higher CD5 levels compared to two other strains from
326 the DN to DP stages, and notably, in the CD8SP stage, NOD8.3 cells exhibited the highest CD5
327 expression, followed by NOD and then BDC2.5 cells (Supplementary Figure 4A). Interestingly,
328 NOD8.3 cells displayed enhanced proliferation (Supplementary Figure 4, B and C), suggesting a
329 potential link between perceived TCR basal signals during thymocyte selection and peripheral
330 lymphocyte proliferation.
331

332 **Downregulation of TCR signaling strength by transgenic phosphatase Pep**
333 **expression does not confer the protection in dLPC/NOD8.3 mice.**

334 Based on the insights gained from thymocyte development in NOD, BDC2.5 and NOD8.3
335 mice, where the TCR signal strength influences intrinsic T cell response and subsequent effector
336 function, we investigated whether the manipulation on TCR basal signal strength influences
337 autoimmune potential of peripheral T cells in NOD mice. To address this issue, we utilized two
338 transgenic mouse model, dLPC/NOD and dLPE/NOD mice, which express a T cell-specific
339 phosphatase Pep to downregulate proximal TCR signaling (27). A significant decrease in
340 autoimmune diabetes, in terms of a delayed onset, less insulitis severity and lower incidence of
341 disease, was found in dLPC/NOD and dLPE/NOD mice compared to NOD controls (27). As
342 expected, transgenic Pep expression in dLPC/NOD mice delayed the onset of diabetes and reduced
343 insulitis. However, Pep overexpression in dLPC/NOD8.3 mice did not provide protection (Figure

344 6A), suggesting that intrinsic high CD5-associated self-reactivity in NOD8.3 T cells overrides the
345 transgenic Pep-mediated protection observed in dLPC/NOD mice. Moreover, overexpression of
346 Pep in dLPC/NOD and dLPC/NOD8.3 mice did not change the CD5 expression of T cells in the
347 spleen compared to their controls, NOD and NOD8.3, respectively. Interestingly, we observed a
348 transgenic Pep-mediated CD5 downregulation in $CD8^+$ T cells in PLNs, enriched with islet-
349 specific autoantigens, of dLPC/NOD mice compared to NOD controls (Figure 6B), suggesting that
350 the transgenic Pep-mediated TCR signaling strength modulates CD5 expression in a context-
351 specific manner. However, CD5 expression level in $CD8^+$ T cells in PLNs of dLPC/NOD8.3 was
352 similar to NOD8.3 mice (Figure 6B), suggesting that NOD8.3 T cells with an intrinsic high CD5-
353 associated self-reactivity are more resistant to transgenic Pep-mediated change in TCR signaling
354 and CD5 expression. These observations are further supported by our data that the CD5-correlated
355 basal TCR signaling molecule, p-CD3ζ, was attenuated in dLPC/NOD mice but not in
356 dLPC/NOD8 .3 mice, both in the spleen and PLNs (Figure 6C). Collectively, our results suggest
357 that $CD8^+$ T cells with intrinsic high CD5-linked self-reactivity are more resistant to transgenic
358 Pep-mediated TCR signaling downregulation and sustain the diabetogenic susceptibility in
359 NOD8.3 mice.

360 Consistently, isolated naïve $CD8^+$ T cells (Supplementary Figure 5 A, left panel) from high
361 CD5-expressing NOD8.3 mice exhibited superior proliferation compared to cells from NOD mice
362 upon anti-CD3/CD28 or PMA/Iono stimulation (Supplementary Figure 5A, middle and right panel,
363 respectively). Moreover, transgenic Pep expression attenuated $CD8^+$ T cell proliferation in both
364 dLPC/NOD and dLPE/NOD mice compared to NOD controls (Supplementary Figure 5B).
365 However, transgenic Pep expression did not alter cell proliferation in dLPE/NOD8.3 T cells when
366 stimulated with the autoantigen-specific self-peptide $IGRP_{206-214}$ (Supplementary Figure 5C),

367 suggesting that a high TCR basal signal conferred by elevated intrinsic self-reactivity overrides
368 the transgenic Pep-mediated reduction of T cell proliferation. Further analysis of p-Erk level also
369 showed a significant decrease in dLPC/NOD compared to NOD mice. Similarly, transgenic Pep
370 did not attenuate the p-Erk level in dLPC/NOD8.3 mice (Figure 6D), consistent with the
371 observation of p-CD3ζ level in these Pep transgenic mice (Figure 6C). Additionally, CD69 and
372 KLRG1 (Figure 6E) and other activation markers including CD44 and CXCR3 (Supplementary
373 Figure 5D) were decreased in dLPC/NOD or dLPE/NOD mice compared to NOD controls. Similar
374 to previous observations, transgenic Pep-mediated attenuation of T cell activation was abolished
375 in dLPC/NOD8.3 mice, supporting again that an intrinsic high CD5-linked self-reactivity is able
376 to confer the impact by transgenic Pep-mediated TCR signaling change.

377 In addition, transgenic Pep expression downregulated CD25 level in T cells of PLNs, not
378 in spleen, in dLPC/NOD mice compared to NOD mice, whereas there was no significant change
379 in CD25 expression between dLPC/NOD8.3 and NOD8.3 mice (Figure 6F). Moreover, memory
380 T cell homeostasis molecules, such as CD122 and CD44, were also reduced in T cells of PLNs,
381 not in spleen, in dLPC/NOD mice compared to NOD mice (Figure 6F and Supplementary Figure
382 5D), but were indistinguishable between dLPC/NOD8.3 and NOD8.3 mice (Figure 6F). Notably,
383 transgenic Pep expression in dLPC/NOD mice significantly reduced production of effector T cell
384 cytokines, such as IL-2, TNF-α and IFN-γ in $CD8^+$ T cells compared to NOD mice (Figure 6G and
385 Supplementary Figure 5E). Nevertheless, transgenic Pep-mediated reduction in cytokine
386 production was abolished in dLPC/NOD8.3 mice (Figure 6G). Collectively, our results indicate
387 that CD5-associated high self-reactivity is able to abolish transgenic Pep-mediated attenuation of
388 effector/memory T cell functions in NOD8.3 mice.

389

390 **Analysis of the CD5^{hi} population identifies TCR repertoires associated with**
391 **autoimmune diseases.**

392 To investigate whether pathogenic feature in CD5^{hi}CD8^{+} population reflects in their TCR
393 repertoire, we divided naïve CD8^{+} T cells into CD5^{hi}CD8^{+} and CD5^{lo}CD8^{+} groups, conducted bulk
394 RNA sequencing on two groups, and applied the MiXCR pipeline to analyze TCR repertoire
395 composition in CD5^{hi} and CD5^{lo} groups (Figure 7A and Supplementary Figure 6). Analysis of T-
396 cell receptor-α chain (*TRAV* and *TRAJ*) and T-cell receptor-β chain (*TRBV* and *TRBJ*) gene usages
397 in CD5^{hi}CD8^{+} and CD5^{lo}CD8^{+} T cells revealed increased utilization of *TRAV13-2*, *TRAV16D-*
398 *DV11*, *TRAV3-3*, *TRAJ32*, *TRBV14*, *TRBV16*, *TRBJ2-1* and *TRBJ2-7* in CD5^{hi}CD8^{+} cells, with the
399 exception of *TRAV9-1*, which exhibited lower utilization in CD5^{hi}CD8^{+} T cells (Figure 7, B-E).
400 The CDR3 loops of TRA (CDR3α) and TRB (CDR3β), crucial for antigen recognition by TCRs
401 on T cells, are shaped by the diverse recombination events that assemble TRA VJ gene segments
402 and TRB V(D)J gene segments (55). The distinct utilization of V or J gene families of TCRα and
403 TCRβ, as shown in Figure 7, B-E, may lead to variable CDR3 characteristics between CD5^{hi}CD8^{+}
404 and CD5^{lo}CD8^{+} T cells. Additionally, emerging evidence suggests a potential association of
405 shorter CDR3 length in T1D patients (56). Therefore, we analyzed whether the CD5^{hi}CD8^{+} cells
406 have similar pathogenic CDR3 patterns. Interestingly, examination of CDR3α and CDR3β length
407 distribution in the TCR repertoire revealed a bias toward shorter length in the CD5^{hi} compared to
408 the CD5^{lo} group, particularly with a significantly shorter CDR3β length (Figure 7F). Shared TCR
409 pools were reported to be enriched in clonotypes with fewer insertions in CDR3 (57). To confirm
410 this, the overlapped clonal count matrix for CDR3α or CDR3β motif was calculated among all
411 groups (Figure 7G), indicating increased similarity between the CD5^{hi} groups based on its own
412 pairing comparison. Strikingly, the IGRP-recognizing CDR3 motif was found in CDR3α of the

413 $CD5^{hi}$ group (Figure 7H), which has been identified in the TCR repertoire of T1D patients (58).
414 Moreover, analysis of CDR3α and CDR3β amino acid characteristics revealed a hydrophobicity
415 enrichment in TRA of $CD5^{hi}CD8^{+}$ cells (Figure 7I), consistent with a previous study demonstrating
416 that the generation of high self-reactive T cells was promoted by hydrophobic residues within the
417 CDR3 region (59). Furthermore, in alignment with a previous study illustrating greater diversity
418 in TCR repertoires from T1D patients than in healthy donors (56), $CD5^{hi}CD8^{+}$ cells exhibited
419 higher diversity in clonotypes compared to their $CD5^{lo}$ counterpart (Figure 7J). Additionally, our
420 results align with a previous study that employed high-throughput TCR-seq analyses in mice,
421 identifying highly shared CDR3 sequences among mice characterized by restricted V and J
422 segment usage (60). These CDR3 sequences, exhibiting lower nucleotide insertions and shorter
423 lengths, were more abundant, particularly in individuals displaying autoimmune and allograft-
424 related reactions, further affirming their association with self-antigen reactivity. In conclusion,
425 these results suggest that $CD5^{hi}CD8^{+}$ T cells, with elevated self-reactivity and increased clonal
426 diversity, are intrinsically linked to the utilization of specific V and J genes within $CD5^{hi}$ cells.
427
428
429
430
431
432
433
434

435 **Discussion**

436 In our study, $CD5^{hi}CD8^{+}$ T cells, with heightened basal signals and increased self-ligand
437 reactivity, show enhanced avidity for the autoantigen IGRP (Figure 8). These cells transition
438 quickly into effector/memory cells upon encountering autoantigens, expressing markers like CD69
439 and CD44. Activation via CD122 and CD127 promotes cytokine secretion, contributing to
440 inflammation and β cell destruction. The upregulation of CD5 in autoreactive $CD8^{+}$ T cells within
441 the PLNs may reflect ongoing antigen encounter and TCR engagement with self-peptides
442 presented by dendritic cells or β cell-derived antigen-presenting cells. This localized antigen
443 stimulation may enhance CD5 expression dynamically, as observed in previous studies where TCR
444 self-reactivity correlates with CD5 levels in both naïve and memory T cells. Additionally, the
445 increased activation marker expression (e.g., CD69 and CD44) in $CD5^{hi}CD8^{+}$ T cells suggests that
446 these cells are actively engaging in self-antigen-driven priming, potentially accelerating their
447 transition to an effector-like phenotype. Future studies employing *in vivo* antigen tracking or CD5
448 fate-mapping approaches could provide deeper insights into whether $CD5^{hi}$ cells within the PLNs
449 are newly activated by antigen encounter or preconditioned for heightened self-reactivity due to
450 thymic selection. Moreover, further investigation is needed to understand the role of these
451 memory-like $CD8^{+}$ T cells in autoreactivity. The loss of Pep-conferred protection in high CD5-
452 expressing NOD8.3 mice highlights the significance of elevated TCR basal signals from positive
453 selection in autoimmune responses, suggesting potential targets for treating T1D and related
454 disorders.

455 CD5 expression in DN thymocytes reflects the strength of pre-TCR signaling during early
456 selection, where successful TCRβ rearrangement drives proliferation and differentiation into the
457 DP stage. The phosphorylation of CD3ζ (pCD3ζ) at this stage indicates activation of Lck/ZAP-70

458 signaling, essential for lineage commitment and self-reactivity tuning. As addressed in a previous
459 study, this early self-MHC interaction calibrates activation thresholds, ensuring appropriate TCR
460 sensitivity while preventing excessive autoreactivity (61). The high expression of CD5 in DP
461 TCRβ^{-}CD69^{-} thymocytes from 8.3-TCR NOD mice may indicate early self-reactivity, even
462 before overt TCR signaling. This raises the possibility that low-level self-pMHC recognition
463 occurs at this stage, priming these cells for selection. To address this hypothesis, future
464 experiments will assess TCR expression and activation states at this intermediate developmental
465 phase, helping to clarify the role of CD5 in shaping the autoreactive potential of these cells. While
466 bulk TCR-seq provided valuable insights into TCR repertoire differences between CD5^{hi} and
467 CD5^{lo}CD8^{+} T cells, it lacks the resolution to assess clonotype-specific self-reactivity. Single-cell
468 TCR-seq would allow a more precise evaluation of individual T cell reactivity and clonal
469 expansion, helping to determine whether CD5^{hi}CD8^{+} cells preferentially retain higher-affinity self-
470 reactive TCRs. Future studies will incorporate this approach to better define the relationship
471 between CD5 expression and antigen specificity.

472 In contrast to previous studies that compared TCR signaling in NOD and wild-type B6
473 mice (11), we investigate how thymic self-recognition impacts TCR signal strength and CD8^{+} T
474 cell pathogenicity in NOD mice. Our research also differs from studies focusing on the CD5^{lo}CD4^{+}
475 T-cell population (12), which resembles central memory T cells and is linked to spontaneous
476 autoimmunity in NOD mice. Instead, we find distinct TCR signal strength variations between
477 CD5^{hi} and CD5^{lo} cells, with CD5^{hi}CD8^{+} cells showing enhanced activation, proliferation and
478 disease transfer potential. This discrepancy may arise from the higher CD5-expressing distribution
479 in the naïve CD4^{+} T cells compared to the naïve CD8^{+} T cells, suggesting distinct TCR signaling
480 sensitivity when stimulated and resulting in different functional activation thresholds between

481 $CD4^+$ and $CD8^+$ T cells (62, 63). Our results reveal that $CD5^{hi}CD8^+$ T cells exhibit elevated CD25
482 and CD122 expression compared to their $CD5^{lo}CD8^+$ counterparts, indicating increased sensitivity
483 to IL-2 stimulation. While exposure to IL-2 may enhance cell expansion in $CD8^+$ cells, it can lead
484 to overstimulation in $CD4^+$ T cells, resulting in activation-induced cell death. Surprisingly, clinical
485 cases of type 1 diabetes reflect similar findings to our animal mouse model study. Children with
486 T1D exhibit higher CD5 expression in $CD8^+$ T cells compared to healthy controls (64). These
487 observations underscore the complexity of immune responses in autoimmune diseases and warrant
488 further exploration to unravel the underlying mechanisms and hold promise for therapeutic
489 interventions in autoimmune diseases.

490 Nevertheless, the role of CD5 itself in shaping the distinctive functions of $CD5^{hi}$ and $CD5^{lo}$
491 cells remains largely unclear (65, 66). A previous research has indicated that CD5 serves as a
492 scaffold protein, retaining the NF-κB inhibitor IκBα in the cytosol to prevent its inhibition of NF-
493 κB signaling (67), though studies of $Cd5^{-/-}$ mice do not appear to support this concept (68). This
494 mechanism confers survival advantages to $CD5^{hi}$ T cells. This observation may help elucidate the
495 seemingly paradoxical result that CD5's primary function is to attenuate TCR-proximal signaling;
496 however interestingly, antigen-specific T cells with higher initial CD5 expression exhibit enhanced
497 persistence as effector/memory cells following a peripheral challenge. Whether $CD5^{hi}CD8^+$ T cells
498 execute potent autoimmune responses through the modulation of NF-κB-dependent signaling
499 needs further investigation.

500 Exploring how TCR composition contributes to the distinct responses between $CD5^{hi}$ and
501 $CD5^{lo}$ cells is beyond the scope of our study. Nonetheless, prior research, which involved screening
502 autoimmune disease databases such as arthritis, diabetes, etc., has revealed a trend in specific TCR
503 repertoire usage characterized by germline-encoded TCRs with fewer nucleotide insertions and

504 shorter CDR3 length (60). It is consistent with our results, demonstrating that $CD5^{hi}$ T cells,
505 skewed toward shorter CDR3 lengths in the TCR repertoire, have a higher potential for
506 autoreactivity. Consequently, the high self-pMHC reactivity of T cells provides a stronger TCR
507 basal signal, potentially priming T cells with specific TCR compositions for robust responses to
508 foreign antigens in the future. From an evolutionary perspective, this TCR design may have
509 initially conferred an advantage by enhancing immune responses against pathogen infections.
510 However, it might have come at the cost of an increased risk of autoimmune diseases. A previous
511 study explored the TCR repertoire of $CD8^+$ T cells recognizing the islet-specific peptide $IGRP_{206–}$
512 $_{214}$ in both grafted and endogenous islet infiltrates, revealing a shared repertoire favoring specific
513 gene segments and limited diversity and clonotypic expansion within $IGRP_{206–214}$-specific $CD8^+$
514 T cells in NOD mice (58). Another study of effector/memory $CD4^+$ and $CD8^+$ T cells involved in
515 autoimmune rejection of islet grafts in diabetic NOD mice demonstrated a comparable pattern of
516 TCR repertoire diversity (69). Our analysis of TCR gene usage in $CD5^{hi}CD8^+$ and $CD5^{lo}CD8^+$ T
517 cells also revealed distinct patterns, suggesting potential functional differences between these
518 subsets. The identified differences included increased usage of TRAV13-2, TRAV16D-DV11,
519 TRAV3-3, TRAJ32, TRBV14, TRBV16, TRBJ2-1, and TRBJ2-7 in $CD5^{hi}$ compared to $CD5^{lo}$
520 cells, while TRAV9-1 was reduced in $CD5^{hi}$ cells. Notably, previous studies identified specific
521 gene segments associated with autoimmune diseases like Sjögren's syndrome (TRAV13-2) (70),
522 inflammatory bowel disease, ulcerative colitis (TRBJ2-1 and TRBJ2-7) (71, 72), and type 1
523 diabetes (TRBV14 and TRBV16) (73), underscoring the importance of understanding T-cell
524 receptor dynamics in autoimmune pathogenesis across various disorders.

525 Several studies have highlighted the impact of TCR-self-pMHC interactions during
526 positive selection on signaling molecules' localization, such as p-Erk, particularly in B cells and

527 $CD4^+$ T cells (4, 74, 75). Similarly, our $CD5^{hi}CD8^+$ T cells may consistently receive stronger
528 signals, leading to better synchronization and activation of Erk at the cell membrane. However,
529 despite using PMA/Iono to bypass proximal TCR signaling and elicit downstream responses,
530 differences in T cell proliferation response persisted between $CD5^{hi}$ and $CD5^{lo}$ or between NOD
531 and NOD8.3 $CD8^+$ T cells. This suggests that TCR-self-peptide interaction influences T cells
532 beyond just proximal TCR signaling intensity. There may be pre-existing transcriptional
533 differences influenced by genes involved in T-cell receptor signaling established during thymic
534 development among naïve NOD $CD8^+$ T cells, affecting their effector lineage fate (76).
535 Additionally, in a previous experimental autoimmune diabetes model, OVA antigen-specific $CD8^+$
536 T cells with a virtual memory phenotype and high CD5 expression showed a low capacity to induce
537 diabetes (77), contrasting with the pathogenic features of our $CD5^{hi}CD8^+$ cells. This suggests that
538 naïve $CD5^{hi}CD8^+$ T cells in NOD mice may only partially resemble virtual memory T cells, posing
539 intriguing questions requiring further investigation.
540
541
542
543
544
545
546
547
548

549 **Materials and methods**

550 *Mice*. The mice utilized in this study included NOD/Sytwu, NOD8.3, and NOD.BDC2.5 TCR
551 transgenic mice, alongside Ptpn22-transgenic NOD mice, designated dLck–Ptpn22 C (dLPC/NOD)
552 and dLck–Ptpn22 E (dLPE/NOD), previously generated by cloning Ptpn22 from NOD mouse
553 splenocytes and microinjecting it into single-cell NOD embryos. The resulting dLck–Ptpn22
554 transgenic mice were genotyped by PCR and evaluated by Southern blot analysis for confirmation.
555 Western blot analysis revealed the expression of transgenic Pep in thymocytes and splenic T cells
556 of dLPC and dLPE mice, with a stepwise increase in Pep protein levels from nontransgenic
557 littermates, dLPC/NOD to dLPE/NOD mice (27). The transgenic mice dLPC/NOD, dLPE/NOD,
558 dLPC/NOD8.3 and dLPE/NOD8.3 used in the study were hemizygous for the Ptpn22 transgene
559 (Supplementary Figure 7). dLPC/NOD8.3 and dLPE/NOD8.3 were established by mating
560 dLPC/NOD or dLPE/NOD mice with NOD8.3 mice. NOD/Sytwu, NOD8.3 and NOD.BDC2.5
561 TCR transgenic mice were originally obtained from The Jackson Laboratory, while NOD Rag1$^{-/-}$
562 mice were procured from the National Laboratory Animal Center. The study adhered to
563 institutional guidelines and was approved by the National Defense Medical Center Institutional
564 Animal Care and Use Committee.

565 *Sex as a biological variable.* Our study exclusively examined female mice because the disease
566 modeled is relevant in females.

567 *Statistics.* The log-rank (Mantel–Cox) test was employed for survival curve comparisons. Two-
568 group comparisons utilized a 2-tailed Student's unpaired t-test, two-sample comparison utilized

569 Welch two sample t-test, and multigroup comparisons utilized one-way ANOVA with Tukey's
570 post-test. A significance level of $P < 0.05$ was considered significant.

571 *Study approval*. All protocols involving live animals adhered to institutional guidelines and
572 received approval from the Institutional Animal Care and Use Committee at the National Defense
573 Medical Center (Taipei, Taiwan).
574
575 Additional methods can be found in the Supplementary Material.
576
577 *Supplementary material.* Supplementary material provided with this study includes Supplementary
578 Figures 1-7, Supplementary Tables 1-6 and Supplementary methods.
579

580 **Data availability**

581 The TCR repertoires of $CD5^{hi}$ and $CD5^{lo}$, along with the data analyzed using R and the
582 corresponding codes, are available in the following GitHub repository: https://github.com/Chia-
583 Lo/TCR-signal-strength-modulates-antigen-specific-CD8-T-cell-pathogenicity-in-non-obese-
584 diabetic-mice.git
585
586
587
588
589
590

591 ## Author contributions

592 CLH and LTY performed experiments and analyzed data. CLH, LTY, YWL and JLD performed
593 experiments. LTY gave advice. CLH and HKS wrote the manuscript.

594

595 ## Acknowledgments

596 This work was supported by the Ministry of Science and Technology of the Republic of China
597 (MOST 109-2320-B-400-018-MY3, MOST 110-2320-B-400-011-MY3), National Science and
598 Technology Council (NSTC 112-2320-B-400-026-MY3) and Tri-Service General Hospital
599 (TSGH-C02-112029, TSGH-C03-113037, VTA112-T-1-1, VTA113-T-1-1). The authors
600 acknowledge the technical services provided by Instrument Center of National Defense Medical
601 Center.

602

603 ## Abbreviations

604 dLPC/NOD, *Lck* distal promoter– *Ptpn22* C line in NOD background; dLPE/NOD, *Lck* distal
605 promoter– *Ptpn22* E line in NOD background. NOD, non-obese diabetic.

606

607

608

609

610

611

612

613

614 ## *References*

615

616 1. Gascoigne NR, Rybakin V, Acuto O, and Brzostek J. TCR Signal Strength and T Cell
617 Development. *Annu Rev Cell Dev Biol.* 2016;32:327-48.
618 2. Persaud SP, Parker CR, Lo WL, Weber KS, and Allen PM. Intrinsic CD4+ T cell sensitivity
619 and response to a pathogen are set and sustained by avidity for thymic and peripheral
620 complexes of self peptide and MHC. *Nat Immunol.* 2014;15(3):266-74.
621 3. Fulton RB, Hamilton SE, Xing Y, Best JA, Goldrath AW, Hogquist KA, et al. The TCR's
622 sensitivity to self peptide-MHC dictates the ability of naive CD8(+) T cells to respond to
623 foreign antigens. *Nat Immunol.* 2015;16(1):107-17.
624 4. Myers DR, Zikherman J, and Roose JP. Tonic Signals: Why Do Lymphocytes Bother?
625 *Trends Immunol.* 2017;38(11):844-57.
626 5. Mandl JN, Monteiro JP, Vrisekoop N, and Germain RN. T cell-positive selection uses self-
627 ligand binding strength to optimize repertoire recognition of foreign antigens. *Immunity.*
628 2013;38(2):263-74.
629 6. Deshpande NR, Parrish HL, and Kuhns MS. Self-recognition drives the preferential
630 accumulation of promiscuous CD4(+) T-cells in aged mice. *Elife.* 2015;4:e05949.
631 7. Sadigh S, Scott BB, Mageed RA, Malcolm A, Andrew EM, and Maini RN. Identification of
632 hybridomas derived from mouse CD5+ B lymphocytes by fluorescent staining for
633 cytoplasmic CD5 expression. *Immunology.* 1994;81(4):558-63.
634 8. Tarakhovsky A, Kanner SB, Hombach J, Ledbetter JA, Muller W, Killeen N, et al. A role
635 for CD5 in TCR-mediated signal transduction and thymocyte selection. *Science.*
636 1995;269(5223):535-7.
637 9. Perez-Villar JJ, Whitney GS, Bowen MA, Hewgill DH, Aruffo AA, and Kanner SB. CD5
638 negatively regulates the T-cell antigen receptor signal transduction pathway: involvement of
639 SH2-containing phosphotyrosine phosphatase SHP-1. *Mol Cell Biol.* 1999;19(4):2903-12.
640 10. Azzam HS, Grinberg A, Lui K, Shen H, Shores EW, and Love PE. CD5 expression is
641 developmentally regulated by T cell receptor (TCR) signals and TCR avidity. *J Exp Med.*
642 1998;188(12):2301-11.
643 11. Dong M, Audiger C, Adegoke A, Lebel ME, Valbon SF, Anderson CC, et al. CD5 levels
644 reveal distinct basal T-cell receptor signals in T cells from non-obese diabetic mice. *Immunol*
645 *Cell Biol.* 2021.

646 12. Kong Y, Jing Y, Allard D, Scavuzzo MA, Sprouse ML, Borowiak M, et al. A dormant T-
647 cell population with autoimmune potential exhibits low self-reactivity and infiltrates islets
648 in type 1 diabetes. *Eur J Immunol.* 2022.
649 13. Lutes LK, Steier Z, McIntyre LL, Pandey S, Kaminski J, Hoover AR, et al. T cell self-
650 reactivity during thymic development dictates the timing of positive selection. *Elife.* 2021;10.
651 14. Han B, Serra P, Yamanouchi J, Amrani A, Elliott JF, Dickie P, et al. Developmental control
652 of CD8 T cell-avidity maturation in autoimmune diabetes. *J Clin Invest.* 2005;115(7):1879-
653 87.
654 15. Amrani A, Verdaguer J, Serra P, Tafuro S, Tan R, and Santamaria P. Progression of
655 autoimmune diabetes driven by avidity maturation of a T-cell population. *Nature.*
656 2000;406(6797):739-42.
657 16. Mingueneau M, Jiang W, Feuerer M, Mathis D, and Benoist C. Thymic negative selection
658 is functional in NOD mice. *J Exp Med.* 2012;209(3):623-37.
659 17. Eisenbarth GS. Type I diabetes mellitus. A chronic autoimmune disease. *N Engl J Med.*
660 1986;314(21):1360-8.
661 18. Ziegler AG, and Nepom GT. Prediction and pathogenesis in type 1 diabetes. *Immunity.*
662 2010;32(4):468-78.
663 19. Herold KC, Vignali DA, Cooke A, and Bluestone JA. Type 1 diabetes: translating
664 mechanistic observations into effective clinical outcomes. *Nat Rev Immunol.*
665 2013;13(4):243-56.
666 20. Pearson JA, Wong FS, and Wen L. The importance of the Non Obese Diabetic (NOD) mouse
667 model in autoimmune diabetes. *J Autoimmun.* 2016;66:76-88.
668 21. Anderson MS, and Bluestone JA. The NOD mouse: a model of immune dysregulation. *Annu*
669 *Rev Immunol.* 2005;23:447-85.
670 22. Fousteri G, Liossis SN, and Battaglia M. Roles of the protein tyrosine phosphatase PTPN22
671 in immunity and autoimmunity. *Clin Immunol.* 2013;149(3):556-65.
672 23. Ivashkiv LB. PTPN22 in autoimmunity: different cell and different way. *Immunity.*
673 2013;39(1):91-3.
674 24. Bottini N, and Peterson EJ. Tyrosine phosphatase PTPN22: multifunctional regulator of
675 immune signaling, development, and disease. *Annu Rev Immunol.* 2014;32:83-119.

676 25. Verdaguer J, Yoon JW, Anderson B, Averill N, Utsugi T, Park BJ, et al. Acceleration of
677 spontaneous diabetes in TCR-beta-transgenic nonobese diabetic mice by beta-cell cytotoxic
678 CD8+ T cells expressing identical endogenous TCR-alpha chains. *J Immunol.*
679 1996;157(10):4726-35.
680 26. Verdaguer J, Schmidt D, Amrani A, Anderson B, Averill N, and Santamaria P. Spontaneous
681 autoimmune diabetes in monoclonal T cell nonobese diabetic mice. *J Exp Med.*
682 1997;186(10):1663-76.
683 27. Yeh LT, Miaw SC, Lin MH, Chou FC, Shieh SJ, Chuang YP, et al. Different modulation of
684 Ptpn22 in effector and regulatory T cells leads to attenuation of autoimmune diabetes in
685 transgenic nonobese diabetic mice. *J Immunol.* 2013;191(2):594-607.
686 28. Kaech SM, and Cui W. Transcriptional control of effector and memory CD8+ T cell
687 differentiation. *Nat Rev Immunol.* 2012;12(11):749-61.
688 29. Pearce EL, Mullen AC, Martins GA, Krawczyk CM, Hutchins AS, Zediak VP, et al. Control
689 of effector CD8+ T cell function by the transcription factor Eomesodermin. *Science.*
690 2003;302(5647):1041-3.
691 30. Intlekofer AM, Takemoto N, Wherry EJ, Longworth SA, Northrup JT, Palanivel VR, et al.
692 Effector and memory CD8+ T cell fate coupled by T-bet and eomesodermin. *Nat Immunol.*
693 2005;6(12):1236-44.
694 31. Zhu Y, Ju S, Chen E, Dai S, Li C, Morel P, et al. T-bet and eomesodermin are required for
695 T cell-mediated antitumor immune responses. *J Immunol.* 2010;185(6):3174-83.
696 32. Lord GM, Rao RM, Choe H, Sullivan BM, Lichtman AH, Luscinskas FW, et al. T-bet is
697 required for optimal proinflammatory CD4+ T-cell trafficking. *Blood.* 2005;106(10):3432-
698 9.
699 33. Banerjee A, Gordon SM, Intlekofer AM, Paley MA, Mooney EC, Lindsten T, et al. Cutting
700 edge: The transcription factor eomesodermin enables CD8+ T cells to compete for the
701 memory cell niche. *J Immunol.* 2010;185(9):4988-92.
702 34. Palmer MJ, Mahajan VS, Chen J, Irvine DJ, and Lauffenburger DA. Signaling thresholds
703 govern heterogeneity in IL-7-receptor-mediated responses of naive CD8(+) T cells. *Immunol*
704 *Cell Biol.* 2011;89(5):581-94.
705 35. Boyman O, Letourneau S, Krieg C, and Sprent J. Homeostatic proliferation and survival of
706 naive and memory T cells. *Eur J Immunol.* 2009;39(8):2088-94.

707 36. Lenz DC, Kurz SK, Lemmens E, Schoenberger SP, Sprent J, Oldstone MB, et al. IL-7
708 regulates basal homeostatic proliferation of antiviral CD4+T cell memory. *Proc Natl Acad*
709 *Sci U S A*. 2004;101(25):9357-62.
710 37. Rubinstein MP, Lind NA, Purton JF, Filippou P, Best JA, McGhee PA, et al. IL-7 and IL-15
711 differentially regulate CD8+ T-cell subsets during contraction of the immune response.
712 *Blood.* 2008;112(9):3704-12.
713 38. Cibrian D, and Sanchez-Madrid F. CD69: from activation marker to metabolic gatekeeper.
714 *Eur J Immunol.* 2017;47(6):946-53.
715 39. Rea IM, McNerlan SE, and Alexander HD. CD69, CD25, and HLA-DR activation antigen
716 expression on CD3+ lymphocytes and relationship to serum TNF-alpha, IFN-gamma, and
717 sIL-2R levels in aging. *Exp Gerontol.* 1999;34(1):79-93.
718 40. Ahn E, Araki K, Hashimoto M, Li W, Riley JL, Cheung J, et al. Role of PD-1 during effector
719 CD8 T cell differentiation. *Proc Natl Acad Sci U S A*. 2018;115(18):4749-54.
720 41. Agata Y, Kawasaki A, Nishimura H, Ishida Y, Tsubata T, Yagita H, et al. Expression of the
721 PD-1 antigen on the surface of stimulated mouse T and B lymphocytes. *Int Immunol.*
722 1996;8(5):765-72.
723 42. Herndler-Brandstetter D, Ishigame H, Shinnakasu R, Plajer V, Stecher C, Zhao J, et al.
724 KLRG1(+) Effector CD8(+) T Cells Lose KLRG1, Differentiate into All Memory T Cell
725 Lineages, and Convey Enhanced Protective Immunity. *Immunity.* 2018;48(4):716-29 e8.
726 43. Park JH, Adoro S, Lucas PJ, Sarafova SD, Alag AS, Doan LL, et al. 'Coreceptor tuning':
727 cytokine signals transcriptionally tailor CD8 coreceptor expression to the self-specificity of
728 the TCR. *Nat Immunol.* 2007;8(10):1049-59.
729 44. Cho JH, Kim HO, Surh CD, and Sprent J. T cell receptor-dependent regulation of lipid rafts
730 controls naive CD8+ T cell homeostasis. *Immunity.* 2010;32(2):214-26.
731 45. Lovering RC, Camon EB, Blake JA, and Diehl AD. Access to immunology through the Gene
732 Ontology. *Immunology.* 2008;125(2):154-60.
733 46. Dorner BG, Dorner MB, Zhou X, Opitz C, Mora A, Guttler S, et al. Selective expression of
734 the chemokine receptor XCR1 on cross-presenting dendritic cells determines cooperation
735 with CD8+ T cells. *Immunity.* 2009;31(5):823-33.

736 47. Best JA, Blair DA, Knell J, Yang E, Mayya V, Doedens A, et al. Transcriptional insights
737 into the CD8(+) T cell response to infection and memory T cell formation. *Nat Immunol.*
738 2013;14(4):404-12.
739 48. Godfrey DI, Kennedy J, Suda T, and Zlotnik A. A developmental pathway involving four
740 phenotypically and functionally distinct subsets of CD3-CD4-CD8- triple-negative adult
741 mouse thymocytes defined by CD44 and CD25 expression. *J Immunol.* 1993;150(10):4244-
742 52.
743 49. Michie AM, and Zuniga-Pflucker JC. Regulation of thymocyte differentiation: pre-TCR
744 signals and beta-selection. *Semin Immunol.* 2002;14(5):311-23.
745 50. Yamasaki S, and Saito T. Molecular basis for pre-TCR-mediated autonomous signaling.
746 *Trends Immunol.* 2007;28(1):39-43.
747 51. Hoffman ES, Passoni L, Crompton T, Leu TM, Schatz DG, Koff A, et al. Productive T-cell
748 receptor beta-chain gene rearrangement: coincident regulation of cell cycle and clonality
749 during development in vivo. *Genes Dev.* 1996;10(8):948-62.
750 52. Fu G, Vallee S, Rybakin V, McGuire MV, Ampudia J, Brockmeyer C, et al. Themis controls
751 thymocyte selection through regulation of T cell antigen receptor-mediated signaling. *Nat*
752 *Immunol.* 2009;10(8):848-56.
753 53. Kim S, Park GY, Park JS, Park J, Hong H, and Lee Y. Regulation of positive and negative
754 selection and TCR signaling during thymic T cell development by capicua. *Elife.* 2021;10.
755 54. Miller CH, Klawon DEJ, Zeng S, Lee V, Socci ND, and Savage PA. Eomes identifies thymic
756 precursors of self-specific memory-phenotype CD8(+) T cells. *Nat Immunol.*
757 2020;21(5):567-77.
758 55. Hughes MM, Yassai M, Sedy JR, Wehrly TD, Huang CY, Kanagawa O, et al. T cell receptor
759 CDR3 loop length repertoire is determined primarily by features of the V(D)J recombination
760 reaction. *Eur J Immunol.* 2003;33(6):1568-75.
761 56. Gomez-Tourino I, Kamra Y, Baptista R, Lorenc A, and Peakman M. T cell receptor beta-
762 chains display abnormal shortening and repertoire sharing in type 1 diabetes. *Nat Commun.*
763 2017;8(1):1792.
764 57. Zvyagin IV, Pogorelyy MV, Ivanova ME, Komech EA, Shugay M, Bolotin DA, et al.
765 Distinctive properties of identical twins' TCR repertoires revealed by high-throughput
766 sequencing. *Proc Natl Acad Sci U S A.* 2014;111(16):5980-5.

767 58. Fuchs YF, Eugster A, Dietz S, Sebelefsky C, Kuhn D, Wilhelm C, et al. CD8(+) T cells
768 specific for the islet autoantigen IGRP are restricted in their T cell receptor chain usage. *Sci*
769 *Rep.* 2017;7:44661.
770 59. Stadinski BD, Shekhar K, Gomez-Tourino I, Jung J, Sasaki K, Sewell AK, et al.
771 Hydrophobic CDR3 residues promote the development of self-reactive T cells. *Nat Immunol.*
772 2016;17(8):946-55.
773 60. Madi A, Shifrut E, Reich-Zeliger S, Gal H, Best K, Ndifon W, et al. T-cell receptor
774 repertoires share a restricted set of public and abundant CDR3 sequences that are associated
775 with self-related immunity. *Genome Res.* 2014;24(10):1603-12.
776 61. Huseby ES, and Teixeiro E. The perception and response of T cells to a changing
777 environment are based on the law of initial value. *Sci Signal.* 2022;15(736):eabj9842.
778 62. Sood A, Lebel ME, Dong M, Fournier M, Vobecky SJ, Haddad E, et al. CD5 levels define
779 functionally heterogeneous populations of naive human CD4(+) T cells. *Eur J Immunol.*
780 2021;51(6):1365-76.
781 63. Hogquist KA, and Jameson SC. The self-obsession of T cells: how TCR signaling thresholds
782 affect fate 'decisions' and effector function. *Nat Immunol.* 2014;15(9):815-23.
783 64. Wadenpohl J, Seyfarth J, Hehenkamp P, Hoffmann M, Kummer S, Reinauer C, et al. CD5-
784 expressing CD8(+) T-cell subsets differ between children with type 1 diabetes and controls.
785 *Immunol Cell Biol.* 2021;99(10):1077-84.
786 65. Voisinne G, Gonzalez de Peredo A, and Roncagalli R. CD5, an Undercover Regulator of
787 TCR Signaling. *Front Immunol.* 2018;9:2900.
788 66. Lozano F, Simarro M, Calvo J, Vila JM, Padilla O, Bowen MA, et al. CD5 signal
789 transduction: positive or negative modulation of antigen receptor signaling. *Crit Rev*
790 *Immunol.* 2000;20(4):347-58.
791 67. Matson CA, Choi S, Livak F, Zhao B, Mitra A, Love PE, et al. CD5 dynamically calibrates
792 basal NF-kappaB signaling in T cells during thymic development and peripheral activation.
793 *Proc Natl Acad Sci U S A.* 2020;117(25):14342-53.
794 68. Axtell RC, Xu L, Barnum SR, and Raman C. CD5-CK2 binding/activation-deficient mice
795 are resistant to experimental autoimmune encephalomyelitis: protection is associated with
796 diminished populations of IL-17-expressing T cells in the central nervous system. *J Immunol.*
797 2006;177(12):8542-9.

798 69. Wong CP, Li L, Frelinger JA, and Tisch R. Early autoimmune destruction of islet grafts is
799 associated with a restricted repertoire of IGRP-specific CD8+ T cells in diabetic nonobese
800 diabetic mice. *J Immunol.* 2006;176(3):1637-44.
801 70. Hong X, Meng S, Tang D, Wang T, Ding L, Yu H, et al. Single-Cell RNA Sequencing
802 Reveals the Expansion of Cytotoxic CD4(+) T Lymphocytes and a Landscape of Immune
803 Cells in Primary Sjogren's Syndrome. *Front Immunol.* 2020;11:594658.
804 71. Rosati E, Pogorelyy MV, Dowds CM, Moller FT, Sorensen SB, Lebedev YB, et al.
805 Identification of Disease-associated Traits and Clonotypes in the T Cell Receptor Repertoire
806 of Monozygotic Twins Affected by Inflammatory Bowel Diseases. *J Crohns Colitis.*
807 2020;14(6):778-90.
808 72. Ihantola EL, Ilmonen H, Kailaanmaki A, Rytkonen-Nissinen M, Azam A, Maillere B, et al.
809 Characterization of Proinsulin T Cell Epitopes Restricted by Type 1 Diabetes-Associated
810 HLA Class II Molecules. *J Immunol.* 2020;204(9):2349-59.
811 73. Shizuru JA, Taylor-Edwards C, Livingstone A, and Fathman CG. Genetic dissection of T
812 cell receptor V beta gene requirements for spontaneous murine diabetes. *J Exp Med.*
813 1991;174(3):633-8.
814 74. Wucherpfennig KW, and Gagnon E. Positively selecting peptides: their job does not end in
815 the thymus. *Nat Immunol.* 2009;10(11):1143-4.
816 75. Daniels MA, Teixeiro E, Gill J, Hausmann B, Roubaty D, Holmberg K, et al. Thymic
817 selection threshold defined by compartmentalization of Ras/MAPK signalling. *Nature.*
818 2006;444(7120):724-9.
819 76. Rogers D, Sood A, Wang H, van Beek JJP, Rademaker TJ, Artusa P, et al. Pre-existing
820 chromatin accessibility and gene expression differences among naive CD4(+) T cells
821 influence effector potential. *Cell Rep.* 2021;37(9):110064.
822 77. Drobek A, Moudra A, Mueller D, Huranova M, Horkova V, Pribikova M, et al. Strong
823 homeostatic TCR signals induce formation of self-tolerant virtual memory CD8 T cells.
824 *EMBO J.* 2018;37(14).
825
826
827

828

829

830 ## Figure legends

831 **Figure 1 Unique phenotypic traits of naïve NOD CD8$^+$ T cells are stratified by CD5**
832 **expression.** Flow cytometry analysis of naïve CD8$^+$ T cells with the upper 5% (CD5^{hi}CD8$^+$) and
833 lower 5% (CD5^{lo}CD8$^+$) CD5 expression from the spleen and PLNs of normoglycemia female NOD
834 mice at the age of 6 to 8 weeks old. (**A**) Representative flow cytometry histograms and the
835 corresponding (**B**) geometric mean fluorescence intensity (gMFI) of CD5, p-CD3ζ and p-Erk
836 expression shown in the indicated samples. Additionally, the percentages of (**C**) transcription
837 factors T-bet and Eomes, along with (**D**) cytokines Granzyme B, TNF-α, IFN-γ and IL-2 in CD8$^+$
838 T cells are also presented in the indicated samples. The gMFI for effector/memory T cell-related
839 markers includes (**E**) CXCR3, CD122, CD127 and (**F**) CD69, PD-1, KLRG-1, CD44 and CD25.
840 (**G**) Representative flow cytometry plots (left) and gMFI (right) of positive IGRP-tetramer staining
841 in CD8$^+$ T cells compared among naive total CD8$^+$ T cells, CD5^{hi} and CD5^{lo} populations. In (**A**)
842 to (**G**), the naïve total CD8 (grey), CD5^{hi} (red) and CD5^{lo} (blue) populations are represented. Data
843 represent mean ± SD. The data presented in (**A**) to (**F**) represent two experiments. The sample size
844 was n = 5-10 (**B**), n = 6-10 (**C**), n = 7-10 (**D**), n = 5-10 (**E**) n = 6-10 (**F**) and n = 3 (**G**) per group.
845 *$P < 0.05$, **$P < 0.01$, ***$P < 0.001$, ****$P < 0.0001$, by one-way ANOVA (**B-D** and **G**) and
846 unpaired, two-tailed t test (**E** and **F**).

847

848 **Figure 2 The gene expression profile of naïve CD5^{hi}CD8$^+$ T cells reveals a poised phenotype**
849 **for effector T cells in autoimmune diseases.** (**A**) RNA-Seq performed on the sorted 10% upper
850 and lower CD5-expressing of naïve CD8$^+$ T cells (CD5^{hi}CD8$^+$ and CD5^{lo}CD8$^+$) from 6-8-week-

851 old normoglycemia female NOD mice to understand the gene expression profile of $CD5^{hi}CD8^{+}$ T
852 cells and comparing that to the $CD5^{lo}$ counterpart to gain insights into their potential role in
853 autoimmune diseases. (**B**) The volcano plot displaying the transcripts that are upregulated and
854 downregulated by RNA sequencing of naïve $CD5^{hi}CD8^{+}$ T cells compared to $CD5^{lo}CD8^{+}$ T cells.
855 The plot shows the log10 fold change of each transcript and the significance of the change,
856 measured by the negative log10 of the adjusted *P*-value (adj.p). Genes with higher fold changes
857 and lower adj.p values (red plots) indicate a significant change in expression between the two
858 groups. (**C**) The gene set enrichment score plot for gene ontology terms (T cell activation, external
859 side of plasma membrane, positive regulation of immune system process, and regulation of
860 catalytic activity). Higher scores indicate a higher degree of enrichment of these processes in naïve
861 $CD5^{hi}CD8^{+}$ T cells compared to the $CD5^{lo}$ counterpart. (**D**) The dot plots of the significant KEGG
862 gene set enrichment in the top 10 enriched pathways, reinforcing the presence of a poised
863 phenotype for effector T cells in autoimmune diseases in naïve $CD5^{hi}CD8^{+}$ T cells. The data
864 presented in (**A**) to (**D**) represent two experiments. In (**A**) to (**D**), n=10 mice per $CD5^{hi}CD8^{+}$ or
865 $CD5^{lo}CD8^{+}$ group, with pooled spleen and PLN cells for sorting obtained from a total of 20
866 normoglycemia female NOD mice aged 6 to 8 weeks old. Significance is determined using a false
867 discovery rate (FDR) adjusted *P*-value < 0.05 and validated using multiple testing correction
868 method Benjamini-Hochberg correction.
869
870 **Figure 3 CD5 expression distinguishes $CD8^{+}$ T cell subsets with differential activation and**
871 **proliferation.** (**A**) Diagram depicting naïve $CD8^{+}$ T cells from normoglycemic female NOD mice
872 aged 6 to 8 weeks, stimulated with indicated concentrations of anti-CD3 (0-10 μg/ml) and anti-
873 CD28 (2 μg/ml; 0 μg/ml for control) for 2 days. Flow cytometry diagrams (**B** and **G**, upper and

874 left panel, respectively) and statistical results (**B-H**) were derived from FLOW analysis.
875 Comparison of CD5 (**B**), p-CD3ζ (**C**), p-Erk (**D**), CD69 (**E**), CD44 (**F**) expression, proliferation
876 levels (CTV dilution percentage) (**G**), and CD127 expression (**H**) between 5% of upper ($CD5^{hi}$)
877 and lower ($CD5^{lo}$) CD5-expressing $CD8^+$ populations was conducted using gMFI of indicated
878 markers. (**I**) Histogram comparing CD69 expression between the upper and lower 10% of CD5-
879 expressing $CD8^+$ T cells ($CD5^{hi}CD8^+$ and $CD5^{lo}CD8^+$). Naïve T cells from normoglycemic female
880 NOD mice aged 6 to 8 weeks were stimulated with anti-CD3/CD28 dynabeads or PMA plus
881 Ionomycin for specified durations and analyzed for CD69 expression by flow cytometry. (**J**)
882 Comparison of Ki-67 expression and IFN-γ production by flow cytometry between $CD5^{hi}CD8^+$
883 and $CD5^{lo}CD8^+$ T cells isolated from normoglycemic female NOD mice aged 6 to 8 weeks. (**K**)
884 Stimulation of $CD5^{hi}CD8^+$ and $CD5^{lo}CD8^+$ T cells isolated from normoglycemic female NOD
885 mice aged 6 to 8 weeks with indicated amounts of anti-CD3/CD28 dynabeads or PMA plus
886 Ionomycin for 2 days. Cell proliferation was assessed by [methyl-3H] thymidine incorporation
887 (cpm; counts per minute). (**L**) Comparison of CD5 gMFI in $CD8^+CD69^+$ (upper gate of flow dot
888 plot) to that in $CD8^+CD69^-$ (lower gate of flow dot plot) population by histogram ($CD8^+CD69^+$ in
889 solid red line; $CD8^+CD69^-$ in grey), across spleen and PLNs from normoglycemic female NOD
890 mice aged 6 to 8 weeks. The statistical results of the percentages of activated ($CD8^+CD69^+$)
891 population (left) and the ratio of activated to non-activated CD5 gMFI (right) are shown. Data
892 represent mean ± SD. The data presented in (**B**) to (**H**) represent two experiments. The sample size
893 was n = 10 (**B-H**), n = 3 (**J**), n = 3-7 (**K**), and n = 4 (**L**) per group. *$P < 0.05$, **$P < 0.01$, ***$P <$
894 0.001, ****$P < 0.0001$, by two-way ANOVA (**B-K**) and unpaired, two-tailed t test (**L**).
895
896 **Figure 4 $CD5^{hi}CD8^+$ T cells-transferred group exhibits severe insulitis and disease phenotype.**

897 (**A**) Diabetes incidence (left) in NOD Rag1$^{-/-}$ mice transferred with CD5^{hi}CD8^{+}, CD5^{lo}CD8^{+}, or
898 CD8^{+} T cells, combined with CD4^{+} T cells, respectively. The islet histological analyses and
899 insulitis scoring (right) for the mice after a 4-week transfer in the respective transferred groups
900 showed a higher diabetes frequency in the CD5^{hi}CD8^{+} group compared to the CD5^{lo}CD8^{+} group.
901 The cells were sorted from the 10% upper and lower of CD5 expression of naïve CD8^{+} T cells
902 (CD5^{hi}CD8^{+} and CD5^{lo}CD8^{+} T cells) from 6-8-week-old normoglycemic female NOD mice and
903 adoptively transferred to 6-8-week-old female NOD Rag1$^{-/-}$ recipients via i.p. injection. Urine
904 glucose concentrations of the four groups of mice were monitored weekly for diabetes incidence.
905 Diabetes was defined as glycosuria > 500 mg/dl in two consecutive tests. Insulitis scoring criteria
906 can be found in the supplementary materials and methods. (**B**) Percentages and cell numbers of
907 CD8^{+} T cells in spleen and PLNs, analyzed from CD5^{hi}CD8^{+} and CD5^{lo}CD8^{+} cells-transferred
908 group, respectively, after 4-week adoptive transfer. (**C**) Percentages of TNF-α, IFN-γ and IL-2
909 production in CD5^{hi}CD8^{+} and CD5^{lo}CD8^{+} group, respectively, from spleen or PLNs, analyzed by
910 flow cytometry, with representative flow dot plots (left) and statistical results (right). (**D**)
911 Percentages of T-bet, Eomes and Granzyme B-expressing in CD5^{hi}CD8^{+} and CD5^{lo}CD8^{+} group,
912 respectively, from spleen or PLNs, analyzed by flow cytometry, with representative flow dot plots
913 (left) and statistical results (right). (**E**) Comparison of differential gMFI expression of CD5, CD25,
914 CD44, CD69, CD122, CD127, KLRG1 and PD-1 between CD5^{hi}CD8^{+} and CD5^{lo}CD8^{+} group from
915 spleen or PLNs. (**F**) Comparison of percentages of central memory T cells (defined by
916 CD44^{hi}CD62L^{hi}) (upper) and positive IGRP-tetramer staining (lower) between CD5^{hi}CD8^{+} and
917 CD5^{lo}CD8^{+} groups from PLNs, with representative flow dot plots (left) and statistical results
918 (right). Data represent mean ± SD. Sample size was n = 5-11 (**A**), and n = 3 (**B**-**F**) per group. *P
919 < 0.05, **P < 0.01, ***P < 0.001, by log-rank test (**A**), by two-way ANOVA (**B**) and (**E**) and

920 unpaired, two-tailed t test (**C**), (**D**) and (**F**).

921 **Figure 5 The high CD5-linked TCR basal signals positively correlate with thymic selection**
922 **in autoimmune-poised NOD8.3 mice.** (**A**) CD5, p-CD3ζ, p-Erk and IL-2 expression levels
923 compared between the lower 5% (hollow blue) and upper 5% (hollow red) CD5 expression in
924 thymocytes of normoglycemia female NOD mice aged 6 to 8 weeks old across DN, DP and CD8SP
925 stages. (**B-H**) Comparison of various marker expression levels between thymocytes of
926 normoglycemia female NOD (solid blue) and NOD8.3 (solid red) mice aged 6 to 8 weeks old
927 across different selection stages. (**B**) CD5 gMFI in NOD and NOD8.3 thymocytes across DN, DP
928 and CD8SP stages. (**C**) Percentages of p-CD3ζ (left) and the corresponding gMFI of p-CD3 (right)
929 compared between NOD and NOD8.3 thymocytes in the indicated stages DN, DP and CD8SP. (**D**)
930 Percentages of DN, DP and CD8SP composition compared between NOD and NOD8.3
931 thymocytes. (**E**) Percentages of indicated DN stages (DN1, DN2, DN3 and DN4) in the DN subset
932 compared between NOD and NOD8.3 mice. DN stages are defined as follows: DN1
933 ($CD44^+CD25^-$), DN2 ($CD44^+CD25^+$), DN3 ($CD44^-CD25^+$) and DN4 ($CD44^-CD25^-$), as depicted
934 in the gating shown in Supplementary Figure 3A, middle panels. (**F**) CD5 gMFI (upper) and
935 corresponding percentages (lower) in the pre-positive selection ($TCR\beta^-CD69^-$) and post-positive
936 selection ($TCR\beta^+CD69^+$) populations in DP thymocytes compared between NOD and NOD8.3
937 mice. The presence of higher TCR basal signals (indicated by higher CD5 gMFI) in NOD8.3 in
938 the pre-positive selection stage leads to an increased percentage of $TCR\beta^+CD69^+$ cells in the post-
939 selection stage compared to NOD mice, as shown in Supplementary Figure 3F. (**G**) gMFI of
940 CD122, CD127, CD44 and CD25 assessed in DP thymocytes compared between NOD and
941 NOD8.3 mice. (**H**) Percentages of virtual memory (V_{memory}) cells in CD8SP thymocytes compared
942 between NOD and NOD8.3 mice. Data represent mean ± SD. The data presented in (**B**) to (**H**)

943 represent two experiments. The sample size was n = 10 (**A**), n = 10-11 (**B**), n = 3-6 (**C**), n = 9-11
944 (**D**), n = 7-11 (**E**), n = 8-11 (**F**) n = 10-11 (**G**) and n = 8-9 (**H**) per group. *$P < 0.05$, **$P < 0.01$,
945 ****$P < 0.0001$, by unpaired, two-tailed t test (**A**-**H**).
946
947 **Figure 6 The protective effect of transgenic Pep on diabetogenesis is negated in**
948 **dLPC/NOD8.3 mice.** (**A**) Spontaneous diabetes incidence (left) and insulitis scoring (right) of
949 female non-Tg NOD, dLPC/NOD, NOD8.3 and dLPC/NOD8.3 mice. Insulitis scoring was
950 performed on the islets from the pancreata of 6-8-week-old mice before the onset of diabetes in
951 each group. Insulitis scoring criteria can be found in the supplementary materials and methods.
952 Urine glucose concentrations of mice were monitored weekly for spontaneous diabetes incidence.
953 Diabetes was defined as glycosuria > 500 mg/dl at two consecutive tests. (**B**-**G**) Characterization
954 of various aspects of TCR signal strength and effector/memory T cell phenotypes among female
955 normoglycemia non-Tg NOD (blue), dLPC/NOD (black), NOD8.3 (red) and dLPC/NOD8.3 (grey)
956 mice at the age of 6 to 8 weeks old. (**B**) CD5 gMFI of $CD8^+$ T cells in the spleen (left) and PLNs
957 (right). (**C**) Percentage of p-$CD3\zeta^+CD8^+$ T cells in the spleen (left) and PLNs (right). (**D**)
958 Percentage of p-Erk^+CD8^+ T cells in the spleen (left) and PLNs (right). (**E**) gMFI of effector T cell
959 markers CD69 and KLRG1 in $CD8^+$ T cells from the spleen (upper) and PLNs (lower). (**F**) gMFI
960 of memory T cell markers CD25, CD122 and CD44 in $CD8^+$ T cells from the spleen (upper) and
961 PLNs (lower). (**G**) Percentage of IL-2^+-, TNF-α^+-, and IFN-γ^+CD8^+ T cells in PLNs. Data in (**B**)
962 to (**G**) represent mean ± SD. The data presented in (**B**) to (**G**) represent two experiments. The
963 sample size was n = 7-10 (**A**), n = 4-11 (**B**), n = 3-7 (**C**), n = 3-7 (**D**), n = 5-11 (**E**), n = 5-11 (**F**)
964 and n = 3-9 (**G**) per group. *$P < 0.05$, **$P < 0.01$, ***$P < 0.001$, ****$P < 0.0001$, by log-rank
965 test (**A**), by one-way ANOVA (**B**-**F**) and unpaired, two-tailed t test (**G**).

966

967 **Figure 7 Examination of the CD5^{hi} population reveals TCR repertoires linked to**
968 **autoimmune disorders.** (**A**) Comparison of TCR repertoire differences between CD5^{hi}CD8^{+} and
969 CD5^{lo}CD8^{+} T cell populations conducted using bulk RNA sequencing, followed by TCR repertoire
970 analysis using the MiXCR pipeline. Naïve CD5^{hi}CD8^{+} and CD5^{lo}CD8^{+} cells were sorted from
971 female normoglycemia NOD mice aged 6 to 8 weeks old following a similar procedure as outlined
972 in Figure 2A, with 1.5 x 10^{6} cells per group. The TCR repertoire of naïve CD5^{hi}CD8^{+} T cells
973 exhibited shorter CDR3 lengths, higher clone overlap values within group comparisons,
974 pathogenic-related CDR3 motifs, and greater hydrophobicity and diversity in the TRA chain
975 compared to CD8^{+}CD5^{lo} cells. (**B**-**E**) Comparison of the TRAV gene segment usage (**B**), TRAJ
976 gene segment usage (**C**), TRBV gene segment usage (**D**), and TRBJ gene segment usage (**E**) within
977 TRA variable and TRB variable genes between CD5^{hi}CD8^{+} (red) and CD5^{lo}CD8^{+} (blue) cells. (**F**-
978 **J**) Comparison of CDR3α (left) or CDR3β (right) length in amino acids (**F**), CDR3 clonal overlap
979 by overlapped count matrix (**G**), top 20 CDR3 motifs (**H**), average hydrophobicity score (**I**) and
980 diversity (**J**) of CDR3α (left) and CDR3β (right) between CD5^{hi}CD8^{+} and CD5^{lo}CD8^{+} T cells. In
981 (**G**), number in cell indicates count number shared within the comparison group. (**H**) Occurrence
982 frequencies of the top 20 CDR3 motifs from mapped-CDR3α (left) and CDR3β (right) sequencings
983 in CD5^{hi}CD8^{+} and CD5^{lo}CD8^{+} cells, with the high-occurrence rate of the CDR3α motif
984 "SGGSNYKLTF" (underlined in red) specific to T1D-related IGRP peptide in the CD8^{+}CD5^{hi}
985 population. (**I**) Average hydrophobicity score defined by summing up the hydrophobicity score in
986 each amino acid in the CDR3 motif and dividing by the CDR3 length, then averaging by total
987 counts in each group. Diversity definition in (**J**) is shown in Materials and Methods section
988 Clonotype repertoire metrics formulas. In (**B**-**E**), each point represents 10 mice, with two points

989 for each group, totaling n = 20 mice (**F-J**) for all $CD5^{hi}$ or $CD5^{lo}$ samples. *$P < 0.05$, **$P < 0.01$,

990 ***$P < 0.001$, by two-way ANOVA (**B-E**), by Welch two sample t-test (**F**), and unpaired, two-

991 tailed t test (**I**) and (**J**).

992 **Figure 8 Thymocyte self-reactivity impacts the effector functions and memory cell formation**

993 **of auto-reactive T cells in the T1D model NOD mice.**

994

995 ## Table

996 **Table 1 Naïve $CD5^{hi}CD8^{+}$ and $CD5^{lo}CD8^{+}$ T cells exhibit distinct expression in**

997 **effector/memory T cell gene-expression clusters.**

Cluster	Characteristics	$CD5^{lo}$	$CD5^{hi}$	*P*	Proportion
I	Initial cytokine or effector response	2	21	6.66555E-45	0.913
II	Preparation for cell division	98	406	1.7815E-173	0.806
III	Cell cycle & division	81	175	2.20063E-29	0.684
IV	Naive and late memory	44	25	5.78321E-06	0.362
V	Early effector, late memory	33	150	2.31501E-70	0.820
VI	Short-term effector and memory	18	30	0.000881688	0.625
VII	Memory precursor	47	41	0.251118001	0.466
VIII	Naive or late effector or memory	103	98	0.492702408	0.488
IX	Short-term effector or memory	27	45	6.4806E-05	0.625
X	Late effector or memory	28	49	1.77113E-06	0.636

998

999 Variation in gene-expression clusters between naïve $CD5^{hi}CD8^{+}$ and $CD5^{lo}CD8^{+}$ T cells and gene-

1000 set clusters in $CD8^{+}$ T cells evaluated by the Immunological Genome Project (published clusters

1001 with designated characteristics). In the '$CD5^{lo}$' and '$CD5^{hi}$' columns, values represent the count of

1002 genes predominantly expressed in each subset; 'Proportion' indicates the fraction of those genes

1003 expressed in the $CD5^{hi}$ subset. Statistical significance of expression differences was determined

1004 using the $\chi 2$ test (*P*).

Figures and figure legends

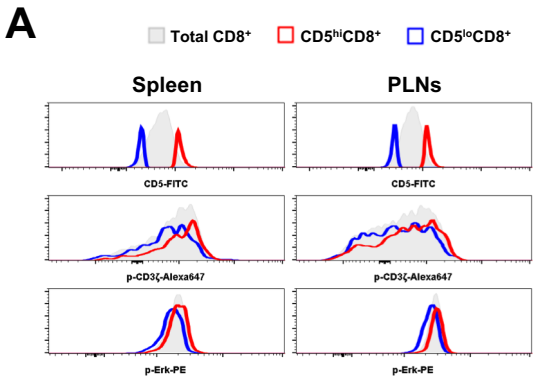

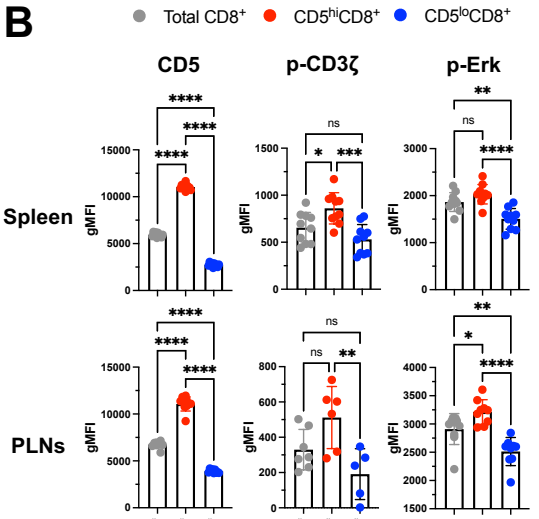

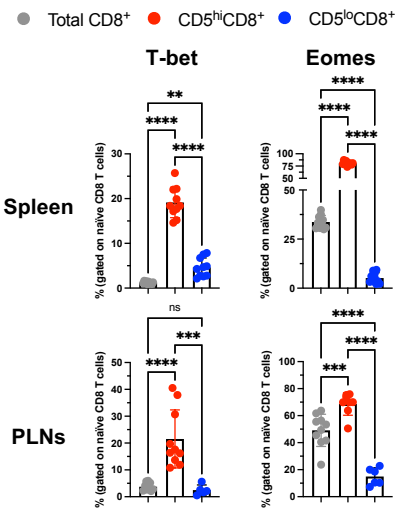

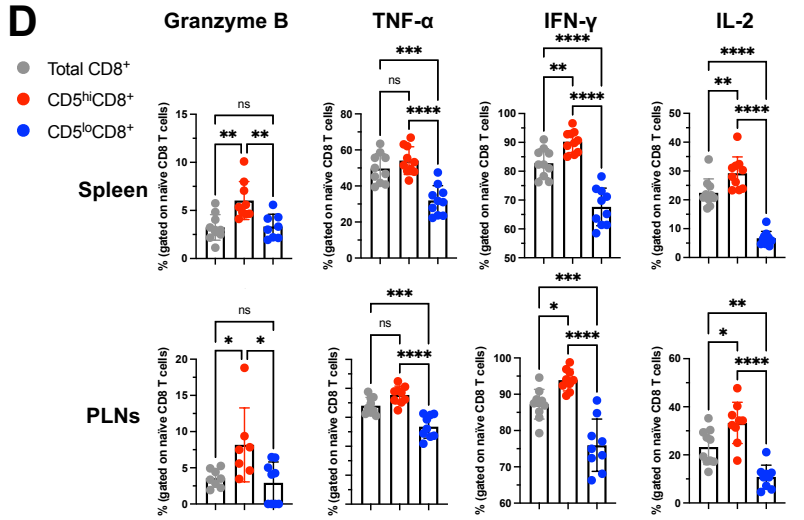

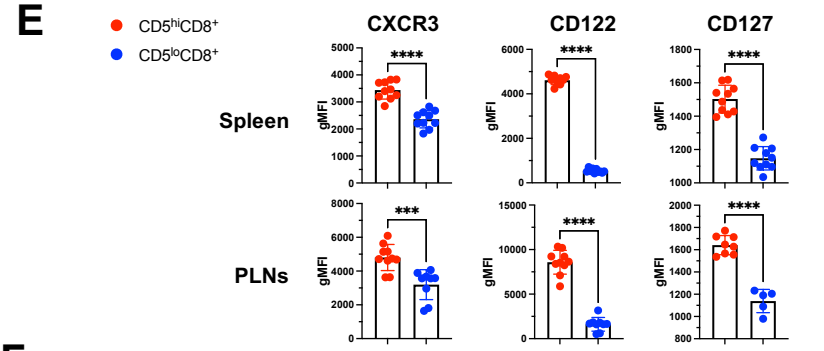

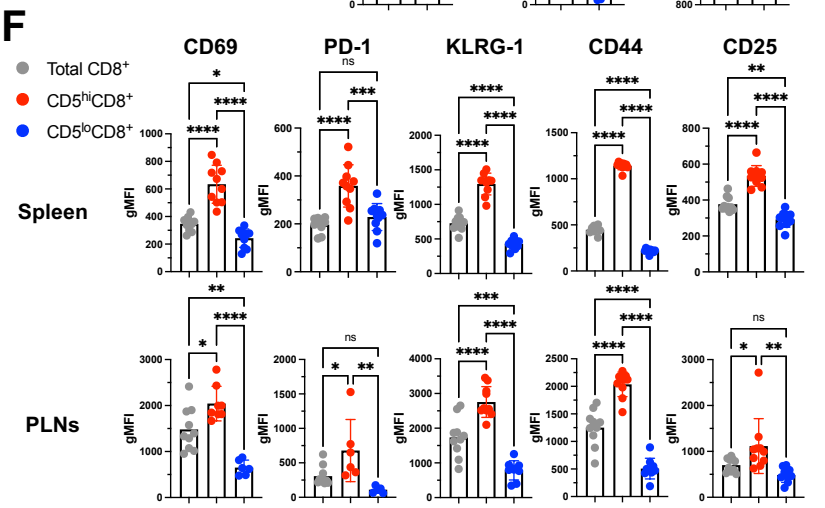

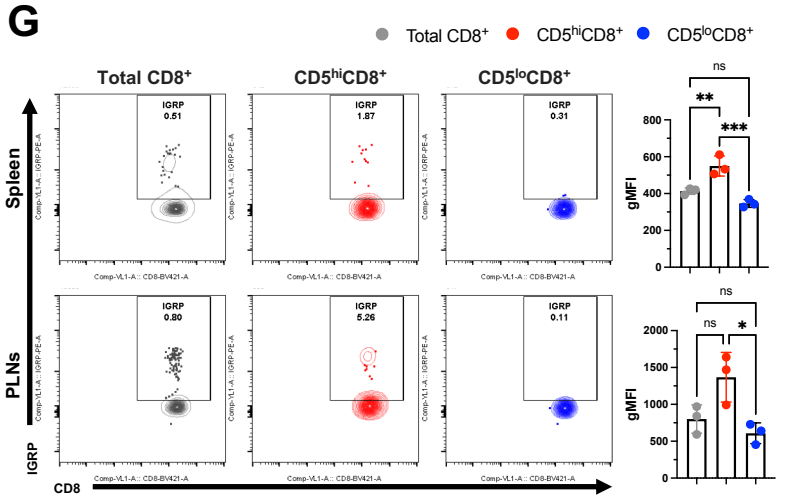

Figure 1 Unique phenotypic traits of naïve NOD CD8⁺ T cells are stratified by CD5 expression. In (**A**) to (**G**), flow cytometry analysis of total naïve CD8⁺ T cells (CD44^{lo}CD62L^{hi}; grey), and the upper 5% (CD5^{hi}CD8⁺; red) and lower 5% (CD5^{lo}CD8⁺; blue) based on CD5 expression, from the spleen and PLNs of normoglycemic female NOD mice aged 6 to 8 weeks. (**A**) Representative flow cytometry histograms and the corresponding (**B**) geometric mean fluorescence intensity (gMFI) of CD5, p-CD3ζ and p-Erk expression shown in the indicated samples. Additionally, the percentages of (**C**) transcription factors T-bet and Eomes, along with (**D**) cytokines Granzyme B, TNF-α, IFN-γ and IL-2 in CD8⁺ T cells are also presented in the indicated samples. The gMFI for effector/memory T cell-related markers includes (**E**) CXCR3, CD122, CD127 and (**F**) CD69, PD-1, KLRG-1, CD44 and CD25. (**G**) Representative flow cytometry plots (left) and gMFI (right) of positive IGRP-tetramer staining in CD8⁺ T cells compared among naive total CD8⁺ T cells, CD5^{hi}CD8⁺ and CD5^{lo}CD8⁺ populations. Data represent mean ± SD. The data presented in (**A**) to (**F**) represent two experiments. The sample size was n = 5-10 (**B**), n = 6-10 (**C**), n = 7-10 (**D**), n = 5-10 (**E**) n = 6-10 (**F**) and n = 3 (**G**) per group. *P < 0.05, **P < 0.01, ***P < 0.001, ****P < 0.0001, by one-way ANOVA (**B**–**D**, **F**, **G**) and unpaired, two-tailed t test (**E**).

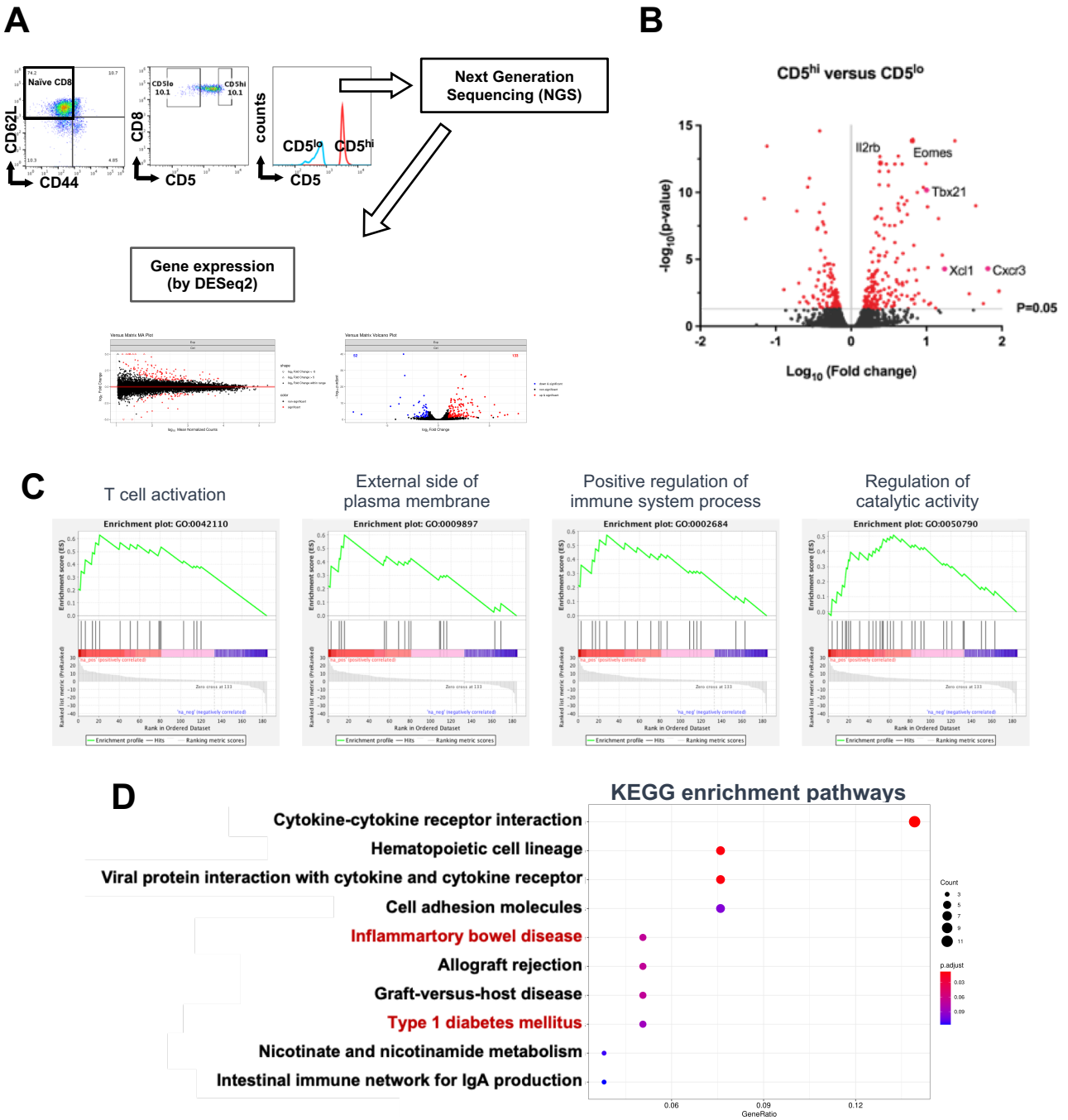

Figure 2 The gene expression profile of naïve CD5^{hi}CD8^{+} T cells reveals a poised phenotype for effector T cells in autoimmune diseases. (**A**) RNA-Seq performed on the sorted 10% upper and lower CD5-expressing of naïve CD8^{+} T cells (CD5^{hi}CD8^{+} and CD5^{lo}CD8^{+}) from 6-8-week-old normoglycemia female NOD mice to understand the gene expression profile of CD5^{hi}CD8^{+} T cells and comparing that to the CD5^{lo} counterpart to gain insights into their potential role in autoimmune diseases. (**B**) The volcano plot displaying the transcripts that are upregulated and downregulated by RNA sequencing of naïve CD5^{hi}CD8^{+} T cells compared to CD5^{lo}CD8^{+} T cells. The plot shows the log10 fold change of each transcript and the significance of the change, measured by the negative log10 of the adjusted *P*-value (adj.p). Genes with higher fold changes and lower adj.p values (red plots) indicate a significant change in expression between the two groups. (**C**) The gene set enrichment score plot for gene ontology terms (T cell activation, external side of plasma membrane, positive regulation of immune system process, and regulation of catalytic activity). Higher scores indicate a higher degree of enrichment of these processes in naïve CD5^{hi}CD8^{+} T cells compared to the CD5^{lo} counterpart. (**D**) The dot plots of the significant KEGG gene set enrichment in the top 10 enriched pathways, reinforcing the presence of a poised phenotype for effector T cells in autoimmune diseases in naïve CD5^{hi}CD8^{+} T cells. The data presented in (**A**) to (**D**) represent two experiments. In (**A**) to (**D**), n=10 mice per CD5^{hi}CD8^{+} or CD5^{lo}CD8^{+} group, with pooled spleen and PLN cells for sorting obtained from a total of 20 normoglycemia female NOD mice aged 6 to 8 weeks old. Significance is determined using a false discovery rate (FDR) adjusted *P*-value < 0.05 and validated using multiple testing correction method Benjamini-Hochberg correction.

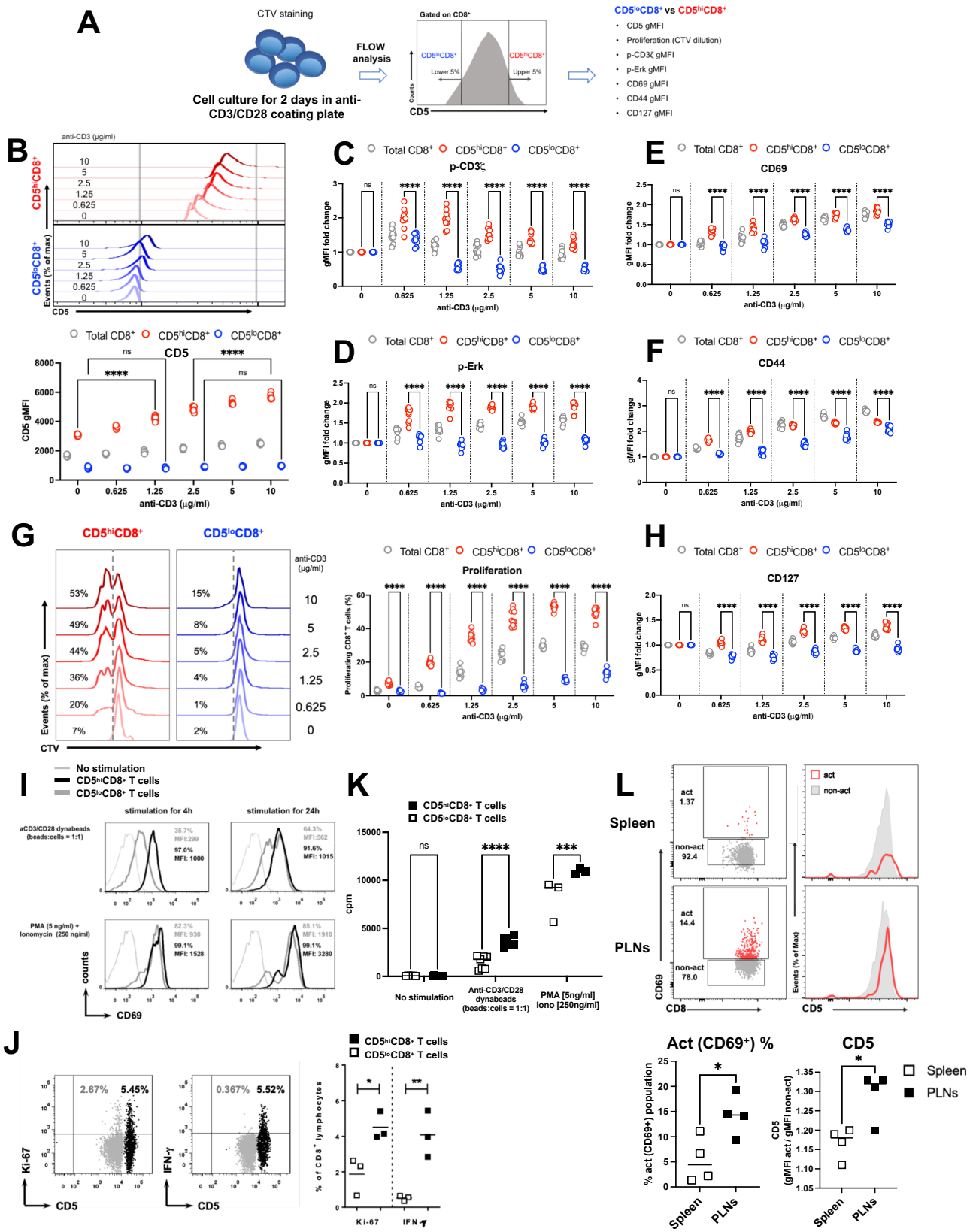

Figure 3 CD5 expression distinguishes CD8⁺ T cell subsets with differential activation and proliferation. (**A-K**) Naïve CD8⁺ T cells were isolated from the spleen of 6–8-week-old normoglycemic female NOD mice and stimulated with the indicated conditions. (**A**) Diagram depicting experimental setup using varying concentrations of anti-CD3 (0–10 μg/ml) and anti-CD28 (2 μg/ml; 0 μg/ml for control) for 2 days. (**B**, **G** upper/left panels) Representative flow cytometry plots, with statistical summaries shown in (**B-H**). Comparison of CD5 (**B**), fold change of p-CD3ζ (**C**), p-Erk (**D**), CD69 (**E**), CD44 (**F**), proliferation levels (CTV dilution %) (**G**) and fold change of CD127 expression (**H**) between the upper and lower 5% of CD5-expressing CD8⁺ T cells (CD5^{hi}CD8⁺ and CD5^{lo}CD8⁺, respectively). Fold change values in (**C-F**, **H**) were normalized to each group's baseline at 0 μg/ml anti-CD3 stimulation, where total CD8⁺ T cells, CD5^{hi}CD8⁺ and CD5^{lo}CD8⁺ were each set to 1. (**I**) Histogram comparing CD69 expression between the upper and lower 10% of CD5-expressing CD8⁺ T cells (CD5^{hi}CD8⁺ and CD5^{lo}CD8⁺) after stimulation with anti-CD3/CD28 dynabeads or PMA plus Ionomycin for specified durations. (**J**) Comparison of Ki-67 expression and IFN-γ production between CD5^{hi}CD8⁺ and CD5^{lo}CD8⁺ T cells. (**K**) Proliferation of CD5^{hi}CD8⁺ and CD5^{lo}CD8⁺ T cells assessed by [methyl-3H] thymidine incorporation (cpm; counts per minute) after stimulation with the indicated amounts of anti-CD3/CD28 dynabeads or PMA plus Ionomycin for 2 days. (**L**) Comparison of CD5 gMFI in CD8⁺CD69⁺ (upper gate of flow dot plot) to that in CD8⁺CD69⁻ (lower gate of flow dot plot) population by histogram (CD8⁺CD69⁺ in solid red line; CD8⁺CD69⁻ in grey), across spleen and PLNs from normoglycemic female NOD mice aged 6 to 8 weeks. The statistical results of the percentages of activated (CD8⁺CD69⁺) population (left) and the ratio of activated to non-activated CD5 gMFI (right) are shown. Data represent mean ± SD. The data presented in (**B**) to (**H**) represent two experiments. The sample size was n = 10 (**B-H**), n = 3 (**J**), n = 3-7 (**K**), and n = 4 (**L**) per group. *$P < 0.05$, **$P < 0.01$, ***$P < 0.001$, ****$P < 0.0001$, by two-way ANOVA (**B**)-(**K**) and unpaired, two-tailed t test (**L**).

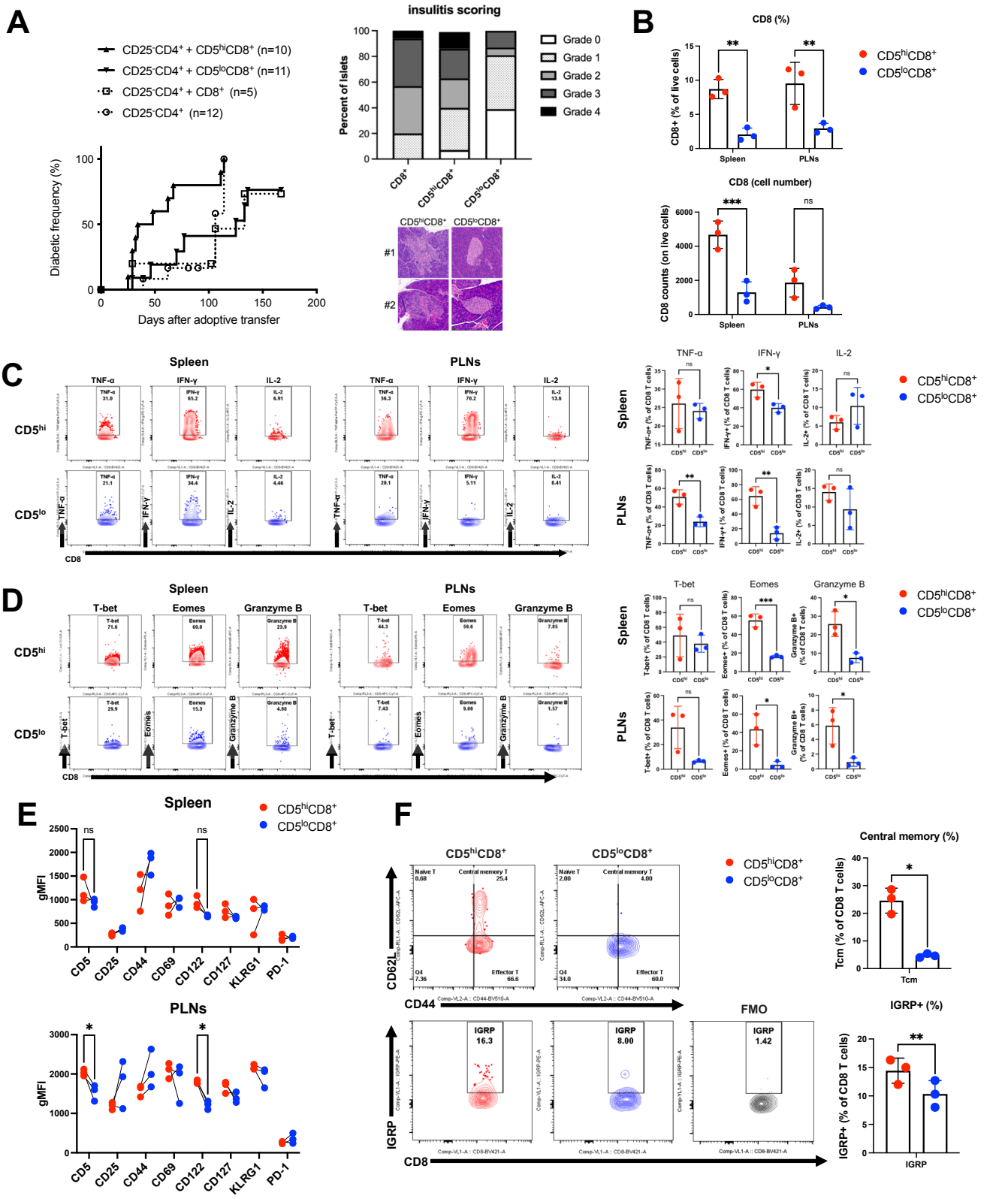

Figure 4 CD5^{hi}CD8^{+} T cells-transferred group exhibits severe insulitis and disease phenotype. (**A**) Diabetes incidence (left) in NOD Rag1$^{-/-}$ mice transferred with naïve CD5^{hi}CD8^{+}, CD5^{lo}CD8^{+}, or CD8^{+} T cells, combined with CD4^{+} T cells, respectively. The islet histological analyses and insulitis scoring (right) for the mice after a 4-week transfer in the respective transferred groups showed a higher diabetes frequency in the CD5^{hi}CD8^{+} group compared to the CD5^{lo}CD8^{+} group. The cells were sorted from the 10% upper and lower of CD5 expression of naïve CD8^{+} T cells (CD5^{hi}CD8^{+} and CD5^{lo}CD8^{+} T cells) from the spleen and PLNs 6-8-week-old normoglycemic female NOD mice and adoptively transferred to 6-8-week-old female NOD Rag1$^{-/-}$ recipients via i.p. injection. Urine glucose concentrations of the four groups of mice were monitored weekly for diabetes incidence. Diabetes was defined as glycosuria > 500 mg/dl in two consecutive tests. Insulitis scoring criteria can be found in the supplementary materials and methods. (**B**) Percentages and cell numbers of CD8^{+} T cells in spleen and PLNs, analyzed from CD5^{hi}CD8^{+} and CD5^{lo}CD8^{+} cells-transferred group, respectively, after 4-week adoptive transfer. (**C**) Percentages of TNF-α, IFN-γ and IL-2 production in CD5^{hi}CD8^{+} and CD5^{lo}CD8^{+} group, respectively, from spleen or PLNs, analyzed by flow cytometry, with representative flow dot plots (left) and statistical results (right). (**D**) Percentages of T-bet, Eomes and Granzyme B-expressing in CD5^{hi}CD8^{+} and CD5^{lo}CD8^{+} group, respectively, from spleen or PLNs, analyzed by flow cytometry, with representative flow dot plots (left) and statistical results (right). (**E**) Comparison of differential gMFI expression of CD5, CD25, CD44, CD69, CD122, CD127, KLRG1 and PD-1 between CD5^{hi}CD8^{+} and CD5^{lo}CD8^{+} group from spleen or PLNs. (**F**) Comparison of percentages of central memory T cells (defined by CD44^{hi}CD62L^{hi}) (upper) and positive IGRP-tetramer staining (lower) between CD5^{hi}CD8^{+} and CD5^{lo}CD8^{+} groups from PLNs, with representative flow dot plots (left) and statistical results (right). Representative flow cytometry plots include FMO negative control for accurate IGRP-tetramer gating. Data represent mean ± SD. Sample size was n = 5-11 (**A**), and n = 3 (**B**-**F**) per group. *P < 0.05, **P < 0.01, ***P < 0.001, by log-rank test (**A**), by two-way ANOVA (**B**) and (**E**) and unpaired, two-tailed t test (**C**), (**D**) and (**F**).

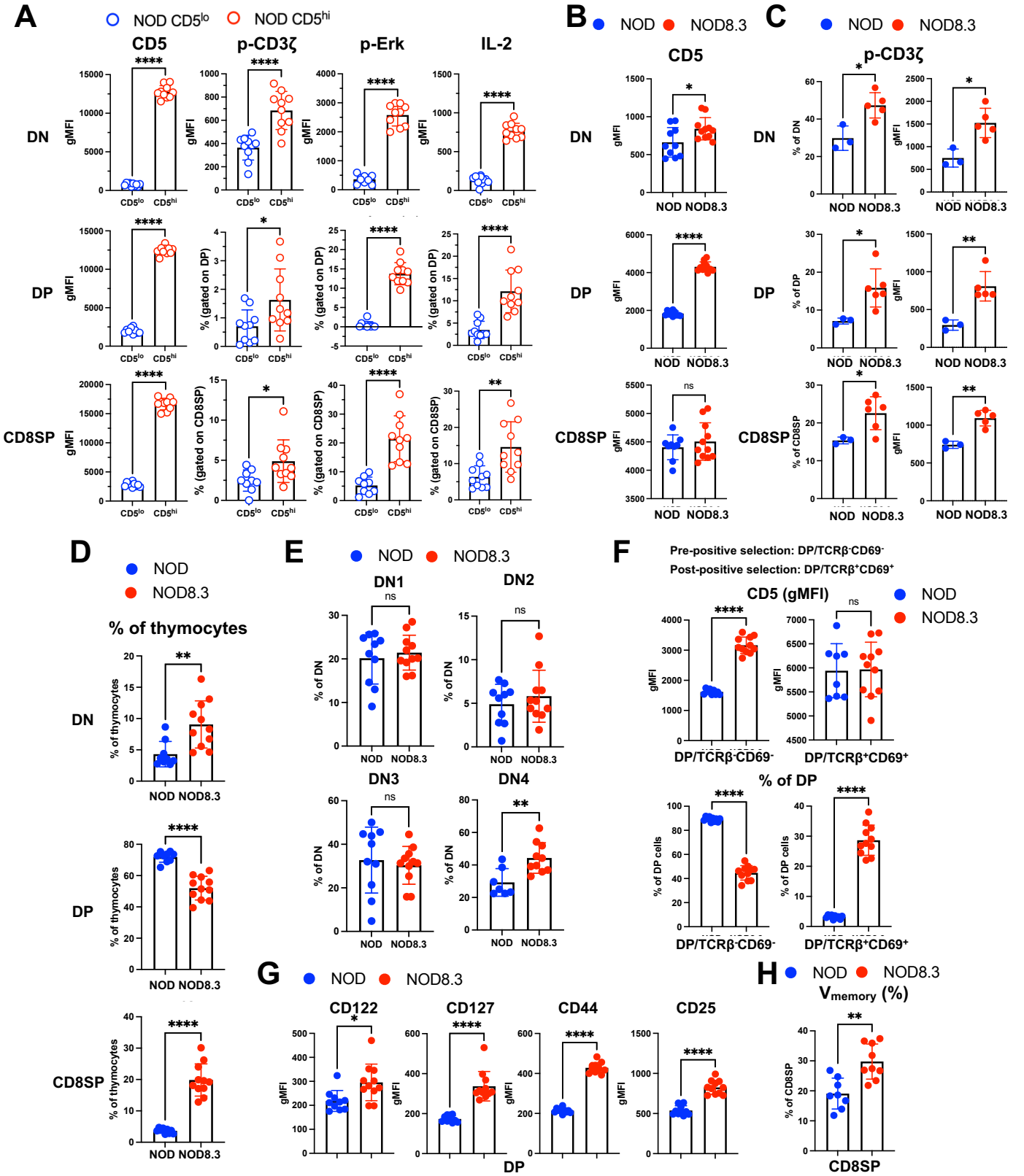

Figure 5 The high CD5-linked TCR basal signals positively correlate with thymic selection in autoimmune-poised NOD8.3 mice. (**A**) CD5, p-CD3ζ, p-Erk and IL-2 expression levels compared between the lower 5% (hollow blue) and upper 5% (hollow red) CD5 expression in thymocytes of normoglycemia female NOD mice aged 6 to 8 weeks old across DN, DP and CD8SP stages. (**B-H**) Comparison of various marker expression levels between thymocytes of normoglycemia female NOD (solid blue) and NOD8.3 (solid red) mice aged 6 to 8 weeks old across different selection stages. (**B**) CD5 gMFI in NOD and NOD8.3 thymocytes across DN, DP and CD8SP stages. (**C**) Percentages of p-CD3ζ (left) and the corresponding gMFI of p-CD3 (right) compared between NOD and NOD8.3 thymocytes in the indicated stages DN, DP and CD8SP. (**D**) Percentages of DN, DP and CD8SP composition compared between NOD and NOD8.3 thymocytes. (**E**) Percentages of indicated DN stages (DN1, DN2, DN3 and DN4) in the DN subset compared between NOD and NOD8.3 mice. DN stages are defined as follows: DN1 ($CD44^+CD25^-$), DN2 ($CD44^+CD25^+$), DN3 ($CD44^-CD25^+$) and DN4 ($CD44^-CD25^-$), as depicted in the gating shown in Supplementary Figure 3A, middle panels. (**F**) CD5 gMFI (upper) and corresponding percentages (lower) in the pre-positive selection ($TCR\beta^-CD69^-$) and post-positive selection ($TCR\beta^+CD69^+$) populations in DP thymocytes compared between NOD and NOD8.3 mice. The presence of higher TCR basal signals (indicated by higher CD5 gMFI) in NOD8.3 in the pre-positive selection stage leads to an increased percentage of $TCR\beta^+CD69^+$ cells in the post-selection stage compared to NOD mice, as shown in Supplementary Figure 3F. (**G**) gMFI of CD122, CD127, CD44 and CD25 assessed in DP thymocytes compared between NOD and NOD8.3 mice. (**H**) Percentages of virtual memory (V_{memory}) cells in CD8SP thymocytes compared between NOD and NOD8.3 mice. Data represent mean ± SD. The data presented in (**B**) to (**H**) represent two experiments. The sample size was n = 10 (**A**), n = 10-11 (**B**), n = 3-6 (**C**), n = 9-11 (**D**), n = 7-11 (**E**), n = 8-11 (**F**) n = 10-11 (**G**) and n = 8-9 (**H**) per group. *$P < 0.05$, **$P < 0.01$, ****$P < 0.0001$, by unpaired, two-tailed t test (**A-H**).

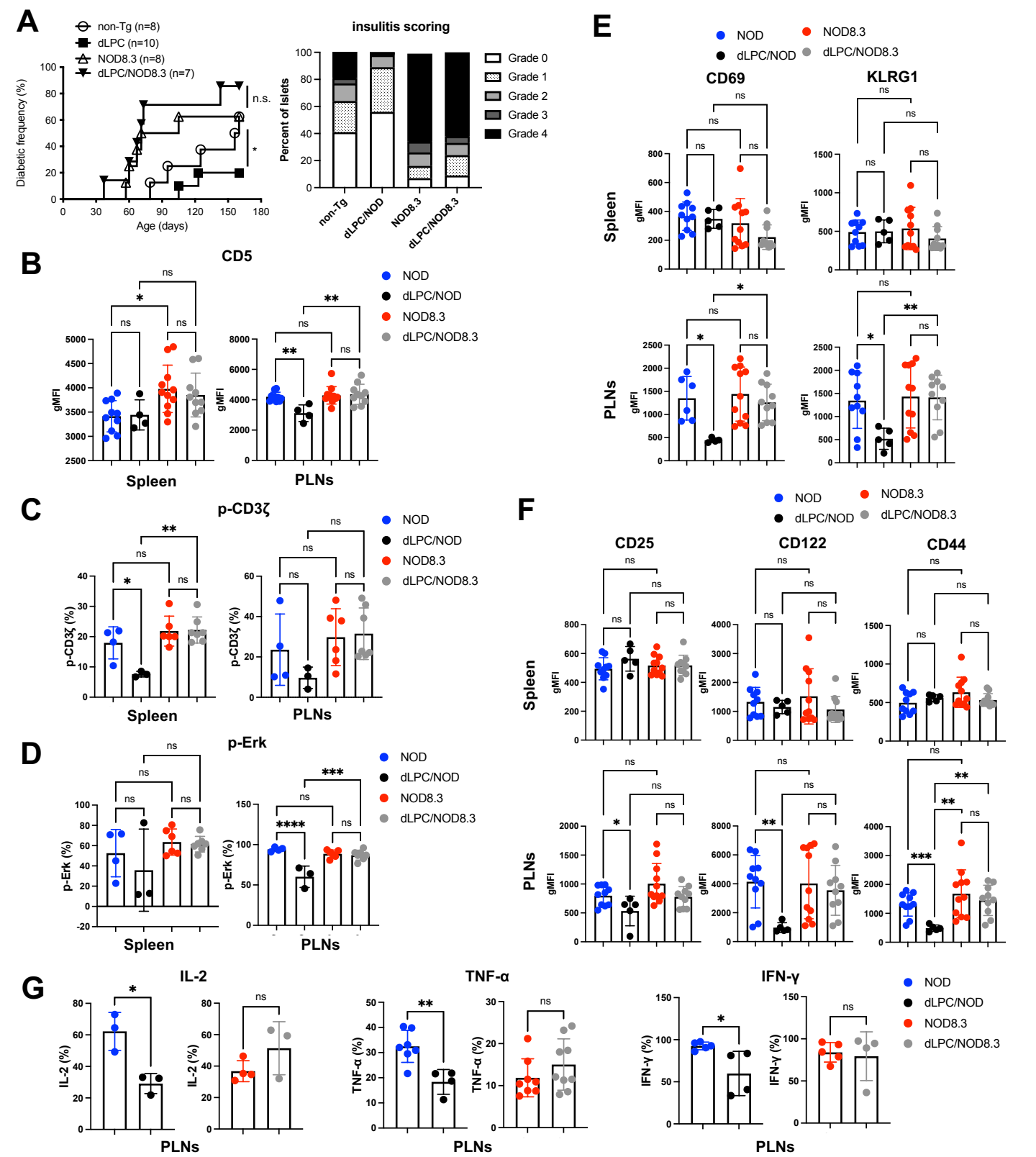

Figure 6 The protective effect of transgenic Pep on diabetogenesis is negated in dLPC/NOD8.3 mice. (**A**) Spontaneous diabetes incidence (left) and insulitis scoring (right) of female non-Tg NOD, dLPC/NOD, NOD8.3 and dLPC/NOD8.3 mice. Insulitis scoring was performed on the islets from the pancreata of 6-8-week-old mice before the onset of diabetes in each group. Insulitis scoring criteria can be found in the supplementary materials and methods. Urine glucose concentrations of mice were monitored weekly for spontaneous diabetes incidence. Diabetes was defined as glycosuria > 500 mg/dl at two consecutive tests. (**B**-**G**) Characterization of various aspects of TCR signal strength and effector/memory T cell phenotypes among female normoglycemia non-Tg NOD (blue), dLPC/NOD (black), NOD8.3 (red) and dLPC/NOD8.3 (grey) mice at the age of 6 to 8 weeks old. (**B**) CD5 gMFI of $CD8^+$ T cells in the spleen (left) and PLNs (right). (**C**) Percentage of p-$CD3\zeta^+CD8^+$ T cells in the spleen (left) and PLNs (right). (**D**) Percentage of p-Erk^+CD8^+ T cells in the spleen (left) and PLNs (right). (**E**) gMFI of effector T cell markers CD69 and KLRG1 in $CD8^+$ T cells from the spleen (upper) and PLNs (lower). (**F**) gMFI of memory T cell markers CD25, CD122 and CD44 in $CD8^+$ T cells from the spleen (upper) and PLNs (lower). (**G**) Percentage of IL-2^+-, TNF-α^+-, and IFN-γ^+CD8^+ T cells in PLNs. Data in (**B**) to (**G**) represent mean ± SD. The data presented in (**B**) to (**G**) represent two experiments. The sample size was n = 7-10 (**A**), n = 4-11 (**B**), n = 3-7 (**C**), n = 3-7 (**D**), n = 5-11 (**E**), n = 5-11 (**F**) and n = 3-9 (**G**) per group. *$P < 0.05$, **$P < 0.01$, ***$P < 0.001$, ****$P < 0.0001$, by log-rank test (**A**), by one-way ANOVA (**B**-**F**) and unpaired, two-tailed t test (**G**).

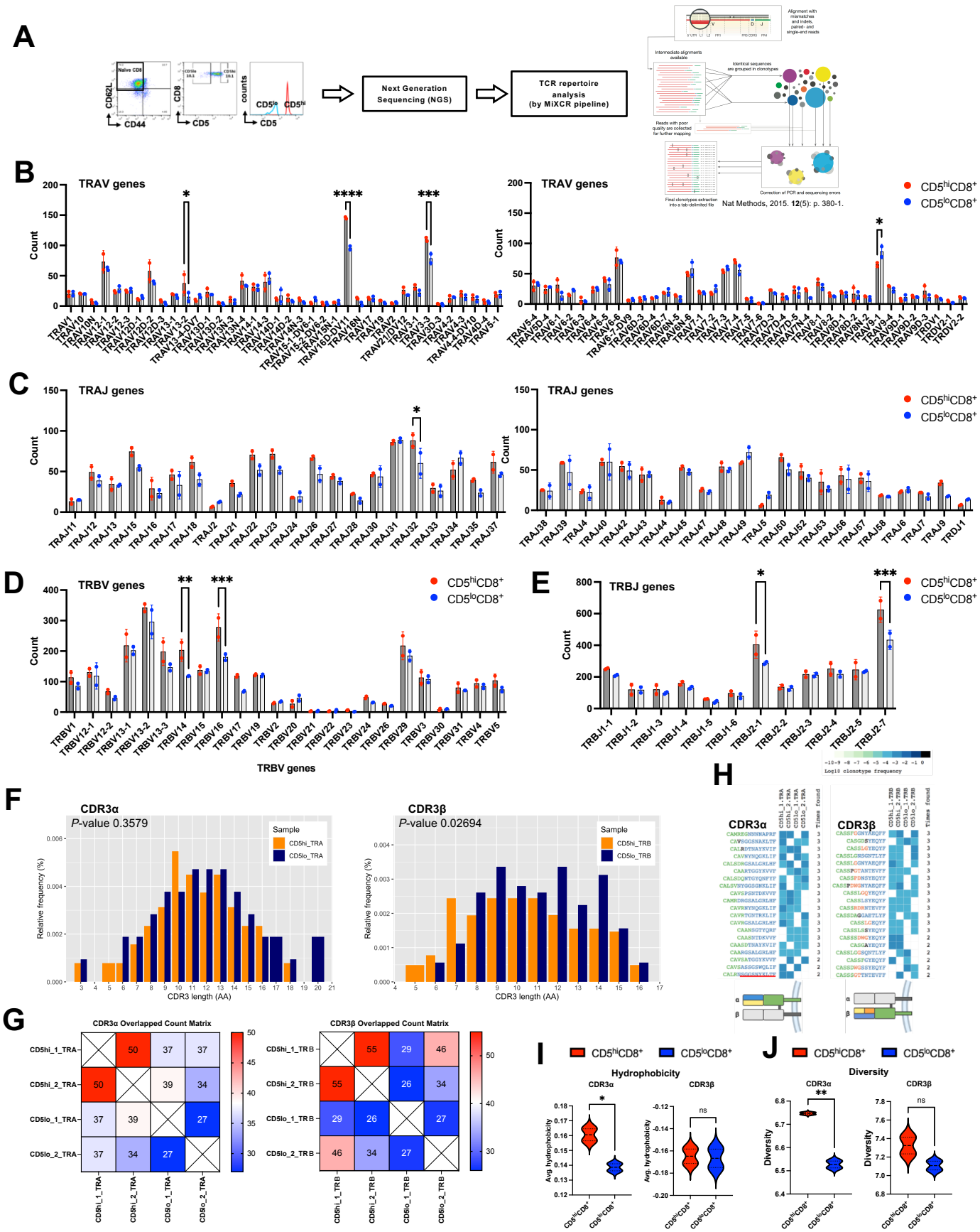

Figure 7 Examination of the CD5^{hi} population reveals TCR repertoires linked to autoimmune disorders. (**A**) Comparison of TCR repertoire differences between CD5^{hi}CD8^{+} and CD5^{lo}CD8^{+} T cell populations conducted using bulk RNA sequencing, followed by TCR repertoire analysis using the MiXCR pipeline. Naïve CD5^{hi}CD8^{+} and CD5^{lo}CD8^{+} cells were sorted from pooled spleens and PLNs of 6–8-week-old normoglycemic female NOD mice, following a similar procedure as outlined in Figure 2A, with 1.5 x 10^{6} cells per group. The TCR repertoire of naïve CD5^{hi}CD8^{+} T cells exhibited shorter CDR3 lengths, higher clone overlap values within group comparisons, pathogenic-related CDR3 motifs and greater hydrophobicity and diversity in the TRA chain compared to CD8^{+}CD5^{lo} cells. (**B-E**) Comparison of the TRAV gene segment usage (**B**), TRAJ gene segment usage (**C**), TRBV gene segment usage (**D**) and TRBJ gene segment usage (**E**) within TRA variable and TRB variable genes between CD5^{hi}CD8^{+} (red) and CD5^{lo}CD8^{+} (blue) cells. (**F-J**) Comparison of CDR3α (left) or CDR3β (right) length in amino acids (**F**), CDR3 clonal overlap by overlapped count matrix (**G**), top 20 CDR3 motifs (**H**), average hydrophobicity score (**I**) and diversity (**J**) of CDR3α (left) and CDR3β (right) between CD5^{hi}CD8^{+} and CD5^{lo}CD8^{+} T cells. In (**G**), the number in each cell indicates the count of shared clonotypes between sample pairs; the detailed method for constructing the Overlapped Count Matrix is provided in the Supplementary methods section. (**H**) Occurrence frequencies of the top 20 CDR3 motifs from mapped-CDR3α (left) and CDR3β (right) sequencings in CD5^{hi}CD8^{+} and CD5^{lo}CD8^{+} cells, with the high-occurrence rate of the CDR3α motif "SGGSNYKLTF" (underlined in red) specific to T1D-related IGRP peptide in the CD8^{+}CD5^{hi} population. (**I**) Average hydrophobicity score defined by summing up the hydrophobicity score in each amino acid in the CDR3 motif and dividing by the CDR3 length, then averaging by total counts in each group. Diversity definition in (**J**) is shown in Materials and Methods section Clonotype repertoire metrics formulas. In (**B-E**), each point represents 10 mice, with two points for each group, totaling n = 20 mice (**F-J**) for all CD5^{hi} or CD5^{lo} samples. *P < 0.05, **P < 0.01, ***P < 0.001, by two-way ANOVA (**B-E**), by Welch two sample t-test (**F**), and unpaired, two-tailed t test (**I**) and (**J**).

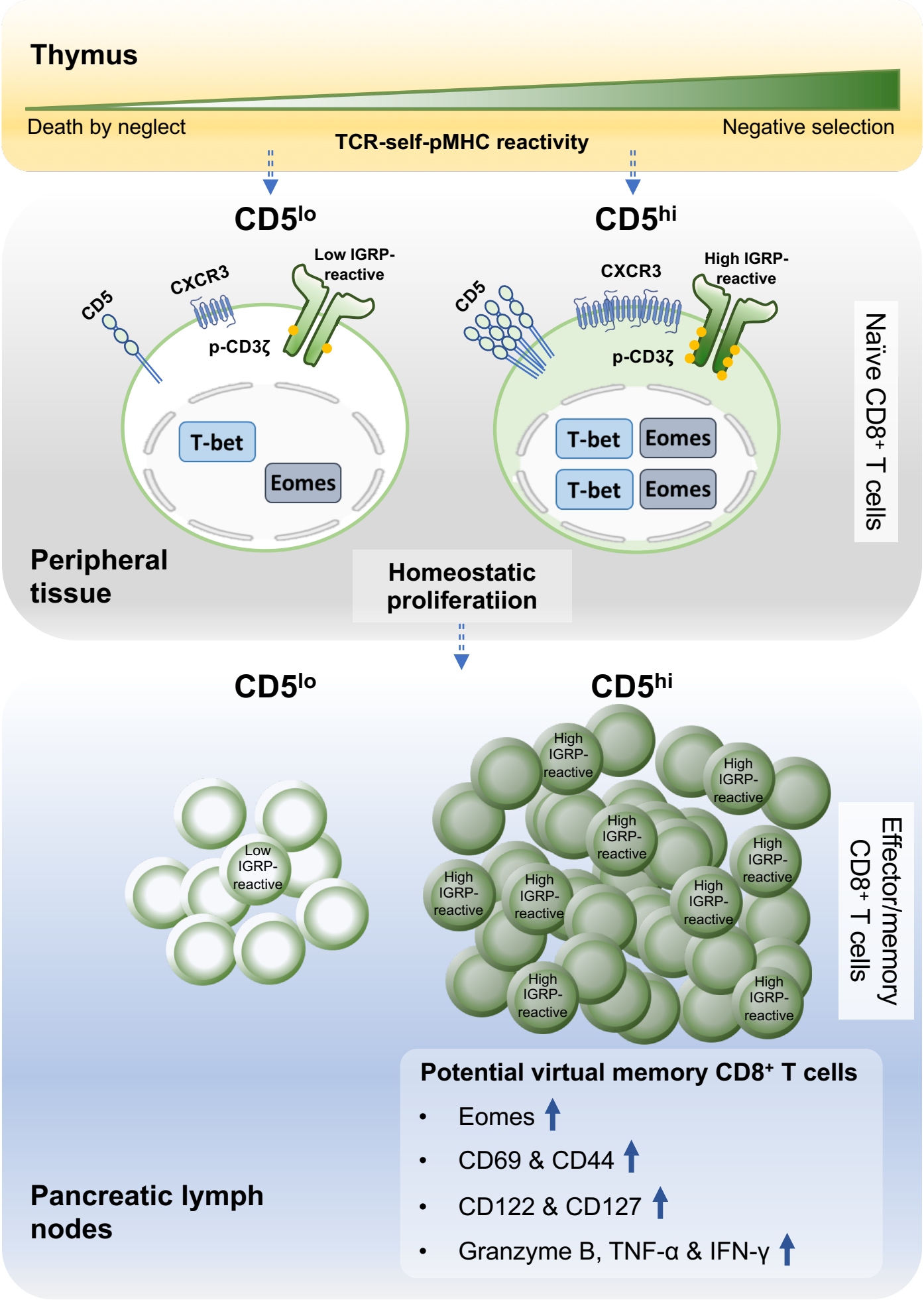

Figure 8 Thymocyte self-reactivity impacts the effector functions and memory cell formation of auto-reactive T cells in the T1D model NOD mice.

Table

Table 1 Naïve $CD5^{hi}CD8^{+}$ and $CD5^{lo}CD8^{+}$ T cells exhibit distinct expression in effector/memory T cell gene-expression clusters.

Cluster	Characteristics	$CD5^{lo}$	$CD5^{hi}$	*P*	Proportion
I	Initial cytokine or effector response	2	21	6.66555E-45	0.913
II	Preparation for cell division	98	406	1.7815E-173	0.806
III	Cell cycle & division	81	175	2.20063E-29	0.684
IV	Naive and late memory	44	25	5.78321E-06	0.362
V	Early effector, late memory	33	150	2.31501E-70	0.820
VI	Short-term effector and memory	18	30	0.000881688	0.625
VII	Memory precursor	47	41	0.251118001	0.466
VIII	Naive or late effector or memory	103	98	0.492702408	0.488
IX	Short-term effector or memory	27	45	6.4806E-05	0.625
X	Late effector or memory	28	49	1.77113E-06	0.636

Variation in gene-expression clusters between naïve $CD5^{hi}CD8^{+}$ and $CD5^{lo}CD8^{+}$ T cells and gene-set clusters in $CD8^{+}$ T cells evaluated by the Immunological Genome Project (published clusters with designated characteristics). In the '$CD5^{lo}$' and '$CD5^{hi}$' columns, values represent the count of genes predominantly expressed in each subset; 'Proportion' indicates the fraction of those genes expressed in the $CD5^{hi}$ subset. Statistical significance of expression differences was determined using the $\chi 2$ test (*P*).

Supplementary Figures

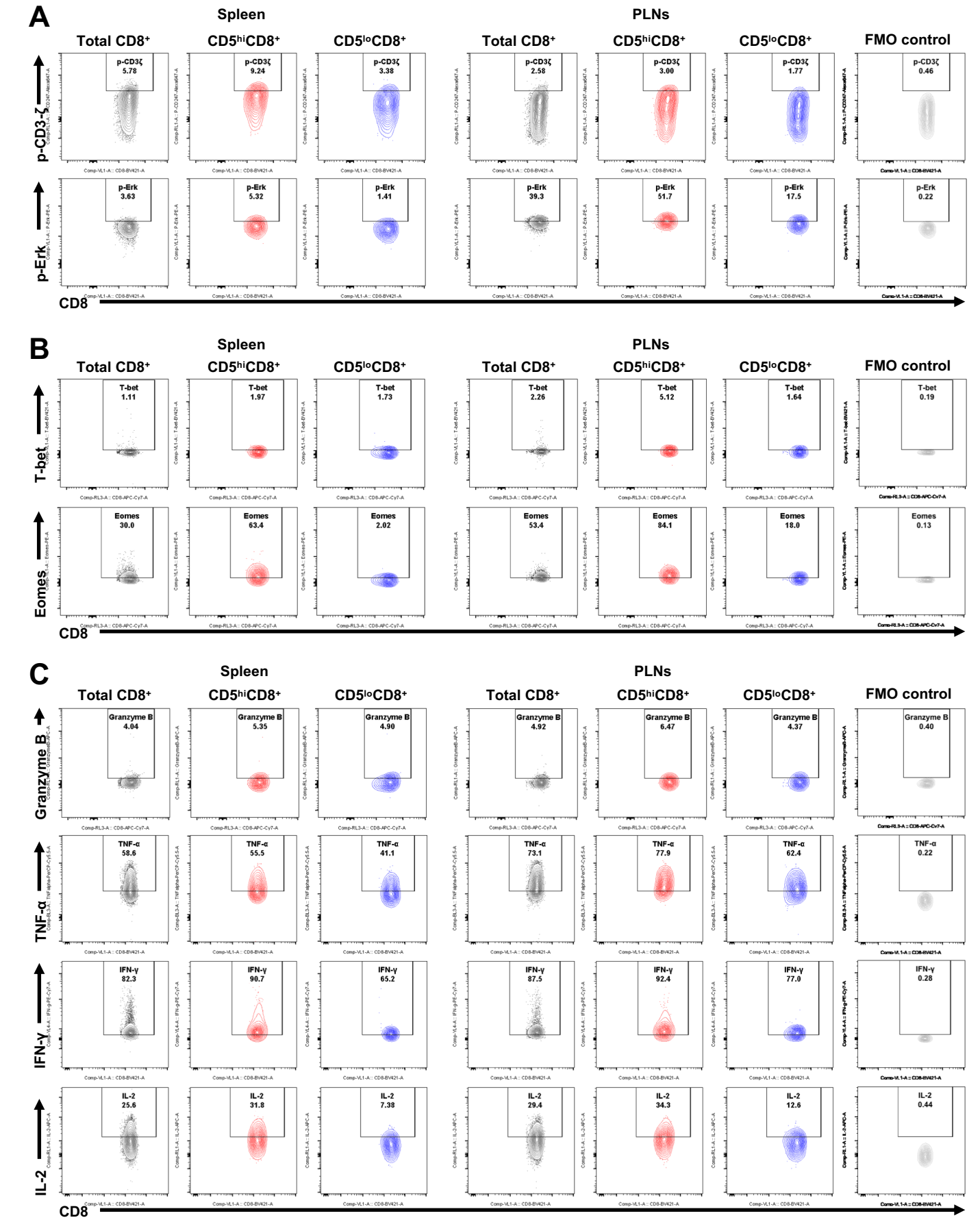

Supplementary Figure 1. CD5^{hi}CD8^{+} T cells display enhanced TCR signaling, effector profiles and autoreactive potential in NOD mice. Representative FLOW analysis plots show a comparison of positive expression percentages in (**A**) proximal TCR signaling molecules p-CD3ζ and p-Erk, (**B**) transcription factors T-bet and Eomes, and (**C**) cytokines Granzyme B, TNF-α, IFN-γ and IL-2 within total naïve CD8^{+} (grey), CD5^{hi}CD8^{+} (red), CD5^{lo}CD8^{+} (blue) cells, and fluorescence minus one (FMO) controls (light grey) from spleen (left) and PLNs (right). (**D**) Corresponding percentages of IGRP-tetramer positive CD8^{+} T cells among total naïve CD8^{+} T cells, CD5^{hi}CD8^{+} and CD5^{lo}CD8^{+} populations from spleen and PLNs. (**E**) Representative flow cytometry plots (left) and corresponding gMFI and proportions (right) of Ins B15-23-pentamer positive CD8^{+} T cells compared among total naïve CD8^{+} T cells, CD5^{hi}CD8^{+} and CD5^{lo}CD8^{+} populations from spleen and PLNs. In (**D**) and (**E**) all panels, total naïve CD8^{+} T cells, CD5^{hi}CD8^{+} and CD5^{lo}CD8^{+} are colored grey, red and blue, respectively. Data represent mean ± SD. Sample size was n = 3–5 per group. *P < 0.05, **P < 0.01, by one-way ANOVA.

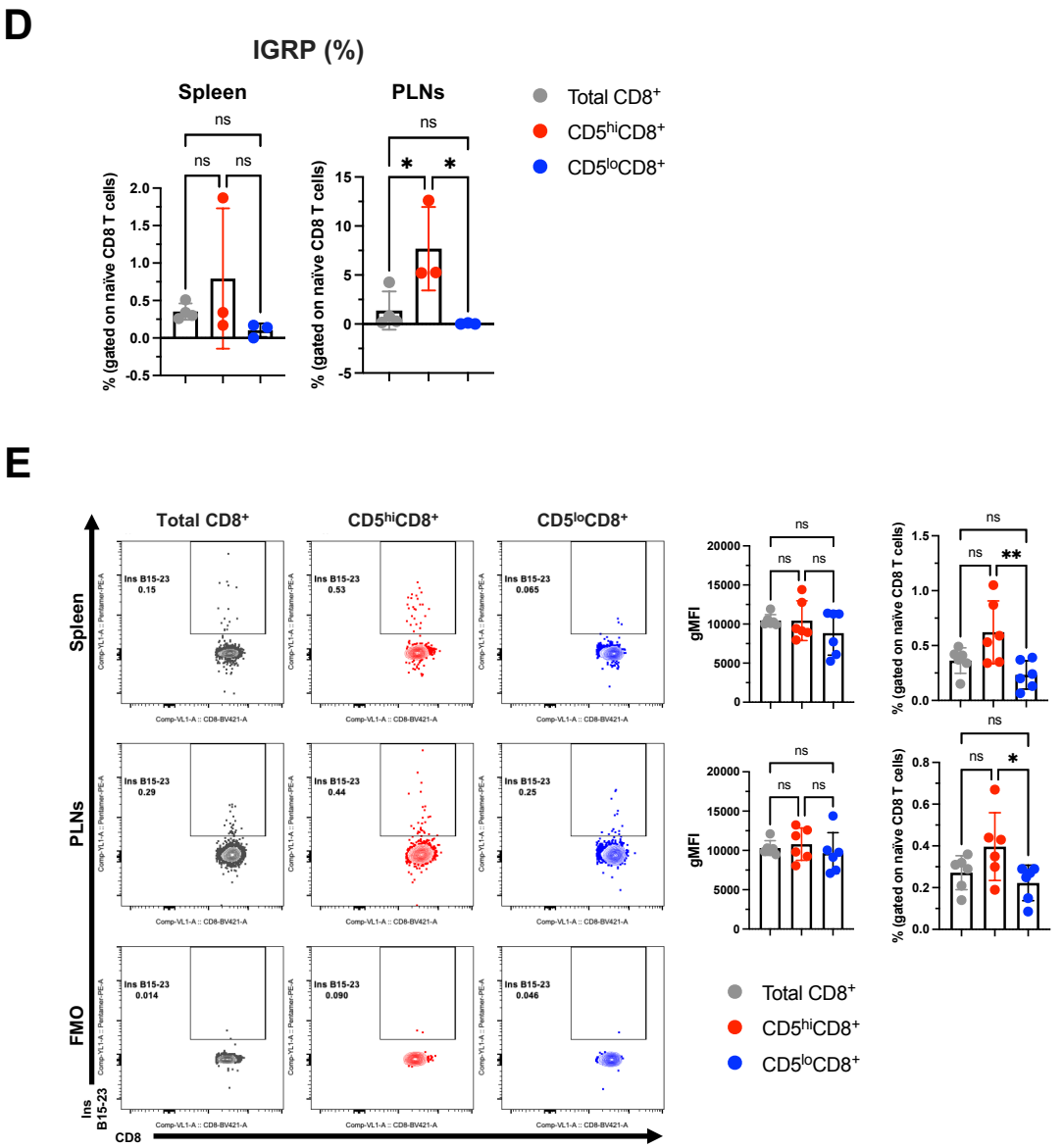

Supplementary Figure 1. CD5^{hi}CD8^{+} T cells display enhanced TCR signaling, effector profiles and autoreactive potential in NOD mice. Representative FLOW analysis plots show a comparison of positive expression percentages in (**A**) proximal TCR signaling molecules p-CD3ζ and p-Erk, (**B**) transcription factors T-bet and Eomes, and (**C**) cytokines Granzyme B, TNF-α, IFN-γ and IL-2 within total naïve CD8^{+} (grey), CD5^{hi}CD8^{+} (red), CD5^{lo}CD8^{+} (blue) cells, and fluorescence minus one (FMO) controls (light grey) from spleen (left) and PLNs (right). (**D**) Corresponding percentages of IGRP-tetramer positive CD8^{+} T cells among total naïve CD8^{+} T cells, CD5^{hi}CD8^{+} and CD5^{lo}CD8^{+} populations from spleen and PLNs. (**E**) Representative flow cytometry plots (left) and corresponding gMFI and proportions (right) of Ins B15-23-pentamer positive CD8^{+} T cells compared among total naïve CD8^{+} T cells, CD5^{hi}CD8^{+} and CD5^{lo}CD8^{+} populations from spleen and PLNs. In (**D**) and (**E**) all panels, total naïve CD8^{+} T cells, CD5^{hi}CD8^{+} and CD5^{lo}CD8^{+} are colored grey, red and blue, respectively. Data represent mean ± SD. Sample size was n = 3–5 per group. *P < 0.05, **P < 0.01, by one-way ANOVA.

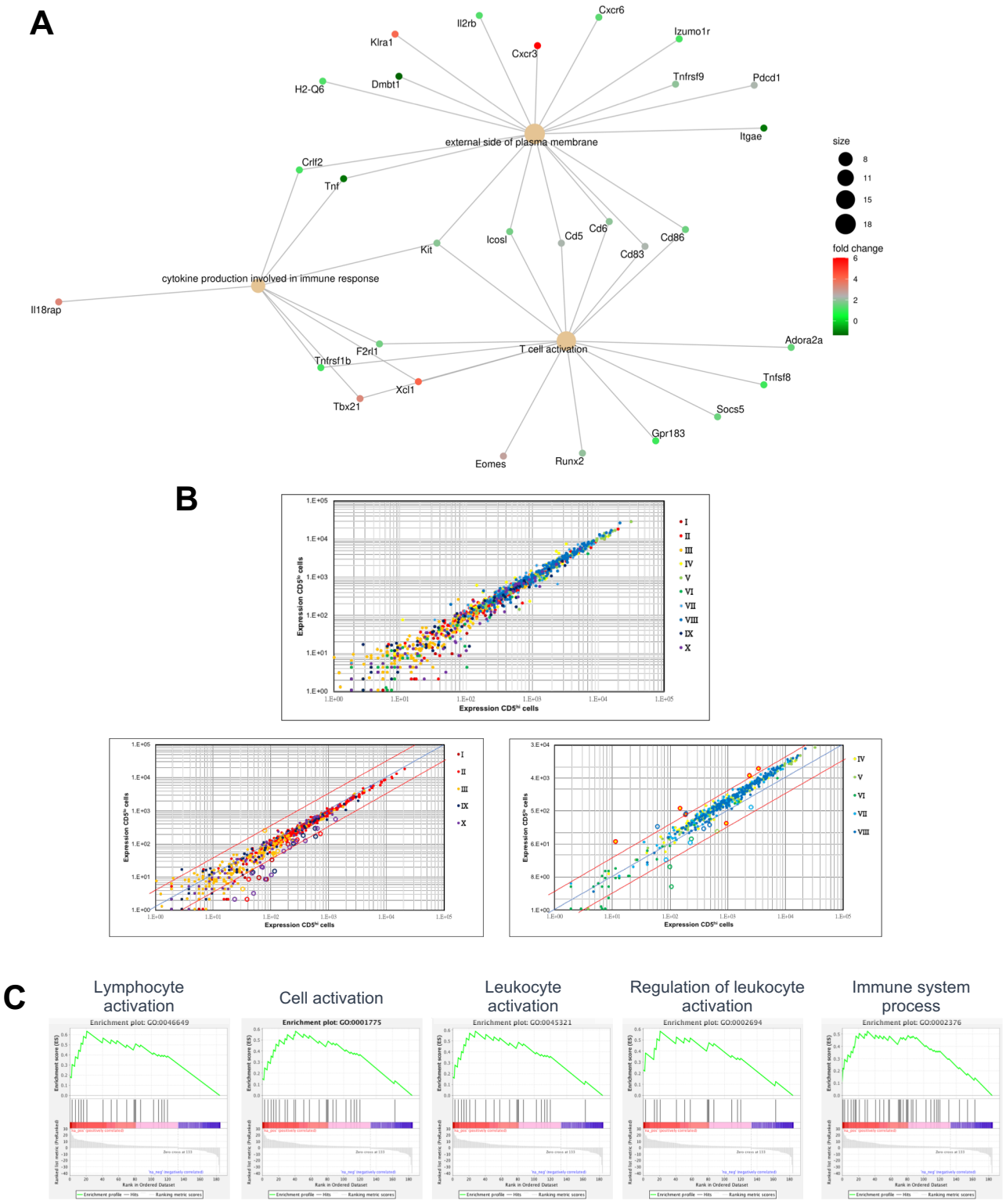

Supplementary Figure 2. Gene expression patterns and enrichment are comparatively analyzed between naïve CD5^{hi} and CD5^{lo}CD8^{+} T cells. (**A**) Gene-concept network of CD5^{hi} versus CD5^{lo} DEGs across key immune process GO terms. This interaction picture displays a gene-concept network highlighting genes associated with the top three GO terms: "external side of plasma membrane" (GO:0009897), "T cell activation" (GO:0042110), and "cytokine production involved in immune response" (GO:0002367) in CD5^{hi} versus CD5^{lo} DEGs. Circle size represents the gene counts, while the color spectrum, ranging from green to red, indicates the fold change in gene expression, spanning from less than 0 to a 6-fold change. (**B**) Comparison of gene expression patterns of CD5^{hi}CD8^{+} (x-axis) versus CD5^{lo}CD8^{+} (y-axis) T cells, using core gene signatures from clusters I to X (top panel). The two lower panels represent a similar comparison to the top panel but specifically focusing on the core gene signature differences in (left) clusters I, II, III, IX, and X, and (right) clusters IV to VIII between CD5^{hi} and CD5^{lo} T cells (lower panel); colors in plots (genes) match colors of clusters (key); red diagonal lines indicate a difference in expression of twofold; blue diagonal line indicates x = y. *P < 0.001 and **P < 0.00001 (t-test). Data are representative of two independent experiments. (**C**) The gene set enrichment score plot for biological process (BP) of GO terms (lymphocyte activation, cell activation, leukocyte activation, regulation of leukocyte activation, and immune system process). Higher scores indicate a higher degree of enrichment of these processes in naïve CD5^{hi}CD8^{+} than in CD5^{lo}CD8^{+} cells.

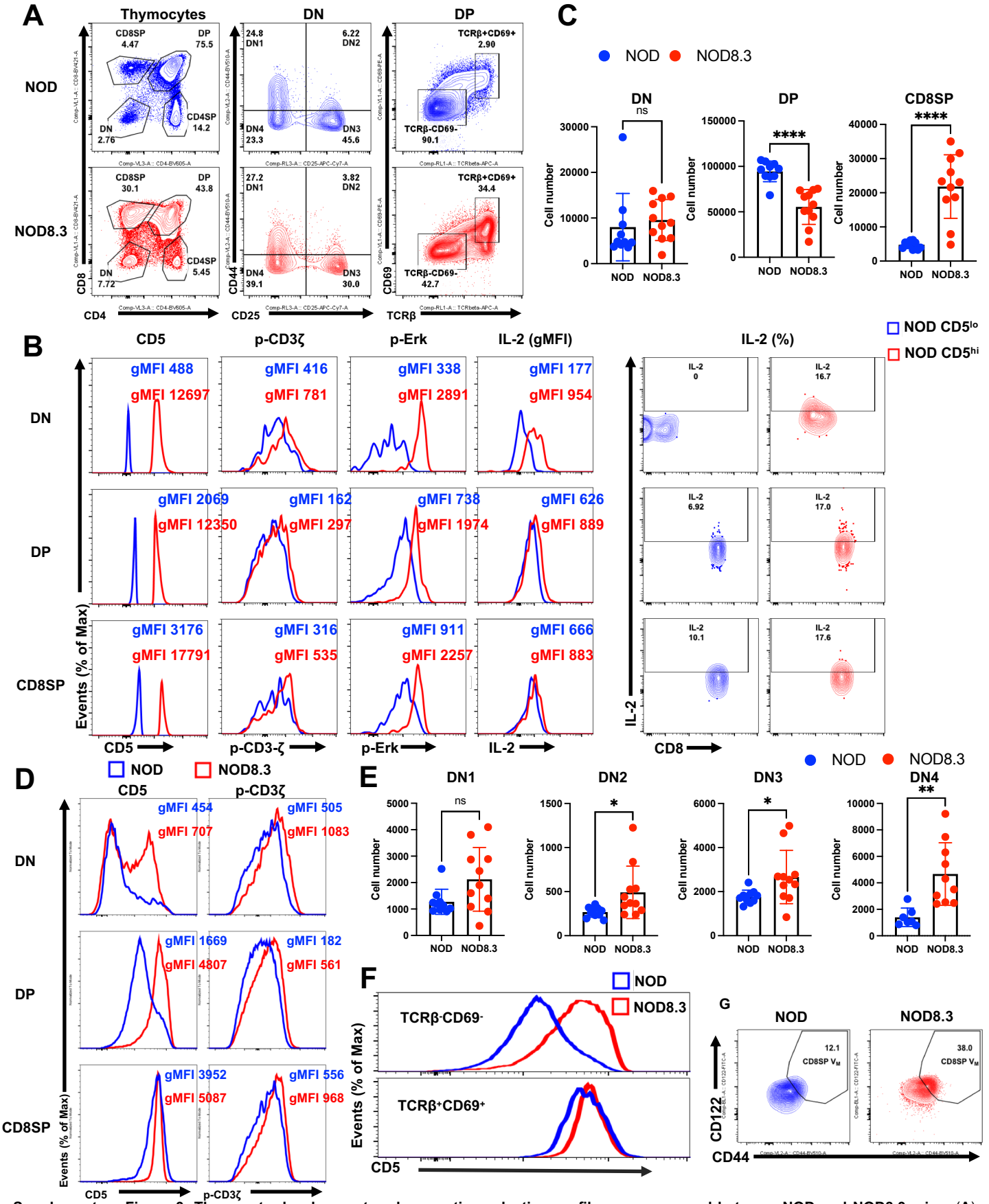

Supplementary Figure 3. Thymocyte development and respective selection profiles are compared between NOD and NOD8.3 mice. (**A**) Representative FLOW dot plots showing thymocytes (CD4 and CD8), DN thymocytes (CD25 and CD44), pre-positive selection (TCRβ$^-$CD69$^-$), and post-positive selection (TCRβ$^+$CD69$^+$) stages in DP thymocytes from NOD and NOD 8.3 mice. (**B**) Representative gMFI histograms of CD5, p-CD3ζ, p-Erk and IL-2 levels (left) and the IL-2 gating representative plot (right) compared between the lower 5% and upper 5% CD5 expression in thymocytes of normoglycemia female NOD mice aged 6 to 8 weeks old across DN, DP and CD8SP stages. (**C**) Cell numbers of thymocytes from NOD and NOD8.3 mice at the DN, DP and CD8SP stages. (**D**) Representative CD5 and p-CD3ζ gMFI histograms in thymocytes across DN, DP and CD8SP stages from NOD and NOD8.3 mice. (**E**) Cell numbers of thymocytes at the indicated DN stages (DN1, DN2, DN3 and DN4) from NOD and NOD8.3 mice. DN stages are defined as presented in Supplementary Figure 3A, middle panels. (**F**) CD5 gMFI distribution at the pre-positive selection (upper; TCRβ$^-$CD69$^-$) or post-positive selection (lower; TCRβ$^+$CD69$^+$) stage in DP thymocytes from NOD and NOD8.3 mice. (**G**) Representative FLOW dot plots for virtual memory (V_{memory}) as shown in Figure 5H in NOD or NOD8.3 mice. In all panels from (**A**) to (**G**), NOD CD5^{lo} cells or NOD mice are represented in blue, and NOD CD5^{hi} cells or NOD8.3 mice are represented in red. Data represent mean ± SD. The data presented in (**C**) and (**E**) represent two experiments. The sample size was n = 10-11 (**C**) and n = 7-11 (**E**) per group. *P < 0.05, **P < 0.01, ****P < 0.0001, by unpaired, two-tailed t test (**C**) and (**E**).

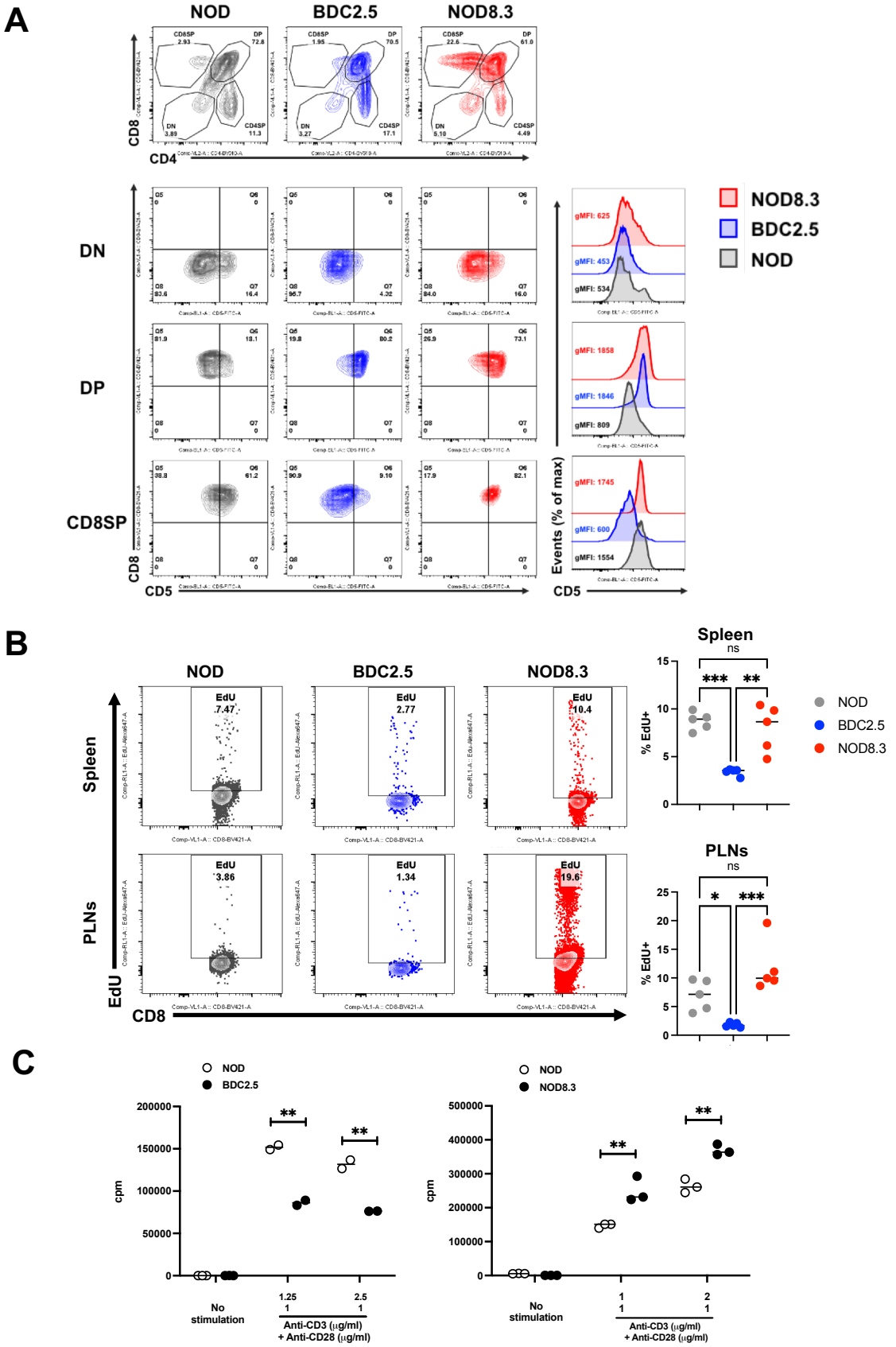

Supplementary Figure 4. Thymocyte-stage self-reactivity correlates peripheral diabetogenic T cell proliferation profiles in NOD, BDC2.5 and NOD8.3 mice. (**A**) CD5 gMFI comparison in the DN, DP and CD8SP stages of thymocytes (upper panel) among NOD (grey), BDC2.5 (blue) and NOD8.3 (red) mice. The received TCR signal (dictated by CD5 level) during thymocyte selection dictates the peripheral cell proliferation level, shown in (**B** and **C**). (**B**) Thymidine analog Edu incorporation in CD8⁺ T cells from spleen (upper) or PLNs (lower) compared among NOD (grey), BDC2.5 (blue) and NOD8.3 (red) mice. Representative FLOW cytometry dot plots (left) and corresponding statistical results (right) are presented. (**C**) T cell proliferation level in BDC2.5 (left panel) and NOD8.3 (right panel) compared to NOD mice. Naïve T cells were isolated from 6-8-week-old normoglycemia female NOD, BDC2.5 and NOD8.3 mice and stimulated with the indicated amounts of anti-CD3 and anti-CD28 (1 μg/ml). Cell proliferation was measured by the incorporation of [methyl-3H] thymidine. Data represent mean ± SD. The data presented in (**B**) represent two experiments. The sample size was n = 5 (**B**) and n = 2-3 (**C**) per group. *$P < 0.05$, **$P < 0.01$, ***$P < 0.001$, by one-way ANOVA (**B**) and unpaired, two-tailed t test (**C**).

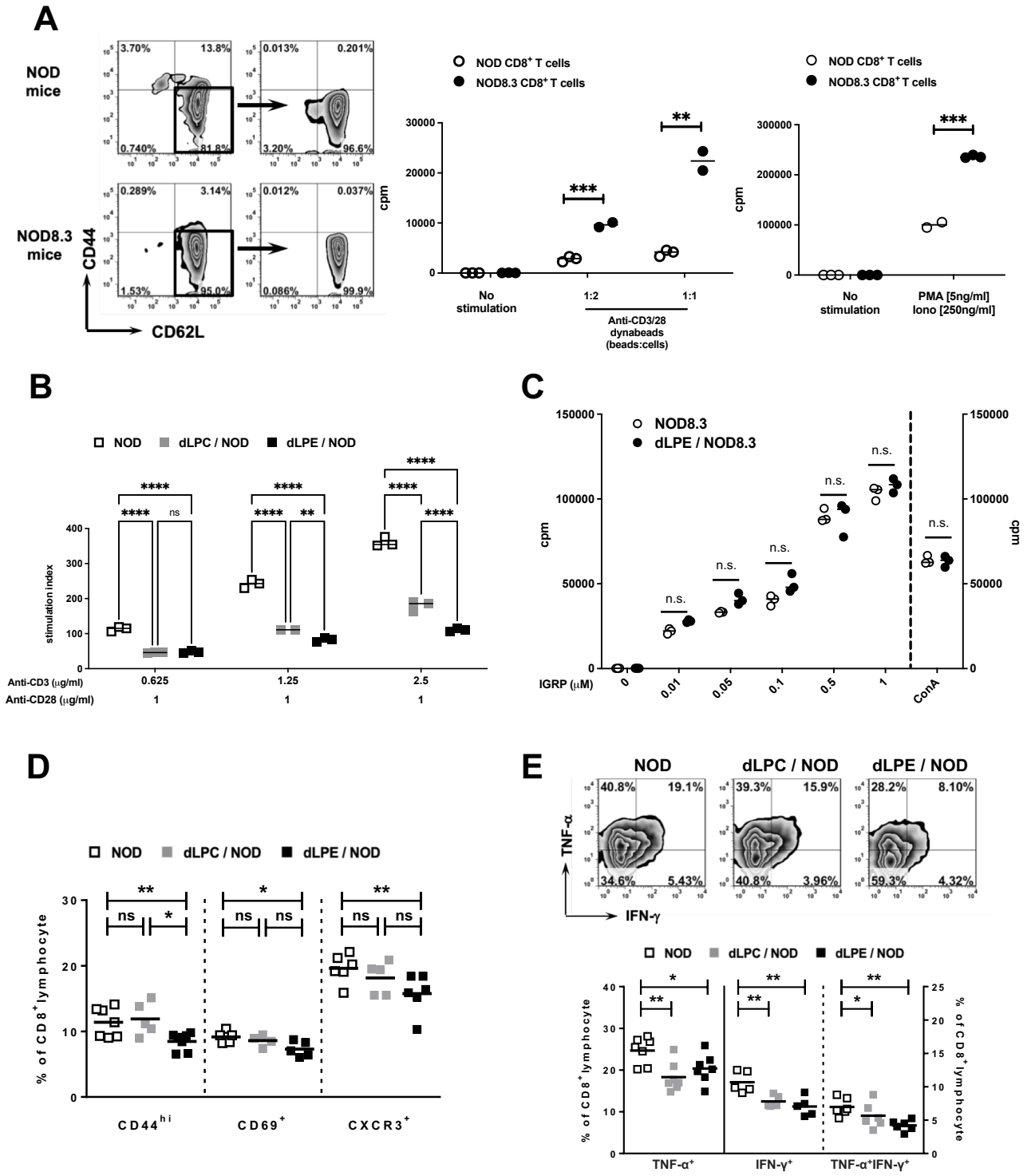

Supplementary Figure 5. Immunomodulatory effects of transgenic Pep on effector T cell functions are analyzed. (**A**) Cell proliferation levels of naïve $CD44^{lo}CD62L^{hi}CD8^{+}$ T cells (left) isolated from 8-10-week-old normoglycemia female NOD or NOD8.3 upon stimulation with anti-CD3/CD28 dynabeads (middle) or PMA/Ionomycin (right) treatment, measured by the incorporation of [methyl-3H] thymidine (cpm; counts per minute). (**B**) Cell proliferation levels of $CD8^{+}$ T cells isolated from 8-10-week-old normoglycemia female NOD, dLPC/NOD and dLPE/NOD mice upon anti-CD3/CD28 stimulation. Purified $CD8^{+}$ T cells were stimulated with the indicated amounts of anti-CD3 (0.625, 1.25 and 2.5 μg/ml, respectively) combined with anti-CD28 (1 μg/ml). Cell proliferation was measured by the incorporation of [methyl-3H] thymidine (shown by simulation index). (**C**) Proliferation levels of splenocytes isolated from 8-10-week-old normoglycemia female NOD8.3 and dLPE/NOD8.3 mice upon stimulation with the indicated amounts of $IGRP_{206-214}$ peptides or ConA. Cell proliferation was measured by the incorporation of [methyl-3H] thymidine (cpm; counts per minute). (**D**) Percentages of effector/memory $CD44^{hi}$-, $CD69^{+}$-, and $CXCR3^{+}CD8^{+}$ T cells in PLNs of NOD, dLPC/NOD and dLPE/NOD mice. (**E**) Percentages of TNF-α^{+}-, IFN-γ^{+}-, and TNF-α^{+}IFN-$\gamma^{+}CD8^{+}$ T cells in 8-10-week-old normoglycemia female NOD, dLPC/NOD and dLPE/NOD mice. Isolated cells were stimulated with anti-CD3/CD28 (1 μg/ml) for 48 hours. After stimulation, the percentages of cytokine-producing $CD8^{+}$ T cells were measured by flow cytometry analysis. Notably, in (**B**), (**D**) and (**E**), a stepwise increase in transgenic Pep expression from nontransgenic NOD to dLPC/NOD and dLPE/NOD mice within the litters born at the same time was confirmed in our previous study (27). Data represent mean ± SD. The data presented in (**A**) to (**E**) represent two experiments. The sample size was n = 5-7 (**A**), n = 5-7 (**B**), n = 6 (**C**), n = 5-7 (**D**) and n = 5-7 (**E**) per group. *P < 0.05, **P < 0.01, ***P < 0.001, by unpaired, two-tailed t test (**A**) and (**C**) and one-way ANOVA (**B**, **D** and **E**).

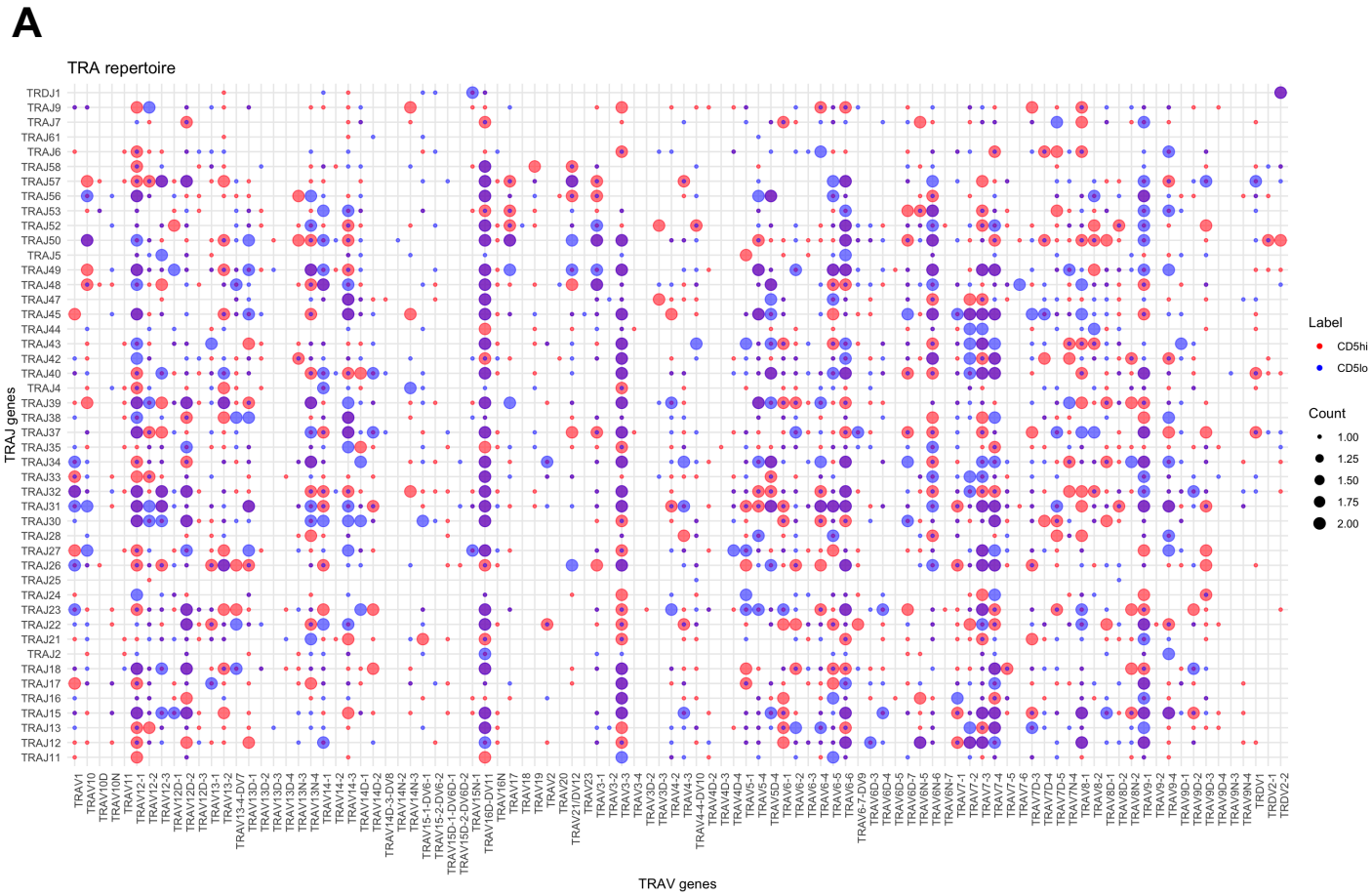

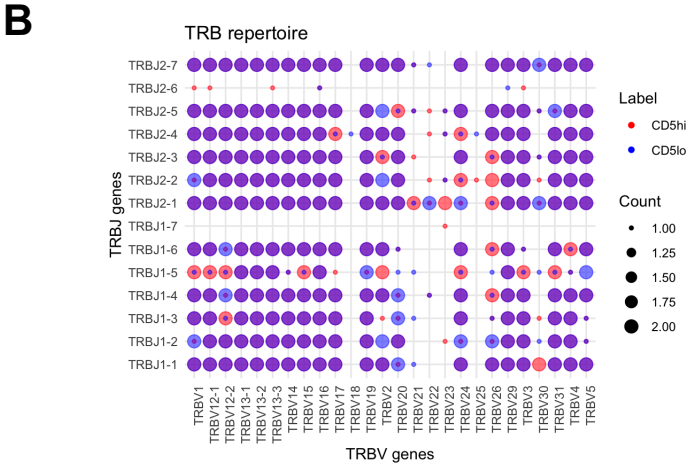

Supplementary Figure 6. The pairing of VJ gene segments in the TCR repertoire is compared between CD5^{hi}CD8^{+} and CD5^{lo}CD8^{+} cells. **(A)** TRA variable (TRAV) and **(B)** TRB variable (TRBV) genes in CD5^{hi} (red dot) and CD5^{lo} (blue dot) groups were examined. Notably, if the same count of a specific VJ gene segment usage occurred in CD5^{hi} and CD5^{lo} cells, the outcome of overlapping dot color would be purple. n = 20 mice for each CD5^{hi} and CD5^{lo} group.

A

Gene	F’	R’
Ptpn22	5’-ATCAGGATGGTTCTCCTCCA-3’	5’-CAAAGGCCAGCTGGTGCAGACGAT-3’
TCRβ8.3	5’-GGCTGCAGTCACCCAAAGTCC-3’	5’-GTACAAGGTGTTTTGAGCATC-3’

B

	35	36	37	38	39	40	41	42	43	44	45	46	47	48	49	50	51	52	53
Pep	-	-	+	+	-	-	+	-	+	+	-	-	-	+	+	-	+	-	+
8.3	-	+	-	+	+	+	+	-	+	-	-	+	+	+	+	-	+	+	+

C **Ptpn22: 853 bp**

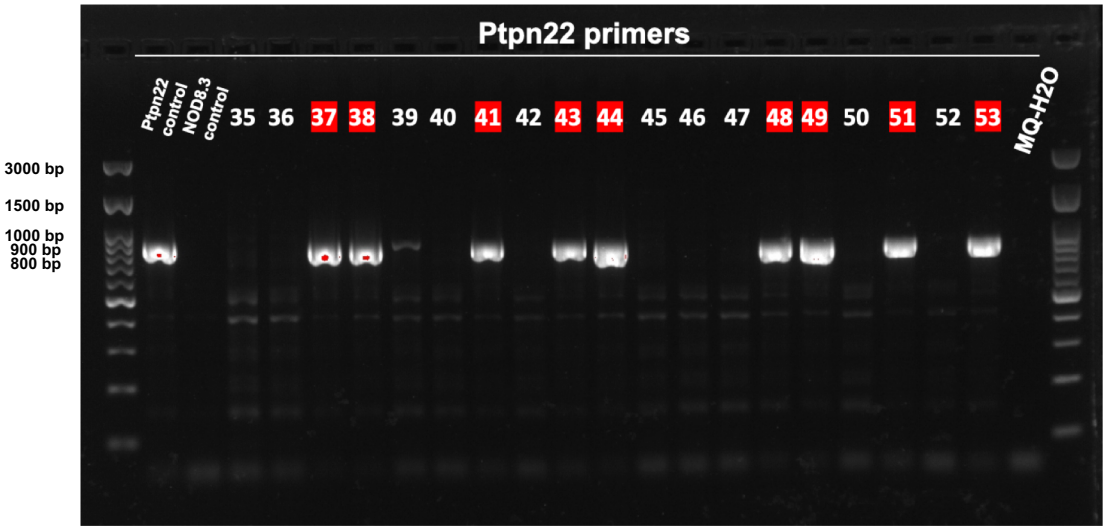

D **TCRβ8.3: 260 bp**

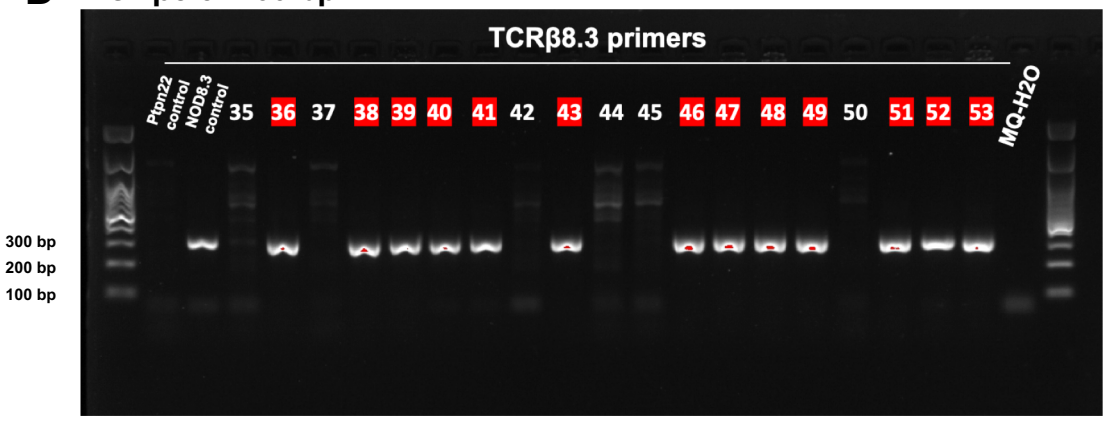

Supplementary Figure 7. The genotyping results of NOD, dLPC/NOD, NOD8.3 and dLPC/NOD8.3 mice using the indicated F’ and R’ primers are shown. (A) The Ptpn22 F’ and R’ primers used for genotyping were designed in our previous study to evaluate the existence of the transgene Ptpn22 (Ptpn22: 853 bp) (27). The primer sequence for TCRβ8.3 can be referred to (Verdaguer et al., 1997) (TCRβ8.3: 260 bp). **(B-D)** Genotyping results for transgenic Ptpn22 and TCRβ8.3 expression in pups #35 to #53 from male NOD8.3 crossed with female dLPC/NOD mice are presented.